Imperial College London

MSc in Quantum Fields and Fundamental Forces

Imperial College London

Department of Physics

A Holographic Perspective of Wormholes in Anti-de Sitter Space

Author:

Shaun Nicholas Swain

Supervisor:

Prof. Toby Wiseman

Submitted in partial fulfilment of the requirements for the degree of Master of Science of Imperial College London

October 11, 2022

Abstract

The topic of wormholes has recently come to the forefront of theoretical research due to the discovery of a remarkable connection between wormholes and entanglement, commonly known as ER=EPR. This relation was realised using the AdS/CFT correspondence, a theory which equates gravitational theories and quantum field theories under certain conditions. In this review, we will discuss how ER=EPR arises and determine some of the properties of these wormholes. We shall also discuss a promising resolution to a current problem of ER=EPR.

Acknowledgements

I would like to express my sincere gratitude to Professor Wiseman for his excellent guidance and patience throughout my dissertation.

To the friends I have made throughout my time at Imperial College London, I would like to thank you for making this experience one that I will treasure forever.

Finally I wish to thank my family, whose support and encouragement throughout my early years in academia is appreciated more than words can say.

Contents

1. Introduction

In 1972, Bekenstein pubished a revolutionary paper describing the relation between the second law of thermodynamics and black holes. He suggested that the entropy of a black hole is proportional to the area of its event horizon [1], providing consistency between the second law of thermodynamics and the idea that the area of a black hole's event horizon cannot decrease. Following this, Bekenstein further proposed the idea of a generalised second law of thermodynamics, whereby the entropy of the universe does not decrease if the entropy of black holes is also included. The entropy of any object that falls into a black hole appears to be lost from the universe. However, this is compensated for by an increase in area, or entropy, of the black hole due to the infalling object. Hence the second law of thermodynamics is still valid if the entropy of black holes is taken in to consideration [2]. Using the idea that black holes emit radiation, Hawking provided further support for Bekenstein's proposal and determined the constant of proportionality of the relation between entropy and area [3]. This led to what is often referred to as the Bekenstein-Hawking entropy [4], which is given by the famous expression

$$S = \frac{k_B A}{4 l_p^2}. \tag{1.1}$$

The important interpretation of Eq. 1.1 states that a black hole can be completely described by information contained on its surface. This was realised by 't Hooft, who suggested that bits of information are defined on two dimensional regions of the order l_p^2 on the event horizon. In other words, the information of a black hole with three spatial dimensions can be realised on the two dimensional event horizon in a similar manner to a hologram; this is the holographic principle [5]. This was given mathematical foundations by Susskind who considered this concept from a string theory perspective [6], thus revealing many possibilities for the future of quantum gravity. One highly researched example of a holographic theory is the AdS/CFT correspondence, typically shortened to AdS/CFT. First proposed by Maldacena, AdS/CFT relates gravitational theories in $d+1$ dimensional spacetimes in asymptotically anti-de Sitter (AdS) space to specific types of quan-

tum field theories called confomal field theories (CFT) in d dimensions [7]. Such theories which are equivalent, i.e. they describe the same physics, are referred to as dual theories. The conformal field theory is said to exist on the spacetime boundary, which establishes AdS/CFT as an example of a holographic theory as the gravitational theory is said to be described by a conformal field theory on the boundary with one less dimension. In principle, AdS/CFT can be used to calculate quantities on one side of the correspondence using its dual theory. However, these computations are usually intractable unless one imposes certain restrictions on the type of theories considered. For example, AdS/CFT is extremely useful for computing quantities in strongly couplied field theories, as classical gravitational dual theories are well understood and can therefore be used to perform calculations that are very difficult to compute in the field theory framework [8]. To avoid confusion, we note AdS/CFT is sometimes referred to as gauge/gravity duality. While these names might be used synonymously, it is important to state that the term gauge/gravity duality refers to the correspondence between quantum gauge theories and more general spacetimes. In other words, AdS/CFT is a specific example of gauge/gravity duality involving Anti-de Sitter spaces and conformal field theories [7]. A detailed review of the AdS/CFT correspondence is given in section 2.

One key point of AdS/CFT is that the CFT is specified by the boundary conditions on the gravitational theory [9]. Therefore, providing sufficient asymptotically AdS boundary conditions are given, one can consider many different spacetime geometries. Recent interest in wormhole geometries has been sparked due to their relevance in the AdS/CFT correspondence. These geometries are given the name 'wormholes' as they connect two distant regions of AdS spacetime [10]. This review will focus on the application of wormhole geometries in AdS/CFT, giving examples where wormholes have been the focal point for much research in the last few decades. The term 'wormhole' is an ambiguous term that can be given many interpretations. In section 3, we will briefly discuss the history of the wormhole and the types of geometries that are associated with this term, providing clarity over what is meant by a 'wormhole'. In particular, we will review the details of the Einstein-Rosen bridge. We will then proceed by reviewing some key aspects of quantum entanglement in section 4, which will become important in later discussions. We will also provide a brief review of black hole thermodynamics in section 5, where we will explain how the Bekenstein-Hawking entropy of Eq. 1.1 arises from the properties of black holes. In section 6, we turn our attention to a simple example in which wormholes have a holographic description. It can be shown that AdS-Schwarzschild geometry, i.e. the geometry surrounding a Schwarzschild black hole in anti-de Sitter space, has two disconnected boundaries which are hidden from each other behind a horizon. The holographic dual of such a gravitational theory is a system of two identical

entangled conformal field theories at finite temperature, each existing on each of the disconnected boundaries [11]. Due to the presence of a horizon, the conformal field theories cannot interact with one another. In this sense, entanglement arises due to the presence of a non-traversable Lorentzian wormhole geometry which connects the two asymptotic boundaries. Maldacena and Susskind summarised this connection using the phrase ER=EPR [12]. In section 6, we introduce the properties of AdS-Schwarzschild black holes before proceeding with a detalied description of how the ER=EPR phenomenon arises. Following this, we use the work of Ryu and Takayanagi [13] to understand how the entanglement entropy of the boundary CFTs affects the dual wormhole geometry. Finally, to conclude this section, a short discussion on the future research possibilities of ER=EPR is provided. As a final remark, we will discuss how the current understanding of AdS/CFT requires slight modification due to the presence of wormhole configurations. A promising proposal is that on the CFT side of the AdS/CFT correspondence, one must consider an ensemble of CFTs [14]. In section 7, we explore the application of the SYK model to AdS/CFT as an example of this proposal. We will briefly discuss the work of Garcia-Garcia and Godet, who demonstrated that at low temperatures, the holographic dual of the SYK model is a Euclidean wormhole [15].

2. The AdS/CFT Correspondence

In this section, we will review the basics of anti-de Sitter spacetime and conformal field theories. Following this, we shall proceed by discussing the correspondence between these two specific theories. However, since there is no formal proof of AdS/CFT, we will discuss a well known example which was initially used to give evidence for the AdS/CFT correspondence. Once we have established the correspondence, we will show how to relate states in the two theories in a conveniently compact expression.

2.1 Anti-de Sitter Space

The geometry of spacetime is governed by the Einstein field equations

$$\mathcal{R}_{\mu\nu} - \frac{1}{2}\mathcal{R}g_{\mu\nu} + \Lambda g_{\mu\nu} = 8\pi\mathcal{T}_{\mu\nu}, \tag{2.1}$$

which relates the spacetime curvature to the matter and energy content. The cosmological constant, Λ, was introduced by Einstein so that a non-dynamical spacetime was predicted by the equations. However, it was discovered by Hubble that the universe is expanding at an accelerating rate. While the cosmological constant was subsequently disregarded, it is now widely believed that the cosmological constant is responsible for this accelerated expansion of the universe [16]. It is clear that the cosmological constant plays a large role in the geometry of spacetime. In particular, there are three maximally symmetric solutions to the vacuum Einstein equations, i.e. spacetimes of constant curvature, or constant $\mathcal{R}$, that possess the maximum possible number of isometries. The spacetime with zero curvature is the well known Minkowski spacetime, while a spacetime with negative (positive) $\mathcal{R}$ is called anti-de Sitter (de Sitter) space [8]. These spacetimes are often referred to as AdS or dS, respectively. While de Sitter space is an interesting area of discussion, we will only discuss anti-de Sitter space in this review. By contracting Eq. 2.1 with $g_{\mu\nu}$ and setting $\mathcal{T}_{\mu\nu} = 0$, the relation $\mathcal{R} = 4\Lambda$ is obtained [17]. Therefore, we can state that AdS is a maximally symmetric spacetime with $\Lambda < 0$.

AdS has a complicated geometrical structure. For this reason there are many different coordinate systems one can use to help uncover useful information. We start by considering the embedding of $d+1$ dimensional AdS, or AdS_{d+1}, into a higher dimensional space. The most intuitive case is the embedding of AdS_{d+1} into a $d+2$ dimensional psuedo-Riemannian manifold with two time-like coordinates, denoted $\mathbb{R}^{2,d}$. The metric of $\mathbb{R}^{2,d}$ is given by

$$ds^2 = -{dx_0}^2 + {dx_1}^2 + ... + {dx_d}^2 - {dx_{d+1}}^2 \tag{2.2}$$

where x_0 and x_{d+1} are timelike coordinates, x_i are spacelike coordinates with $i \in (1, 2, ..., d)$ and $x_\mu \in \mathbb{R}^{2,d}$. AdS_{d+1} is then given by the hyperboloid

$$-{x_0}^2 + {x_1}^2 + ... + {x_d}^2 - {x_{d+1}}^2 = -R_{\mathrm{AdS}}^2 \tag{2.3}$$

where R_{AdS} is the radius of curvature of AdS [8]. We now proceed with a coordinate transformation such that the new coordinates cover the full range of the AdS_{d+1} hypersurface. The new coordinates (τ, ρ, Ω_i), where $i \in (1, 2, ..., d)$, are related to the coordinates of $\mathbb{R}^{2,d}$ by

$$\begin{aligned} x_0 &= R_{\mathrm{AdS}} \cosh(\rho) \cos(\tau), \\ x_i &= R_{\mathrm{AdS}} \sinh(\rho)\, \Omega_i, \\ x_{d+1} &= R_{\mathrm{AdS}} \cosh(\rho) \sin(\tau), \end{aligned} \tag{2.4}$$

where $\rho \in \mathbb{R}_{\geq 0}$, $\tau \in [0, 2\pi)$ and Ω_i are the coordinates of the d sphere. Substituting the coordinates of Eq. 2.4 into Eq. 2.2, we obtain the metric

$$ds^2 = R_{\mathrm{AdS}}^2(-\cosh^2(\rho)d\tau^2 + d\rho^2 + \sinh^2(\rho)d\Omega_{d-1}^2) \tag{2.5}$$

under the condition that $\Omega^i\Omega_i = 1$ [8].

A key feature of Eq. 2.4 is that τ appears to be a periodic coordinate with an identification of the points 0 and 2π. Taking the limit $\rho \ll 1$, where we obtain $\cosh^2(\rho) \simeq 1$ and $\sinh^2(\rho) \simeq \rho^2$, we see that Eq. 2.5 is a metric with the topology $S^1 \times \mathbb{R}^d$, where we identify the coordinate τ with S^1. Thus, as Eq. 2.5 suggests τ is a timelike coordinate, AdS manifests closed timelike curves. From the perspective of causality, this is a problem as the future and past lightcones of causal observers overlap. To bypass this property of AdS, the identification of the τ coordinate must be removed. This is accomplished by extending the range of τ to $\tau \in (-\infty, \infty)$, meaning there are no closed timelike curves. The spacetime described by Eq. 2.5 with the new range of τ is referred to as

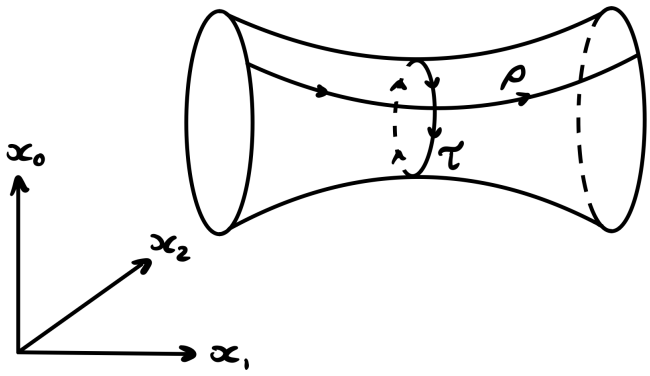

Figure 2.1: The geometry of AdS_2 embedded into $\mathbb{R}^{2,1}$ [8]. In this visualisation, it is clear to see the closed timelike curves which wrap around the hyperboloid.

the universal cover of AdS, denoted $\widetilde{\text{AdS}}$ [18]. Another coordinate transformation is given by the relation $\sinh(\rho) = \tan(\theta)$ with $\theta \in [0, \frac{\pi}{2})$, or $\theta \in (-\frac{\pi}{2}, \frac{\pi}{2})$ for the special case of AdS_2. This allows us to rewrite Eq. 2.5 as

$$ds^2 = \frac{R^2_{\text{AdS}}}{\cos^2(\theta)}(-d\tau^2 + d\theta^2 + \sin^2(\theta)d\Omega^2{}_{d-1}), \tag{2.6}$$

which is a very useful expression of the metric as we can easily perform a conformal compactification of AdS [18]. Before discussing this in more detail, we note a useful parametrisation (τ, r', ψ, ϕ) of AdS_4 given by

$$\begin{aligned}
x_0 &= \sqrt{R^2_{\text{AdS}} + r'^2}\sin\left(\frac{\tau}{R_{\text{AdS}}}\right), \\
x_1 &= r'\cos(\psi), \\
x_2 &= r'\sin(\psi)\cos(\phi), \\
x_3 &= r'\sin(\psi)\sin(\phi), \\
x_4 &= \sqrt{R^2_{\text{AdS}} + r'^2}\cos\left(\frac{\tau}{R_{\text{AdS}}}\right).
\end{aligned} \tag{2.7}$$

Inserting Eq. 2.7 into Eq. 2.2, one obtains the metric

$$ds^2 = -\left(1 + \frac{r'^2}{R^2_{\text{AdS}}}\right)d\tau^2 + \left(1 + \frac{r'^2}{R^2_{\text{AdS}}}\right)^{-1} dr'^2 + r'^2 d\Omega_2{}^2 \tag{2.8}$$

where $d\Omega_2^2 = d\psi^2 + \sin^2(\psi)d\phi^2$ [17]. It is clear to see the similarities between the form of the metric in Eq. 2.8 and the Schwarzschild metric, with the obvious difference being the lack of an event horizon in AdS_4. We will see later that this form of the metric is useful for constructing black hole solutions in AdS_4.

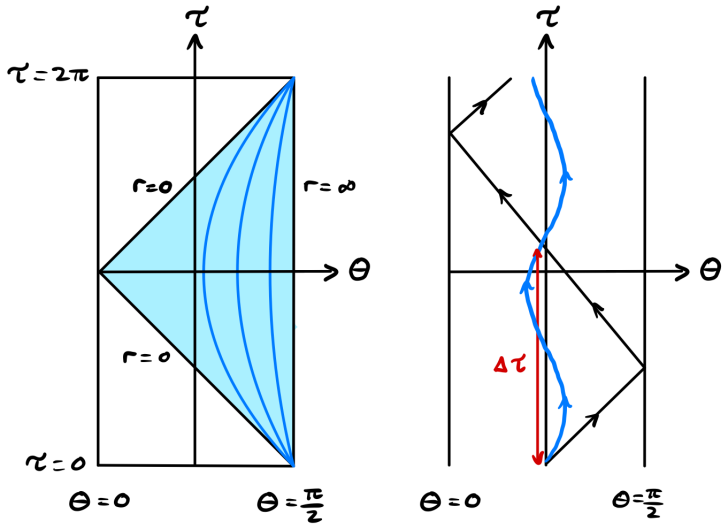

Figure 2.2: Left: Conformally compactified AdS_{d+1}. The Poincaré patch is given by the triangular region, where the blue lines are lines of constant r and the two singularities are shown [8]. Right: Conformally compactified $\widetilde{\mathrm{AdS}}_{d+1}$. Null radial geodesics are given by black lines, while timelike radial geodesics are given by blue lines [19]. Each point on both diagrams is an S^{d-1} sphere.

It is useful to determine the causal structure of the full AdS spacetime in order to understand the boundary structure and the motion of particles. First, we must perform a conformal compactification of AdS_{d+1}. To conformally compactify this spacetime, we use a Weyl transformation to remove the conformal factor, giving the metric

$$ds^2 = -d\tau^2 + d\theta^2 + \sin^2(\theta) d\Omega_{d-1}^2. \tag{2.9}$$

Eq. 2.9 is known as the Einstein static universe, which has the topology $\mathbb{R} \times S^d$ [18]. The origin of AdS in these coordinates corresponds to $\theta = 0$ ($\rho = 0$), while spatial infinity corresponds to $\theta = \frac{\pi}{2}$ ($\rho = \infty$). Following this, we choose to include the point $\theta = \frac{\pi}{2}$ as part of this manifold, which corresponds to what is known as the conformal boundary of AdS. With these conditions, it is clear to see that the conformal boundary of AdS_{d+1}, denoted $\partial\mathrm{AdS}_{d+1}$ with topology $\mathbb{R} \times S^{d-1}$, is equivalent to Minkowski spacetime in d dimensions, $\mathbb{M}^{1,d-1}$ [8]. This will become important later in the discussion of AdS/CFT. An interesting property of Eq. 2.6 and Eq. 2.9 is that radial null geodesics are represented by straight lines with unit gradient [19]; this will be discussed later. The Penrose diagrams of conformally compactified AdS_{d+1} and $\widetilde{\mathrm{AdS}}_{d+1}$ are given in figure 2.2,where each point on these diagrams is a S^{d-1} sphere of radius $\sin(\theta)$. Another common visualisation of conformally compactified AdS is obtained by rotating the spacetimes of figure 2.2 around $\theta = 0$ forming a solid cylinder. These Penrose diagrams are shown in fig 2.3.

We can now go one step further and understand the geometry of the region $0 \leq \theta < \frac{\pi}{2}$, also

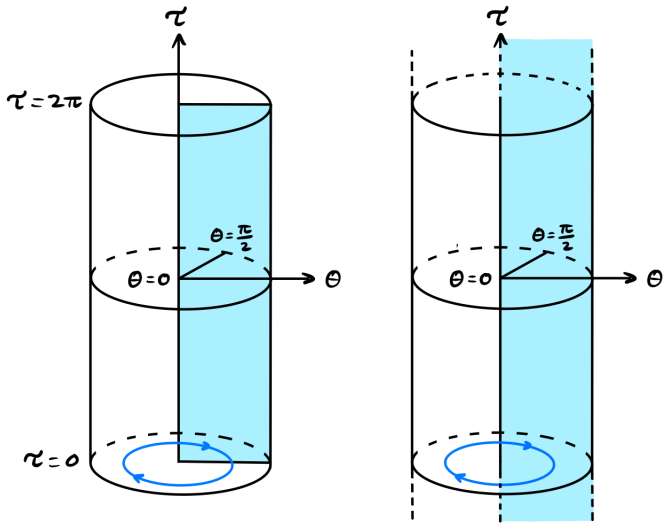

Figure 2.3: Alternative visualisation of conformally compactified AdS_{d+1} and $\widetilde{\mathrm{AdS}}_{d+1}$, where the blue regions are the respective diagrams from figure 2.2 [18]

known as the bulk of AdS. Consider Eq. 2.3 for $d = 2$

$$-{x_0}^2 + {x_1}^2 + {x_2}^2 - {x_3}^2 = -R^2_{\mathrm{AdS}}. \tag{2.10}$$

By considering the surface $x_0 = 0$, we find that Eq. 2.10 becomes a the two dimensional hyperbolic (Lobachevsky) plane, H^2. It is well understood that the hyperbolic plane can be projected onto a disk of finite size called the Poincaré disk [19]. The metric of the Poincaré disk is given by

$$d{s_p}^2 = d{r_p}^2 + {r_p}^2 d{\Omega_1}^2 \tag{2.11}$$

By performing a simple coordinate transformation

$$r_p = R_{AdS}\frac{\sinh(\rho)}{1+\cosh(\rho)}, \tag{2.12}$$

Eq. 2.11 becomes [19]

$$d{s_p}^2 = \frac{R^2_{\mathrm{AdS}}}{(1+\cosh(\rho))^2}(d\rho^2 + \sinh^2(\rho) d{\Omega_1}^2). \tag{2.13}$$

Comparing this metric with a constant τ slice of Eq. 2.5 for $d = 2$. we see that there exists a Weyl transformation between the Poincaré disk and the hyperbolic plane. Therefore, we can see that the full conformally compactified AdS_3, i.e. the bulk and conformal boundary, is given by Poincaré disks stacked in the τ direction. We see that the topology of $\partial\widetilde{\mathrm{AdS}}_3$ is $\mathbb{R} \times S^1$, so to generalise to AdS_{d+1} we simply state that the topology of $\partial\widetilde{\mathrm{AdS}}_{d+1}$ to $\mathbb{R} \times S^{d-1}$, as can be seen from Eq. 2.9

[19]. This is equivalent to stating that AdS_{d+1} is a tower of constant τ spatial sections which are identical to the d dimensional hyperbolic space, H^d.

The full symmetry group of AdS_{d+1} is determined in a similar way to the symmetry group of S^2, i.e. the 2-sphere. S^2 can be embedded into three dimensional Euclidean space, $\mathbb{R}^3$. This has a similar metric to Eq. 2.2 with $d = 2$, apart from having a completely positive metric signature, i.e. diag$(+,+,+)$. We can define the symmetry group of S^2 as the group of rotations that leaves the metric of $\mathbb{R}^3$ invariant. This symmetry group is called the special orthogonal group, $SO(3)$. Therefore, we can immediately see that by embedding AdS_{d+1} into $\mathbb{R}^{2,d}$ as before, the symmetry group of AdS_{d+1} is $SO(2,d)$, the group of rotations that leaves the the metric in Eq. 2.2 invariant [19]. To determine the boundary symmetries, we introduce a new set of coordinates $(T, r, \vec{X})$ called the Poincaré coordinates, given by the parametrisation

$$\begin{aligned} x_0 &= \frac{R^2_{\mathrm{AdS}}}{2r}\left(1 + \frac{r^2}{R^4_{\mathrm{AdS}}}(\vec{X}^2 - T^2 + R^2_{\mathrm{AdS}})\right), \\ x_i &= \frac{rX_i}{R_{\mathrm{AdS}}}, \\ x_d &= \frac{R^2_{\mathrm{AdS}}}{2r}\left(1 + \frac{r^2}{R^4_{\mathrm{AdS}}}(\vec{X}^2 - T^2 - R^2_{\mathrm{AdS}})\right), \\ x_{d+1} &= \frac{rT}{R_{\mathrm{AdS}}}. \end{aligned} \tag{2.14}$$

Here, $i \in 1, ..., d-1$, $T \in \mathbb{R}$, $r \in \mathbb{R}_{>0}$ and $\vec{X} = (X_1, ..., X_d - 1) \in \mathbb{R}^{d-1}$. As $r \in \mathbb{R}_{>0}$, the Poincaré coordinates only cover half of the full AdS_{d+1} spacetime as shown in fig 2.2. For this reason, these coordinates are sometimes called the Poincaré patch [8]. Substituting Eq. 2.14 into Eq. 2.2 gives the metric

$$ds^2 = \frac{R^2_{\mathrm{AdS}}}{r^2}dr^2 + \frac{r^2}{R^2_{\mathrm{AdS}}}(\eta_{\mu\nu}dX^\mu dX^\nu), \tag{2.15}$$

where $X_\mu = (T, \vec{X})$ and $\eta_{\mu\nu}$ is the Minkowski metric. We can immediately see the presence of two singularities at $r \to 0$ and $r \to \infty$, with the former being a coordinate singularity and the latter being a curvature singularity. The $r \to 0$ singularity is called the Poincaré horizon. This horizon separates the $r > 0$ Poincaré patch and the $r < 0$ Poincaré patch, which together cover the full AdS_{d+1} spacetime [8]. It is easy to see that the metric of Eq. 2.15 is invariant under $ISO(1, d-2)$, the Poincaré symmetry group and $SO(1,1)$, the scale symmetry group which acts on the coordinates as $T \to \lambda T$, $\vec{X} \to \lambda\vec{X}$ and $r \to \lambda^{-1}r$ [18]. For further convenience, we can define a new coordinate $z = L^2 r^{-1}$ such that Eq. 2.15 becomes

$$ds^2 = \frac{R^2_{\mathrm{AdS}}}{z^2}(dz^2 + \eta_{\mu\nu}dX^\mu dX^\nu). \tag{2.16}$$

We can see that on the conformal boundary at $z = 0$ [8], the Poincaré symmetry is manifest. A useful concept in AdS/CFT is to consider Euclidean AdS. This is achieved by performing a wick rotation of the T coordinate, i.e. $T \to iX_0$, which gives us the Euclidean AdS metric [7]

$$ds^2 = \frac{R_{\text{AdS}}^2}{z^2}(dz^2 + {dX_0}^2 + d\vec{X}^2). \tag{2.17}$$

We will see in section 2.3 that this form of the metric is used to determine the relation between states on either side of the AdS/CFT correspondence.

The last interesting property of AdS is the fate of future directed curves. First, let's consider a particle of mass $m > 0$ moving along a timelike geodesic in AdS. By setting $d\Omega_{d-1}^2 = 0$ in Eq. 2.6 and read off the Lagrangian as

$$\mathcal{L} = \frac{R_{\text{AdS}}^2}{\cos^2(\theta)}\left(\left(\frac{d\tau}{d\tau'}\right)^2 - \left(\frac{d\theta}{d\tau'}\right)^2\right) \tag{2.18}$$

where τ' is the proper time. We can determine the equations of motion by solving the Euler-Lagrange equation for τ. Plugging the solution to the Euler-Lagrange equation back into Eq. 2.18, we obtain

$$\frac{d\theta}{d\tau'} = \pm\sqrt{1 - \frac{1}{c^2 R_{\text{AdS}}^2 \cos^2(\theta)}}, \tag{2.19}$$

which once integrated uncovers the relation

$$\theta(\tau') = \sin^{-1}\left(\sqrt{1 - \frac{1}{|cR_{\text{AdS}}|^2}}\right)\sin(\tau' - \tau_0'). \tag{2.20}$$

We can see that θ is sinusoidal in τ' and more importantly, the value of the inverse sine function is restricted to the range $[0, \frac{\pi}{2})$. Therefore, the maximum value of $\theta(\tau')$ less than $\frac{\pi}{2}$ for the full range of τ', i.e. a massive particle can never reach the boundary of AdS in finite time [19]. Now, let's consider how this differs from the case for a massless particle. For a null radial geodesic $d\Omega_{d-1}^2 = 0$ and $ds^2 = 0$, so we have the very simple formula $d\theta = d\tau$. Therefore, if a massless particle is sent on a radial trajectory from $\theta = 0$ to $\theta = \frac{\pi}{2}$ and then back to $\theta = 0$, an observer at $\theta = 0$ would calculate the time taken for this journey as

$$\Delta\tau' = \frac{2R_{\text{AdS}}}{\cos(0)}\Delta\theta, \tag{2.21}$$

where $\Delta\theta$ is the distance travelled by the massless particle on the outgoing journey. Therefore, by plugging in $\Delta\theta = \frac{\pi}{2}$, we obtain

$$\Delta\tau' = R_{\text{AdS}}\pi. \tag{2.22}$$

Therefore, a massless particle can be sent on a radial trajectory outwards towards the conformal boundary at infinity, reach the boundary and return back to its origin in finite time [19]. This is different to the massive particle case and we will see that this plays a very important role in the thermodynamics of black holes in AdS.

2.2 Conformal Field Theories

The starting point for a quantum field theory is to specifiy the action, which encodes the full dynamics of the system. The symmetries of the system will restrict the form of the action and therefore, the equations of motion. In AdS/CFT, a specific set of quantum field theories called conformal field theories, or CFTs, is considered. We will start by considering a classical field theory which is invariant under transformaitons of the conformal group. The conformal group is defined as the group of transformations that preserve the metric up to a Weyl scaling factor, $\Omega^2(x) > 0$, as given by [20]

$$g_{\mu\nu}(x) \to g'_{\mu\nu}(x') = \Omega^2(x) g_{\mu\nu}(x). \tag{2.23}$$

In other words, conformal transformations leave the angles at each point of the spacetime invariant, preserving causal structure of the full spacetime [8]. Considering the infinitesimal transformation $x^\mu \to x'^\mu = x^\mu + \xi^\mu(x)$, we see that $g_{\mu\nu}$ transforms as

$$g_{\mu\nu}(x) \to g'_{\mu\nu}(x') = \frac{\partial x^{\mu'}}{\partial x'^{\mu}} \frac{\partial x^{\nu'}}{\partial x'^{\nu}} g_{\mu'\nu'}(x) = (\delta^{\mu'}{}_{\mu} - \partial_\mu \xi^{\mu'})(\delta^{\nu'}{}_{\nu} - \partial_\nu \xi^{\nu'}) g_{\mu'\nu'}(x), \tag{2.24}$$

which to leading order in ξ is

$$g'_{\mu\nu}(x') = g_{\mu\nu}(x) - 2\partial_{(\mu}\xi_{\nu)}. \tag{2.25}$$

Therefore, in order for Eq. 2.25 to be consistent with Eq. 2.23 we require that

$$2\partial_{(\mu}\xi_{\nu)} = f(x) g_{\mu\nu}(x) \tag{2.26}$$

where $f(x)$ is a function related to the infinitesimal expansion of $\Omega^2(x)$ [20]. Now, considering $g_{\mu\nu} = \eta_{\mu\nu}$ with $\mu, \nu \in (0, ..., d-1)$, we contract both sides with the metric and find

$$2\partial_\sigma \xi^\sigma = f(x)d \tag{2.27}$$

for a d dimensional spacetime. After some simple algebra, we see that ξ must satisfy

$$(\eta_{\mu\nu}\partial_\sigma\partial^\sigma + (d-2)\partial_\mu\partial_\nu)\partial_\rho\xi^\rho = 0 \tag{2.28}$$

in order for the transformation to be conformal. For $d > 2$, we see that the most general solution to Eq. 2.28 is second order in x^μ, i.e. [8]

$$\xi^\mu(x) = a^\mu + \omega^\mu{}_\nu x^\nu + \lambda x^\mu + b^\mu x_\sigma x^\sigma - 2b^\sigma x_\sigma x^\mu. \tag{2.29}$$

Here, we have the usual translations and Lorentz transformations given by a^μ and $\omega^\mu{}_\nu$, respectively. In addition to these, we also have two new transformations, λ and b^μ [8]. The transformations given by λ are called dilations, or dilatations, whose finite transformation scales a coordinate as

$$x^\mu \to x'^\mu = \lambda x^\mu. \tag{2.30}$$

The transformations given by b^μ and are called the special conformal transformations. A finite special conformal transformation acts on a coordinate as

$$x^\mu \to x'^{\mu'} = \frac{x^{\mu'} + b^{\mu'} x_\sigma x^\sigma}{1 + 2b_\mu x^\mu + b_\sigma b^\sigma x_\rho x^\rho}. \tag{2.31}$$

The generators of these infinitesimal parameters form the conformal algebra, of which the commutation relations are given by the Poincaré commutation relations and

$$\begin{aligned}
&[M_{\mu\nu}, K_\sigma] = i(\eta_{\nu\sigma}K_\mu - \eta_{\mu\sigma}K_\nu),\\
&[K_\mu, K_\nu] = 0,\\
&[K_\mu, P_\nu] = -2i(\eta_{\mu\nu}D - M_{\mu\nu}),\\
&[D, P_\mu] = iP_\mu,\\
&[D, K_\mu] = -iK_\mu,\\
&[D, M_{\mu\nu}] = 0,
\end{aligned} \tag{2.32}$$

where P_μ, $M_{\mu\nu}$, K_μ and D are the generators of translations, Lorentz transformations, special conformal transformations and dilations, respectively [8]. Immediately, we see that for vanishing D and K_μ, the relations of Eq. 2.32 equal zero, so we recover the Poincaré group. However for non-vanishing D and K_μ, we can combine all four generators into a single matrix given by

$$\widetilde{J}_{AB} = \begin{pmatrix} M_{\mu\nu} & J_{\mu(d)} & J_{\mu(d+1)} \\ -J_{\nu(d)} & 0 & D \\ -J_{\nu(d+1)} & -D & 0 \end{pmatrix} \tag{2.33}$$

where $A, B \in (0, ..., d+1)$ and

$$\begin{aligned} J_{\mu(d)} &= \frac{K_\mu - P_\mu}{2}, \\ J_{\mu(d+1)} &= \frac{K_\mu + P_\mu}{2}, \\ J_{d(d+1)} &= D. \end{aligned} \tag{2.34}$$

The algebra of which $\widetilde{J}$ obeys the algebra of $SO(2,d)$, the conformal group [18]. Therefore, any field theory that is invariant under $SO(2,d)$ transformations is a conformally invariant. It is important to note that the existence of Poincaré and scale symmetry does not make a theory conformally invariant, as the theory must also display special conformal symmetry. However in the majority of cases, scale invariant theories naturally displays special conformal invariance. Therefore, as is usually the case in the literature, we will assume that the combination of Poincaré and scale symmetry is equivalent to conformal symmetry [21].

To understand how conformal symmetries restrict the dynamics of a field theory, we must first determine the irreducible representations of $SO(2,d)$ and how these act on classical fields. Let's consider a scalar field $\Phi(x)$. The action of translation and Lorentz generators on Φ are given by [8]

$$\begin{aligned} \widetilde{P_\mu}\Phi(x) &= [P_\mu, \Phi(x)] = -i\partial_\mu \Phi(x), \\ \widetilde{M_{\mu\nu}}\Phi(x) &= [M_{\mu\nu}, \Phi(x)] = -S_{\mu\nu}\Phi(x) + (x_\nu P_\mu - x_\mu P_\nu)\Phi(x). \end{aligned} \tag{2.35}$$

To proceed, we consider the action of transformations on $\Phi(0)$ such that $x = 0$ remains invariant. This subgroup of the conformal group excludes P_μ as this changes the x coordinate, leaving only $M_{\mu\nu}$, K_μ and D. Taking $x = 0$ in the equation for $M_{\mu\nu}$ in Eq. 2.35 we obtain

$$\widetilde{M_{\mu\nu}}\Phi(0) = -S_{\mu\nu}\Phi(0). \tag{2.36}$$

where $S_{\mu\nu}$ determines the spin of the field at $x = 0$. In a similar manner to $M_{\mu\nu}$, we present the commutation relation for D as [8]

$$\widetilde{D}\Phi(0) = -i\Delta\Phi(0). \tag{2.37}$$

where Δ is the scaling dimension of the field. This suggests that tnder the finite coordinate transformation in Eq. 2.30, Φ transforms as [8, 18]

$$\Phi(x) \to \Phi'(x') = \lambda^{-\Delta}\Phi(x). \tag{2.38}$$

The action of D is to introduce the scaling dimension into the system as shown in Eq. 2.37. Let's consider the action of P_μ and K_μ on the scaling dimension of a field at $x = 0$. From Eq. 2.32 and Eq. 2.37 we have [18]

$$\widetilde{D}(\widetilde{P}_\mu\Phi(0)) = [\widetilde{D}, \widetilde{P}_\mu]\Phi(0) + \widetilde{P}_\mu(\widetilde{D}\Phi(0)) = i(\Delta + 1)\widetilde{P_\mu}\Phi(0) \tag{2.39}$$

and similarly,

$$\widetilde{D}(\widetilde{K_\mu}\Phi(0)) = [\widetilde{D}, \widetilde{K}_\mu]\Phi(0) + \widetilde{K}_\mu(\widetilde{D}\Phi(0)) = i(\Delta - 1)\widetilde{K_\mu}\Phi(0). \tag{2.40}$$

Here, we have assumed that $\widetilde{P_\mu}$, $\widetilde{K_\mu}$ (the special conformal transformation analogue of Eqs. 2.35 & 2.37) and $\widetilde{D}$ obey the respective commutation relations of Eq. 2.32. In fact, $\widetilde{M_{\mu\nu}}$ along with the aformentioned generators, form a representation of the conformal algebra [8]. Therefore, Eq. 2.32 remains valid when $M_{\mu\nu}$, P_μ, K_μ and D are replaced by $\widetilde{M_{\mu\nu}}$, $\widetilde{P_\mu}$, $\widetilde{K_\mu}$ and $\widetilde{D}$, respectively. From Eqs. 2.39 and 2.40, we can see that $\widetilde{P_\mu}$ increases the scaling dimension of Φ by one and $\widetilde{K_\mu}$ decreases the scaling dimension of Φ by one [18]. Given the action of $\widetilde{K_\mu}$ on the scaling dimension, one might expect a lower bound on Δ. This is indeed the case and is given by

$$\Delta \geq \frac{d-2}{2} \tag{2.41}$$

for a d dimensional field theory [8]. Therefore, we can state that a primary field is one whose scaling dimension is equal to this lower bound. We can also define the primary operator, an operator with the minimum value of Δ. Using primary fields, one can construct all other fields by acting on Φ with P_μ, or equivalently by acting on Φ with ∂_μ. These fields are called the conformal descendents of Φ [8]. W define the action of K_μ on a primary field at $x = 0$ as

$$\widetilde{K}_\mu\Phi(0) = [K_\mu, \Phi(0)] = 0, \tag{2.42}$$

where we say that Φ has been annihilated by K_μ. However, we want to understand how $\widetilde{K_\mu}$ and $\widetilde{D}$ act on fields for arbitrary x. Therefore, we use the translation operator to act on Φ as

$$\Phi(0) \to \Phi(x) = e^{-ix^\mu P_\mu}\Phi(0)e^{ix^\mu P_\mu}. \tag{2.43}$$

We can use this expression to find

$$\begin{aligned}\widetilde{K_\mu}\Phi(x) &= (-2x^\nu S_{\mu\nu} + i(-x^\nu x_\nu \partial_\mu + 2x_\mu \Delta + 2x_\mu x^\nu \partial_\nu))\Phi(x),\\ \widetilde{D}\Phi(x) &= -i(\Delta + x^\mu \partial_\mu)\Phi(x)\end{aligned} \tag{2.44}$$

which together with Eq. 2.35 show how the all the generators of the conformal group act on a scalar field [8].

Now we have discussed conformal symmetry at the classical level, we shall now move on to quantum field theories that possess conformal symmetry, i.e, conformal field theories. Consider a classical field theory with scale invariance, which is quantised in the usual way by upgrading the field to operators. Typically, the scale invariance does not remain after quantisation due to the presence of a renormalisation scale, μ. For a simple renormalisation procedure, one introduces a cut-off and bare parameters such as couplings and masses. The renormalised couplings and masses are then determined and usually depend on μ, in addition to the bare parameters and cut-off. Therefore, the coupling depends on the scale of the theory, meaning that a scale invariant quantum field theory is not well defined in this case. Therefore, a renormalised quantum field theory with scale invariance must be independent of μ or equivalently, must have a vanishing beta function, β. This places restrictions on the dynamics of a scale invariant, or conformally invariant quantum field theory [18]. We start by considering the two-point correlation function of fields ϕ_1 and ϕ_2, given by

$$\langle \Phi_1(x)\Phi_2(y)\rangle = \frac{\int [\mathcal{D}\Phi]\, \Phi_1(x)\Phi_2(y)e^{i\int dt \mathcal{L}[\Phi]}}{\int [\mathcal{D}\Phi]\, e^{i\int dt \mathcal{L}[\Phi]}}, \tag{2.45}$$

where $\mathcal{L}$ is a conformally invariant lagrangian [20]. To see how this two-point function transforms under conformal transformations, we must consider how it transforms under Poincaré, scale and special conformal transformations individually. We recall that Poincaré invariance restricts the form of he two-point function to

$$\langle \Phi_1(x)\Phi_2(y)\rangle = \langle \Phi_1(x+a)\Phi_2(y+a)\rangle \tag{2.46}$$

as can be seen by introducing translation operators appropriately. From this we obtain the restricted from of the two-point function, given by

$$\langle \Phi_1(x)\Phi_2(y)\rangle = f(|x-y|) \tag{2.47}$$

where we see that the two-point function only depends the seperation of the fields. Performing a scale transformation on Eq. 2.45 leads to

$$\langle \Phi_1(x)\Phi_2(y)\rangle \to \langle \Phi_1'(x')\Phi_2'(y')\rangle = \frac{\int [\mathcal{D}\Phi']\, \Phi_1'(x')\Phi_2'(y') e^{i\int dt \mathcal{L}[\Phi]}}{\int [\mathcal{D}\Phi']\, e^{i\int dt \mathcal{L}[\Phi]}}. \tag{2.48}$$

Using Eq. 2.38, we can now write

$$\langle \Phi_1'(x')\Phi_2'(y')\rangle = \lambda^{-(\Delta_1+\Delta_2)} \frac{\int [\mathcal{D}\Phi(\tilde{x})]\, \Phi_1(x)\Phi_2(y) e^{i\int dt \mathcal{L}[\Phi(\tilde{x})]}}{\int [\mathcal{D}\Phi(\tilde{x})]\, e^{i\int dt \mathcal{L}[\Phi(\tilde{x})]}} \tag{2.49}$$

where we identify the term on the right as Eq. 2.45 multiplied by a factor. Thus, we can rearrange to find

$$\langle \Phi_1(x)\Phi_2(y)\rangle = \lambda^{\Delta_1+\Delta_2} \langle \Phi_1'(x')\Phi_2'(y')\rangle . \tag{2.50}$$

By comparing Eqs. 2.47 and 2.50, we can see that for a scale invariant quantum field theory, the two-point function must be restricted to [20]

$$\langle \Phi_1(x)\Phi_2(y)\rangle = \frac{C_{\Phi_1\Phi_2}}{|x-y|^{\Delta_1+\Delta_2}}. \tag{2.51}$$

where $C_{\Phi_1\Phi_2}$ is a constant. Finally, while we won't go through the details here, we note that the special conformal transformations impose the additional constraint on the two-point function $\Delta_1 = \Delta_2$ [20]. Therefore, the two-point correlation function for a conformal field theory is given by the expression

$$\langle \Phi_1(x)\Phi_2(y)\rangle = \frac{C_{\Phi_1\Phi_2}}{|x-y|^{2\Delta_1}} \tag{2.52}$$

where $\Delta_1 = \Delta_2$. This is a highly restricted form, highlighting the contraints imposed on the dynamics of a conformal field theory. One can go further with similar arguments and determine the three-point correlation function, given by [20]

$$\langle \Phi_1(x)\Phi_2(y)\Phi_3(z)\rangle = \frac{C_{\Phi_1\Phi_2\Phi_3}}{|x_1-x_2|^{\Delta_1+\Delta_2-\Delta_3}|x_2-x_3|^{\Delta_2+\Delta_3-\Delta_1}|x_3-x_1|^{\Delta_3+\Delta_1-\Delta_2}}. \tag{2.53}$$

An important example of a conformal field theory is $\mathcal{N} = 4$ Super Yang-Mills theory in 4 dimensions. Explicit details of this theory will be given in section 2.3, but we can state that the beta function $\beta = 0$ and so the theory is scale invariant at the quantum level. However, as we have discussed previously, invariance under special conformal transformations is also required to be classified as a conformal field theory. For $\mathcal{N} = 4$ Super Yang-Mills theory in 4 dimensions, we find that this is true and so it is a CFT [18].

2.3 AdS/CFT

As stated in the previously, AdS/CFT is a framework that relates theories of gravity in asymptotically AdS_{d+1} with CFTs in d dimensions. One might be rightfully speculative, as a connection between two such theories seems highly unlikely for many reasons. For example, AdS/CFT is a direct relation between gravity and quantum theory, two theories which notoriously do not combine easily. Additionally, each theory exists in a different number of dimesions, making the correspondence even less clear. These difficulties are summarised by the fact that there is no formal proof for AdS/CFT. However, the conjecture is widely believed to be true and there exist many examples where AdS/CFT holds [7]. The most famous example of AdS/CFT connects $\mathcal{N} = 4$ Super Yang-Mills theory in 4 dimensions and type IIB string theory compactified on $\text{AdS}_5 \times S^5$ [22]. In this section, we will provide a brief overview of these theories and identify the properties which allows the connection between them to arise.

The CFT considered in this correspondence is $\mathcal{N} = 4$ Super Yang-Mills in 4 dimensions, a maximally supersymmetric quantum field theory with the gauge group $SU(N)$. The lagrangian of this theory can be obtained by performing a dimensional reduction on $\mathcal{N} = 1$ Super Yang-Mills in 10 dimensions. In its most useful form, the lagrangian of $\mathcal{N} = 4$ Super Yang-Mills in 4 dimensions is given by

$$\begin{aligned}\mathcal{L}_{SYM} = Tr\Bigg(&-\frac{1}{2g_{YM}^2}F_{\mu\nu}F^{\mu\nu} + \frac{\theta}{16\pi^2}F_{\mu\nu}\tilde{F}^{\mu\nu} - i\sum_a \bar{\lambda}^a\bar{\sigma}^\mu D_\mu\lambda_a - \sum_i D_\mu\phi^i D^\mu\phi^i \\ &+ g_{YM}\sum_{a,b,i} C_i^{ab}\lambda_a[\phi^i,\lambda_b] + g_{YM}\sum_{a,b,i}\bar{C}_{abi}\bar{\lambda}^a[\phi^i,\bar{\lambda}^b] + \frac{g_{YM}^2}{2}\sum_{i,j}[\phi^i,\phi^j]^2\Bigg),\end{aligned} \tag{2.54}$$

where g_{YM} is the Yang-Mills coupling, $F_{\mu\nu}(\tilde{F}_{\mu\nu}$ is the (dual) field strength tensor, θ is called the instanton angle, λ^a ($\bar{\lambda}^a$) are left (right) handed weyl fermions with $a \in (1,..,4)$, ϕ^i are real scalar fields with $i \in (1,...,6)$ and C_i^{ab} are related to a six dimensional generalisation of the pauli matrices. Therefore, we see that there are 6 scalar fields, 4 fermion fields and 1 gauge field, all

of which transform in the adjoint representation of $SU(N)$ [8, 23]. The lagrangian is invariant under $\mathcal{N} = 4$ Poincaré supersymmetry and scale symmetry. Therefore, the theory displays what is known at superconformal symmetry, given by the supergroup $SU(2,2|4)$ [23]. The generators of this group obey the superconformal algebra, a supersymmetric extension of the conformal algebra discussed in section 2.2 [8]. This algebra combines the generators of the conformal algebra with the fermionic supercharges Q^a_α and S^a_α, where $a \in (1, ..., 4)$, in addition to their adjoints $\bar{Q}_{a\dot{\alpha}}$ and $\bar{S}_{a\dot{\alpha}}$. The Q^a_α and $\bar{Q}_{a\dot{\alpha}}$ supercharges arise directly from the Poincaré supersymmetry, while the S^a_α and $\bar{S}_{a\dot{\alpha}}$ supercharges arise due to the fact that the special conformal generators and the generators of Poincaré supersymmetry have a non-vanishing commutator. The anti-commutation relations of the fermionic algebra are given by

$$\begin{aligned}
&\{Q^a_\alpha, Q^b_\beta\} = \{S_{\alpha a}, S_{\beta b}\} = \{Q^a_\alpha, \bar{S}^b_{\dot{\beta}}\} = 0, \\
&\{Q^a_\alpha, \bar{Q}^b_{\dot{\beta}}\} = 2\sigma^\mu_{\alpha\dot{\beta}} P_\mu \delta^a_b, \\
&\{S_{\alpha a}, \bar{S}^b_{\dot{\beta}}\} = 2\sigma^\mu_{\alpha\dot{\beta}} K_\mu \delta^b_a, \\
&\{Q^a_\alpha, S_{\beta b}\} = \epsilon_{\alpha\beta}(\delta^a_b D + T^a_b) + \frac{1}{2}\delta^a_b M_{\mu\nu}\sigma^{\mu\nu}_{\alpha\beta}.
\end{aligned} \tag{2.55}$$

where $\epsilon_{\alpha\beta}$ is the Levi-Civita tensor [23]. We also see the introduction of T^a_b, the components of the R-symmetry generators T^A, where $A \in (1, ..., 15)$. These generate the group $SO(6)_R$ and act by performing a global rotation of a supercharge into a different supercharge [8, 23]. Extending the idea of a primary operator from section 2.2, it is possible to define a superconformal primary operator. In analogy with equations 2.40 and 2.42, one can see from the relation between S^a_α and K_μ, the action of S^a_α changes the dimension of an operator by $-\frac{1}{2}$. Subsequently, S^a_α annihilates a superconformal primary operator as shown by [23]

$$[S^a_\alpha, \mathcal{O}] = 0. \tag{2.56}$$

Continuation of this analogy suggests that we can construct all other operators by acting with the generator that changes the dimension of an operator by $+\frac{1}{2}$. We can see that there exists a relation between Q^a_α and P_μ, which belongs to the super-Poincaré algebra. Therefore, we can construct the superconformal descendent operators, $\tilde{\mathcal{O}}$ using Q^a_α via the equation

$$\tilde{\mathcal{O}} = [Q^a_\alpha, \mathcal{O}], \tag{2.57}$$

where $\Delta_{\tilde{\mathcal{O}}} = \Delta_{\mathcal{O}} + \frac{1}{2}$ [23]. The superconformal primary fields of $\mathcal{N} = 4$ Super Yang-Mills theory are constructed from the fields of Eq. 2.54 and have the property that they are invariant under

the $SU(N)$ gauge group. Simple operators are constructed by taking the trace of the product of these fields. One such important example is

$$\mathcal{O}(x) = \text{Str}\left(\phi^{i_1}(x)\phi^{i_1}(x)...\phi^{i_m}(x)\right), \tag{2.58}$$

where Str means that the trace is fully symmetrised and $\phi^i = \phi^{ia}T_a$ transforms in the adjoint representation of $SO(6)_R$ [8]. In other words, we take Eq. 2.58 and sum over all permutations of the indices. Furthermore, we can construct multi-trace operators by taking the product of single-trace operators like the type in Eq. 2.58 [8]. We have stated that the gauge group of $\mathcal{N} = 4$ Super Yang-Mills is $SU(N)$. We now consider the effect of taking $N \to \infty$ on a general Yang-Mills theory with gauge group $SU(N)$. The beta function for such a theory is given by

$$\mu\frac{dg_{YM}}{d\mu} = -\frac{11}{3}N\frac{g_{YM}^3}{16\pi^2} + ..., \tag{2.59}$$

so the first term, and also higher order terms, remain the same in the $N \to \infty$ if one keeps the combination $\lambda = g_{YM}^2 N$ fixed [22]. This is the 't Hooft limit. Let's further generalise to a theory which contains fields in the adjoint representation of $SU(N)$, ϕ_i^a, where a is an $SU(N)$ index and i is a general index that depends on the type of field considered. The Lagrangian of this theory, omitting terms that don't affect our analysis, is given by

$$\mathcal{L} \sim \frac{1}{g_{YM}^2}\left(Tr(\partial_\mu\tilde{\phi}\partial^\mu\tilde{\phi}) + c^{ijk}Tr(\tilde{\phi}_i\tilde{\phi}_j\tilde{\phi}_k) + d^{ijkl}Tr(\tilde{\phi}_i\tilde{\phi}_j\tilde{\phi}_k\tilde{\phi}_l)\right) + ..., \tag{2.60}$$

where c^{ijk} and d^{ijkl} are constants and $\tilde{\phi}_i = g_{YM}\phi_i$ are the rescaled fields, where the a indices have been suppressed for convenience [22]. The Feynman diagrams for the interactions of this theory are given in double-line notation, where the propagator for an adjoint field is equivalent to the propagator of a fundamental anti-fundamental pair. By considering the orientation of each line, one can compactify the Feynman diagrams and obtain compact surfaces with a topology that depends on the interaction. It can be shown that the coefficient for a diagram with V vertices, E propagators and F loops is of the order $N^\chi\lambda^{E-V}$ [22]. Here, $\chi = V - E + F = 2 - 2g$ is the Euler number. In the large N limit, diagrams with $\chi > 0$ will dominate, while diagrams with $\chi \leq 0$ will be suppressed. The diagrams which dominate for large N are called planar diagrams. We can identify this diagramatic expansion with the Feynman diagrams obtained in string theory. Therefore, this analysis suggests that there exists a relation between Yang-Mills theory and string theories [22]. It is important to note that this argument also holds for $\mathcal{N} = 4$ Super Yang-Mills, suggesting that there exists a dual string theory. However, we have yet to determine the details of

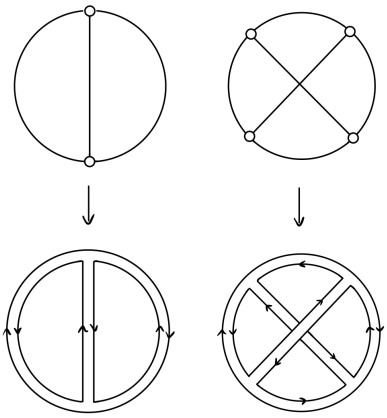

Figure 2.4: Feynman diagrams of adjoint fields at the top, where the lines represent the propagation of the adjoint fields and the circles represent the interaction vertices. These diagrams are converted to double-line notation underneath, whose topology can be identified with string interaction diagrams. Left: The Euler number of the diagram is $\chi = 2$. Right: The Euler number of the diagram is $\chi = 0$ [22].

this string theory, which we discuss in the remainder of this section.

On the other side of the correspondence we have type IIB string theory. There are two consistent superstring theories in ten dimensions that are based on closed strings, namely type IIA string theory and type IIB string theory. While these theories are very similar, they differ by how they change under spacetime parity transformations which can be seen by analysing the massless closed string spectrum. For the case of type IIA, there exists states that transform in the **8**, **8**', **56** and **56**' representations of the $SO(8)$ group. A spacetime parity transformation has the effect of interchanging **8** with **8**' and **56** with **56**', leaving the string spectrum invariant under these transformations and making type IIA string theory achiral [24]. Conversely, in type IIB string theory there are no **8**' or **56** representations of the $SO(8)$ group. Therefore, the theory is not invariant under spacetime parity transformations and so we say that the type IIB string theory is chiral [24]. At low energies, type IIB string theory can be described by type IIB supergravity. The bosonic part of the type IIB supergravity action is given by

$$\begin{aligned} S_{SG} = \frac{1}{(2\pi)^7 \alpha'^4 {g_s}^2} \Bigg(\int d^{10}X \sqrt{-\det(g_{mn})} \Bigg(e^{-2\varphi} \left(\mathcal{R} + 4\partial_m \varphi \partial^m \varphi - \frac{1}{2} |H_{(3)}|^2 \right) \\ - \frac{1}{2} |F_{(1)}|^2 - \frac{1}{2} |\tilde{F}_{(3)}|^2 - \frac{1}{2} |\tilde{F}_{(5)}|^2 \Bigg) - \frac{1}{2} \int C_{(4)} \wedge H_{(3)} \wedge F_{(3)} \Bigg) \end{aligned} \tag{2.61}$$

where X are the coordinates of the worldsheet, α' is related to the length of the string, g_s is the string coupling constant, φ is the dilaton, $m, n \in (0, ..., 9)$ and the field strength tensors are given

by

$$\begin{aligned} H_{(3)} &= dB_{(2)}, \\ F_{(q)} &= dC_{(q-1)}, \\ \tilde{F}_{(3)} &= F_{(3)} - C_{(0)}H_{(3)}, \\ \tilde{F}_{(5)} &= F_{(5)} - \frac{1}{2}C_{(2)} \wedge H_{(3)} + \frac{1}{2}B_{(2)} \wedge F_{(3)}, \end{aligned} \tag{2.62}$$

where $B_{(2)}$ is the totally antisymmetric Kalb-Ramond field and $C_{(q-1)}$ is totally antisymmetric tensor [8]. Furthermore, we have the self dual condition $\star F_{(5)} = F_{(5)}$ and the shorthand

$$|M_{(q)}|^2 = \frac{1}{q!} g_{m_1 n_1} ... g_{m_q n_q} \tilde{M}^{m_1 n_1} ... M^{m_q n_q}, \tag{2.63}$$

for a general field strength tensor M, where $\tilde{M}$ is the complex conjugate of M [8]. An important property of type IIB supergravity is the presence of unique transformations that lead to the concept of dualities. There are two such types, namely T-duality and S-duality. T-duality, also known as target space duality, is the term to describe the physical equivalence of two superstring theories, each compactified on different spacetime manifolds. For example, for a superstring theory with only closed strings and one of the nine spatial dimensions compactified on S^1, one can determine the string spectrum and find the string masses to be [8]

$$M^2 = \left(\frac{wR}{\alpha'}\right)^2 + \left(\frac{n}{R}\right)^2 + \frac{2}{\alpha'}(N + \tilde{N} - 2), \tag{2.64}$$

where w the winding number, i.e. how many times the closed string is wrapped around the compactified coordinate, n is the momentum number related to the quantisation of momentum in the direction of the compactified cordinate, N and $\tilde{N}$ are related to the occupation number of states and R is the radius of S^1. It is easy to notice that by replacing R with $\frac{\alpha'}{R}$ and simultaneously exchanging w and n, we obtain the return to the same expression in Eq. 2.64 [8]. Therefore, we see that the mass spectrum is equivalent for two superstring theories, one with a spatial dimension compactified on S^1 with radius R and the other with a spatial dimension compactified on S^1 with radius $\frac{\alpha'}{R}$. S-duality, also known as strong-weak duality, is the term to describe the map between weak and strong couplings in a superstring theory, in a similar way to the mapping of compactified dimensions in T-duality [8]. The action of type IIB supergravity, given in Eq. 2.61, is invariant under $SL(2, \mathbb{R})$ transformations. By considering a complex field τ with $Im[\tau] = e^{-\varphi}$, we can

express Eq. 2.61 in such a way that it is invariant under $SL(2,\mathbb{R})$ transformations given by

$$\begin{pmatrix} a & b \\ c & d \end{pmatrix} \in SL(2,\mathbb{R}), \tag{2.65}$$

where $ad - bc = 1$. This acts on τ as [18]

$$\tau \to \tau' = \frac{a\tau + b}{c\tau + d}. \tag{2.66}$$

Upon quantisation, type IIB supergravity becomes invariant under a subgroup of $SL(2,\mathbb{R})$ transformations. Within this subgroup is the transformation given by Eq. 2.65 with $a = d = 0$ and $c = -b = 1$. Therefore, the transformation of τ in Eq. 2.66 becomes

$$\tau \to \tau' = -\frac{1}{\tau}. \tag{2.67}$$

If τ has no real component then we have $\varphi \to \varphi' = -\varphi$, or equivalently via the relation $g_s = e^{\varphi}$,

$$g_s \to {g_s}' = \frac{1}{g_s}. \tag{2.68}$$

Therfore, we can say that there is an equivalence between the weak and strong coupling regimes of type IIB supergravity [18, 8]. We can also consider the role of D-branes, or Dirichlet-branes, which are objects on which the ends of open strings can end to satisfy boundary conditions. It is understood that D-branes are dynamical objects and so it is possible to understand the dynamics of p dimensional D-branes, or Dp-branes, from the p dimensional generalisation of the Polyakov action. This is given by

$$S = -T_p \int d^{p+1}\xi \sqrt{-h}, \tag{2.69}$$

where T_p is the tension of the p-brane and h is the induced metric on the worldvolume (or the pull-back of the metric), given by

$$h = \det\left(\frac{\partial X^\mu}{\partial \xi^a}\frac{\partial X^\nu}{\partial \xi^b} g_{\mu\nu}\right) \tag{2.70}$$

where $\mu, \nu, a, b \in (0, ..., p)$ [18]. Of central importance is the interaction of closed strings with Dp-branes. Consider the action which couples a Dp-brane to $g_{\mu\nu}$ and the antisymmetric tensor $B_{\mu\nu}$, given by

$$S = -T_p \int d^{p+1}\xi \sqrt{-\det\left(\partial_a X^\mu \partial_b X^\nu (g_{\mu\nu} + \alpha' B_{\mu\nu})\right)}. \tag{2.71}$$

For the case of $B_{\mu\nu} = 0$ and $g_{\mu\nu}(X) = \eta_{\mu\nu} + 2\kappa h_{\mu\nu}(X)$, expanding the determinant gives the scalar-graviton action

$$S = -T_p \int d^{p+1}\xi \left(T_p + \frac{1}{2}\partial^a \vec{\phi} \partial_a \vec{\phi} + 2\kappa \sqrt{T_p} h_{ai} \partial^a \phi^i + ... \right), \tag{2.72}$$

where the action has reparametrisation invariance, such that we can write $X^a = \xi^a$ for $a \in (0, ..., p)$ [18]. Therefore, we have $\phi^i(\xi^a) = X^i(\xi^a)\sqrt{T_p}$ for $a \in (p+1, ..., d-1)$ where d is the dimension of spacetime, i.e. $d - (p+1)$ scalar fields confined to the worldvolume of the Dp-brane. We can see from the third term in Eq. 2.72 that there are interactions of $h_{ai}(X)$, a closed string that can exist at an arbitrary point in spacetime, with $\phi^i(\xi^a)$, an open string mode confined to the Dp-brane. We can interpret this interaction in the following way [18]: a closed string makes contact with a Dp-brane, which in turn excites an open string mode on the Dp-brane causing the brane to vibrate . Furthermore, we can introduce the dilaton field, φ, by multiplying the integrand of Eq. 2.71 by $e^{-\varphi}$ [18]. Let's also consider the existence of other fields on the Dp-brane worldvolume. One such example is described by the Dirac-Born-Infeld action for electromagnetism, given by

$$S = -T_p \int d^{p+1}\xi \, e^{-\varphi} \sqrt{-\det\left(\partial_a X^\mu \partial_b X^\nu (g_{\mu\nu} + \alpha' B_{\mu\nu}) + 2\pi\alpha' F_{ab}\right)}. \tag{2.73}$$

where F_{ab} are the components of the field strength tensor for the $U(1)$ gauge field, A_a, existing on the Dp-brane [8]. By considering Eq. 2.73 with $g_{\mu\nu} = \eta_{\mu\nu}$, vanishing $B_{\mu\nu}$, and expanding the determinant, we obtain [8]

$$S = -(2\pi\alpha')^2 \frac{T_p}{4g_s} \int d^{p+1}\xi \, F_{ab} F^{ab}. \tag{2.74}$$

Therefore, we can see that the Dirac-Born-Infeld action for a Dp-brane reduces to an expression that can be described by Yang-Mills theory. Note, the tension of the Dp-brane, T_p, is given by

$$T_p = (2\pi)^{-p} \alpha'^{-\frac{(p+1)}{2}}. \tag{2.75}$$

From this, we can define the Yang-Mills coupling constant to be

$$g_{YM}^2 = g_s (2\pi)^{p-2} (\alpha')^{\frac{p-3}{2}} \tag{2.76}$$

where we have inserted Eq. 2.75 into the Dirac-Born-Infeld equation given by Eq. 2.74 [8]. To see that this is the correct way to define the Yang-Mills coupling, consider two seperate systems of interacting open strings, where each system has the coupling constant g_{YM}. By 'fusing' these systems together at the ends of each string, one forms a single system of interacting closed strings

with coupling g_s. From this, we can intuitively see the relation $g_{YM}^2 \sim g_s$ [18]. Furthermore, we can consider N coincident Dp-branes, a system of N Dp-branes such that different ends of open strings can attach to different Dp-branes. While we will omit the details, it can be shown that such

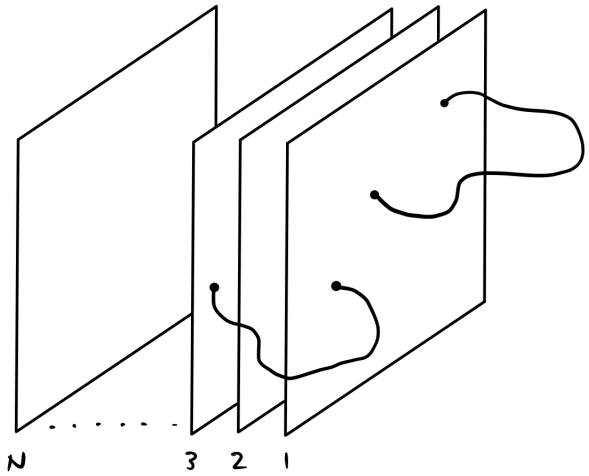

Figure 2.5: N coincident Dp-branes, where we see that it is possible for open strings to end on different branes [22].

a system can be described by a $U(N)$ gauge theory, a simple generalisation of the single Dp-brane case [8].

We are starting to see a potential link between Yang-Mills gauge theories and string theories. However, we need to be more precise and determine further details about these two theories. While so far we have limited the discussion of Dp-branes to bosonic string theory, the main discussion for AdS/CFT surrounds D3-branes in type IIB supergravity. For the case of D3-branes, we find that the worldvolume contains 6 scalar fields, 4 fermions, and 1 gauge field, all of which transform in the adjoint representation of $U(N)$ [18]. It turns out that in this case, one can equivalently consider the gauge group $SU(N)$ [8]. Therefore, as these are the same fields that we discussed for $\mathcal{N} = 4$ Super Yang-Mills, we can conclude that the gauge theory on N coincident D3-branes is equivalent to $\mathcal{N} = 4$ Super Yang-Mills in 4 dimensions with gauge group $SU(N)$ [18]. Furthermore, we have the property that Dp-branes curve spacetime. For type IIB supergravity, the relevant part of the solution for a D3-brane are given by

$$\begin{aligned} ds^2 &= \left(1 + \frac{R^4}{r^4}\right)^{-\frac{1}{2}} {dX_B}^2 + \left(1 + \frac{R^4}{r^4}\right)^{\frac{1}{2}} (dr^2 + r^2 d\Omega_5^2), \\ R^4 &= 4\pi g_s N \alpha'^2 \end{aligned} \tag{2.77}$$

where X_B are the coordinates of the D3-brane worldvolume [9]. To analyse this solution, we take the limit $\alpha' \to 0$ (where supergravity is valid) while keeping the quantity $U = \frac{r}{\alpha'}$ fixed. We can rewrite Eq. 2.77 as

$$ds^2 = \alpha' \left(\frac{U^2}{\sqrt{4\pi g_s N}} {dX_B}^2 + \sqrt{4\pi g_s N} \frac{dU^2}{U^2} + \sqrt{4\pi g_s N} d\Omega_5^2 \right). \tag{2.78}$$

If we also take the 't Hooft limit, i.e. $\lambda = g_{YM}^2 N \sim g_s N$ fixed (by setting $p = 3$ in Eq. 2.76), then we can see that the metric becomes that of $\mathrm{AdS}_5 \times S^5$. [9]. Rearranging the second equation of Eq. 2.77, we obtain the radius of curvature

$$\frac{R^2}{\alpha'} = \sqrt{4\pi g_s N}, \tag{2.79}$$

so we can alternatively say the taking the limit of large λ, i.e. we consider a strongly coupled Yang-Mills theory, we obtain $\mathrm{AdS}_5 \times S^5$ with a large radius of curvature. Therefore, we can now state that in the large N and λ limit, strongly coupled $\mathcal{N} = 4$ Super Yang-Mills is physically equivalent to classical type IIB supergravity in weakly curved $\mathrm{AdS}_5 \times S^5$ spacetime [8]. We can also relax the condition of large λ, i.e. we move away from the supergravity approximation of type IIB string theory, which combined with the large N limit gives $g_s \ll 1$, i.e. classical type IIB string theory. Therefore, we can state the in the large N limit, $\mathcal{N} = 4$ Super Yang-Mills is physically equivalent to classical type IIB string in $\mathrm{AdS}_5 \times S^5$ spacetime [25]. Furthermore, we can obtain the most general statement of the AdS/CFT correspondence by relaxing the large N limit, alleviating the weak string coupling description and leading to the following conjecture: $\mathcal{N} = 4$ Super Yang-Mills in 4 dimensions is physically equivalent to type IIB string theory on $AdS_5 \times S^5$ [9]. The power of AdS/CFT comes from ability to choose the 't Hooft limit. For example, by choosing $\lambda \gg 1$, we obtain the the weak form of the AdS/CFT correspondence. Here, we have a situation where a highly understood gravitational theory is dual to a strongly coupled CFT, in which calculations are intractable. Therefore, it is possible to use classical type IIB supergravity to compute quantities in strongly coupled $\mathcal{N} = 4$ Super Yang-Mills. Additionally, choosing $\lambda \ll 1$ we obtain a situation where a weakly coupled CFT is dual to a string theory, in which calculations are also difficult. Therefore, we can perform calculations in the weakly coupled $\mathcal{N} = 4$ Super Yang-Mills to obtain quantities in string theory. We can see that by tuning the 't Hooft parameter, it is possible use the AdS/CFT to perform calculations in a dual theory that are otherwise intractable in the original theory [7].

A rather simple check of this correspondence is to compare the symmetries of both theories.

We have discussed that the bosonic symmetry of $\mathcal{N} = 4$ Super Yang-Mills in 4 dimensions are $SO(2,4) \times SO(6)$, which comes from the combination of conformal symmetry and the R-symmetry. In section 2.1, we also stated that the symmetry group of AdS_{d+1} is $SO(2,d)$. Therefore, from Eq. 2.78 we can state that the symmetry group of type IIB string theory in $\mathrm{AdS}_5 \times S^5$ spacetime is also $SO(2,4) \times SO(6)$. Therefore, we see that the symmetries of both theories match [8]. From this argument, we should expect a correspondence between states in the two different theories. First, we must determine exactly where the states of $\mathcal{N} = 4$ Super Yang-Mills exist within AdS_5. In section 2.1, we established that $\partial\mathrm{AdS}_{d+1}$ is equivalent to $\mathbb{M}^{1,d-1}$, d dimensional Minkowski space. Therefore, it is natural to consider that 4 dimesional $\mathcal{N} = 4$ Super Yang-Mills exists on the conformal boundary of AdS_5, as the spacetime here is identical to 4 dimensional Minkowski spacetime [8]. From this, we can see that there must exist a correspondence between field theory states on the conformal boundary of AdS_5 and supergravity states in the bulk of AdS_5 . Consider the Euclidean action of a massive scalar field in AdS_{d+1}

$$S = \int d^d X dz \sqrt{g} (\partial_\rho \phi \partial^\rho \phi + m^2 \phi^2) \tag{2.80}$$

where $g_{\rho\sigma}$ is the metric of AdS in Poincaré coordinates as in Eq. 2.17 and $\phi = \phi(z, X)$ [7]. The equation of motion, determined by varying S with respect to ϕ gives the usual Klein-Gordon equation

$$\frac{1}{\sqrt{g}} \partial_\rho (\sqrt{g} g^{\rho\sigma} \partial_\sigma \phi) - m^2 \phi = 0. \tag{2.81}$$

By substituting the metric components of Eq. 2.17 into Eq. 2.81, one obtains

$$\frac{1}{R^2} (z^2 \partial_z{}^2 + z^2 \partial_X^2 + z(1-d)\partial_z)\phi = m^2 \phi. \tag{2.82}$$

where $\partial_X^2 = \partial_{X_0}^2 + \partial_{\vec{X}}^2$ [26]. As Poincaré symmetry is manifest on ∂AdS in these coordinates, we see that ∂AdS is translation invariant. Therfore, we can transition to fourier space and decompose the solution into radial and boundary parts as $\phi(z, X) = e^{ik_\mu X^\mu} f(k, z)$. Substituting this solution into Eq. 2.82, we arrive at the radial equation [7]

$$\partial_z^2 f(k,z) + \frac{(1-d)}{z} \partial_z f(k,z) - \left(k^2 + \frac{m^2 R^2}{z^2} \right) f(k,z) = 0. \tag{2.83}$$

Given that for $z \to \infty$ the field should decay, we look for the solution to Eq. 2.83 that suppresses $f(k,z)$ at large z. Therefore, we find that the solution to Eq. 2.83 for our boundary conditions is

$$\begin{aligned} f(k,z) &= e^{ikz} z^{\frac{d}{2}} K_\alpha(kz), \\ \alpha &= \sqrt{\frac{d^2}{4} + (mR)^2}, \end{aligned} \tag{2.84}$$

where K_α is the modified Bessel function of the second kind [7]. Considering the $z \to 0$ limit, we find that $f(k,z) \sim z^{d-\Delta}$, where $\Delta = \frac{d}{2} + \alpha$. Therefore, we can put a boundary condition at $z = \epsilon \ll 1$ whereby [26]

$$\phi(\epsilon, X) = \phi_0(X)\epsilon^{d-\Delta}. \tag{2.85}$$

Therefore, we can determine the expression for $\tilde{\phi}(k,z)$ satisfying this boundary condition, which is given by

$$\tilde{\phi}(k,z) = \tilde{\phi_0}(k)\epsilon^{d-\Delta}\frac{f(k,z)}{f(k,\epsilon)}, \tag{2.86}$$

where $\tilde{\phi}$ denotes the Fourier transform of ϕ. Substituting this solution into the action of Eq. 2.80, we can integrate by parts, use the equations of motion, take the limit $\epsilon \to 0$ and transform back to real space to arrive at the important expression [7]

$$S = -\frac{2\alpha\Gamma(\Delta)}{\pi^{\frac{d}{2}}\Gamma(\alpha)} R^{d-1} \int d^dX d^dY \frac{\phi_0(X)\phi_0(Y)}{|X-Y|^{2\Delta}}. \tag{2.87}$$

Therefore, if we consider the partition function of the supergravity theory, $Z_{SG}[\phi_0(X)] = e^{-S_{SG}}$, where the saddle point approximation has been taken due to the classical nature of supergravity, we can determine the two point correlation function of the dual CFT by

$$\begin{aligned} \langle \mathcal{O}(X)\mathcal{O}(Y)\rangle_{CFT} &= \left.\frac{\delta^2 e^{-S_{SG}}}{\delta\phi_0(X)\delta\phi_0(Y)}\right|_{\phi_0=0} \\ &\sim \frac{1}{|X-Y|^{2\Delta}}. \end{aligned} \tag{2.88}$$

We can now draw the conclusion that

$$e^{-S_{SG}} = Z_{CFT}[\phi_0(X)] = \left\langle e^{\int d^dX \phi_0(X)\mathcal{O}(X)} \right\rangle_{CFT} \tag{2.89}$$

from the comparison between Eq. 2.52 and Eq. 2.88 [7]. This allows us to perform calculations in AdS/CFT. We call this the field-operator map, or the AdS/CFT dictionary, for the weak form of the AdS/CFT correspondence. We can also generalise this statement to the strong form of the AdS/CFT correspondence, in which type IIB string theory is the gravitational theory. Therefore,

the field-operator map for the strong form is given by [8]

$$Z_{String}[\phi_0(X)] = \left\langle e^{\int d^d X \phi_0(X)\mathcal{O}(X)} \right\rangle_{CFT}. \tag{2.90}$$

An important point is that while we have used Eq. 2.80 to arrive at this conclusion, these results also hold for the full type IIB supergravity action, obtained by performing a dimensional reduction on the 10 dimensional action in Eq. 2.61 [8]. Note that the term $Z_{string}[\phi_0(X)]$ is used to describe the partition function with the condition that $\phi = \phi_0$ on the conformal boundary [22].

3. Fundemental Aspects of Wormholes

The prediction of wormhole structures in Einstein's General Theory of Relativity has been used as a source of inspiration for many works of science fiction. The standard portrayal is that these seemingly futuristic objects allow the travelling of long distances across the universe, usually in a very short amount of time. It is natural to speculate whether this interpretation of wormholes is indeed correct, or even to question their existence entirely. To answer these questions, we first must describe the details of the first, well established interpretation of a wormhole, the Einstein-Rosen bridge. Following this, we will discuss more general interpretations of wormholes and their properties.

3.1 The Einstein-Rosen Bridge

In 1935, Einstein and Rosen published a paper where they considered a theory of particles which only depends on the metric of spacetime and a vector potential, in the absence of singularities. To remove any singularities, they performed a simple coordinate change to alter the gravitational equations. This gave rise to the following conclusion: physical spacetime is mathematically described by two sheets, which are joined by a geometrical structure called a 'bridge'. The interpretation of this bridge is that it represents a physical particle [27]. This geometrical model does not appear to be correct, however, the concept that two seperate sheets of spacetime are connected by a bridge was not disregarded. The modern interpretation of Einstein and Rosen's idea is that in some coordinate systems, we are concerned about the asympototically flat regions of maximally extended Schwarzschild spacetime [28]. Maximally extended Schwarzschild spacetime is the extension of the Schwarzschild solution to the full spacetime manifold. Taking $G = c = 1$ units, the Schwarzschild solution, in Schwarzschild coordinates (t, r, θ, ϕ), is given by

$$ds^2 = -\left(1 - \frac{2M}{r}\right) dt^2 + \left(1 - \frac{2M}{r}\right)^{-1} dr^2 + r^2 d\Omega_2^2, \tag{3.1}$$

where the $d\Omega_2^2 = d\theta^2 + \sin^2(\theta)d\phi^2$ is the metric on S^2 of unit radius. It is important to note that these coordinates are only defined for the region $r > 2M$. One can write this metric using null coordinates $u = t - r_*$ and $v = t + r_*$, where r_* is the Regge-Wheeler (tortoise) coordinate defined by

$$dr_*^2 = \frac{dr^2}{1 - \frac{2M}{r}}, \tag{3.2}$$

which once integrated gives the expression

$$r_*(r) = r + 2M \ln \left| \frac{r - 2M}{2M} \right|. \tag{3.3}$$

Therefore, using the (u, v, θ, ϕ) coordinates, we can write Eq. 3.1 as

$$ds^2 = -\left(1 - \frac{2M}{r}\right) dudv + r^2 d\Omega_2^2 \tag{3.4}$$

where u and v are implicitly given by $r = \frac{1}{2}(v - u)$. Due to the tortoise coordinate, this coordinate system is not well defined at $r = 2M$. Therefore, we define a new coordinate system, namely the Kruskal-Szekeres coordinates (U, V, θ, ϕ). These coordinates are given by

$$\begin{aligned} U &= -e^{-\frac{u}{4M}}, \\ V &= e^{\frac{v}{4M}} \end{aligned} \tag{3.5}$$

where $U < 0$ and $V > 0$. We also note the important relation

$$\frac{V}{U} = -e^{\frac{t}{2M}}. \tag{3.6}$$

We can now write the Schwarzschild metric in Kruskal-Szekeres coordinates, which gives

$$ds^2 = -\frac{32M^3}{r} e^{-\frac{r}{2M}} dUdV + r^2 d\Omega_2^2 \tag{3.7}$$

where r is given implicitly by

$$UV = -e^{\frac{r}{2M}} \left(\frac{r}{2M} - 1\right). \tag{3.8}$$

From Eqs. 3.7 & 3.8, we see that the singularity at $r = 2M$ has disappeared, meaning that the kruskal coordinates are well defined for $0 < r < \infty$. Furthermore, we can see that the ranges of U and V can be extended to $-\infty < U < \infty$ and $-\infty < V < \infty$. The spacetime diagram of the Schwarzschild solution in Kruskal-Szekeres coordinates, denoted the Kruskal diagram, is shown in figure 3.1. We will refer to the spacetime described by the Kruskal diagram as Kruskal

spacetime. Each point on the Kruskal diagram represents a 2-sphere, i.e. we have suppressed the metric of the 2-sphere and restricted any physics to radial motion. The Schwarzschild coordinates

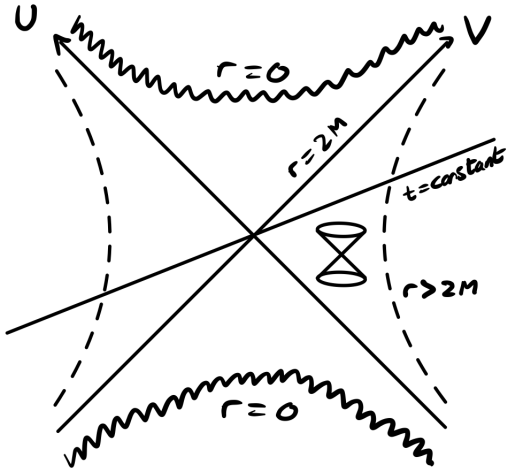

Figure 3.1: The Kruskal diagram with lines of constant r and constant t shown. The jagged lines represent the curvature singularities at $r = 0$. Each point of the diagram corresponds to a 2-sphere.

only cover the $V > 0$ portion of the Kruskal diagram (not including $U = 0$). We see that the region $V > 0$ and $U > 0$ corresponds to the black hole region, while the region $V > 0$ and $U < 0$ corresponds to the exterior of the black hole. Interestingly, the Kruskal diagram gives rise to a new section of spacetime not present in Schwarzschild coordinates. This new section, defined for $V < 0$ is completely isometric to the $V > 0$ region under the transformation $U \to -U$ and $V \to -V$. Therefore, we see that we obtain two new regions The region $U < 0$ and $V < 0$ is called the white hole region, which differs from the black hole region only by the reversal of the coordinates. The consequence of this is that, in contrast to a black hole, a causal observer cannot cross the event horizon from the $r > 2M$ region. Finally, the region $U > 0$ and $V < 0$ is the white hole exterior. The common conception is that the white hole exterior region is indeed a universe of its own. For convenience, we will split these regions of the Kruskal diagram are into 4 regions; top, bottom, left and right. By setting $r = 2M$ in Eq. 3.8, we find $UV = 0$. Therefore, the event horizon at $r = 2M$ in Schwarzschild coordinates corresponds to the surface at $U = 0$ or $V = 0$. We can therefore state that each region of the Kruskal diagram is separated by a horizon. These two horizons at $U = 0$ and $V = 0$ intersect eachother at $U = V = 0$. This point on the Kruskal diagram is called the bifurcation 2-sphere, as it is the only point on the Kruskal diagram that directly joins the left and right regions. It is also referred to as the bifurcate horizon. An important property of the kruskal diagram is that null radial geodesics are given by 45° lines. This can be seen from Eq. 3.7, where setting $ds^2 = 0$ gives one of three results; $dU = 0 \; \forall \; U, V$, $dV = 0 \; \forall \; U, V$ or $dU = 0$ and $dV = 0 \; \forall$

U, V. From this, we also see that light cones remain constant at every point on the diagram, which makes Kruskal coordinates the perfect arena to understand the causal structure. To consider the whole spacetime, we perform a conformal compactification of Kruskal spacetime. To accomplish this, we define two new coordinates

$$\begin{aligned} U &= \tan \tilde{U}, \\ V &= \tan \tilde{V} \end{aligned} \tag{3.9}$$

such that the new finite coordinate ranges are $-\frac{\pi}{2} < U < \frac{\pi}{2}$ and $-\frac{\pi}{2} < V < \frac{\pi}{2}$. Substituting Eq. 3.9 into Eq. 3.7 and performing a necessary Weyl transformation, one obtains the metric for conformally compactified Kruskal spacetime

$$ds^2 = -\frac{32M^3}{r} e^{-\frac{r}{2M}} d\tilde{U} d\tilde{V} + r^2 \cos^2(\tilde{U}) \cos^2(\tilde{V}) d\Omega_2^2. \tag{3.10}$$

where we now add the points at infinity such that the new coordinate ranges are $-\frac{\pi}{2} \leq U \leq \frac{\pi}{2}$ and $-\frac{\pi}{2} \leq V \leq \frac{\pi}{2}$. The diagram of conformally compactified Kruskal spacetime is given in figure 3.2. Here, we have introduced the boundary points $i^{\pm}$, i^0 and $\mathscr{I}^{\pm}$, as well as $\mathcal{H}^+$ and $\mathcal{H}^-$, the future

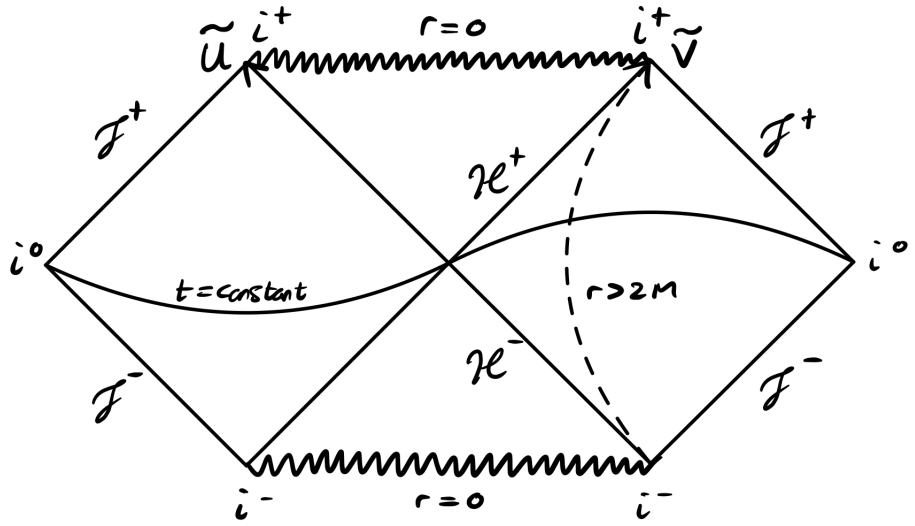

Figure 3.2: Conformally compactified Kruskal spacetime, where we have shown examples of constant t and constant r lines. We have also introduced the notation $\mathcal{H}^+$ and $\mathcal{H}^-$ to denote the future and past event horizons of the black hole exterior, respectively. Once again, each point of the diagram represents a 2-sphere.

and past event horizons of the black hole exterior, respectively. Considering only the right region of the diagram, i^+ labels the point with $\tilde{U} = 0, \tilde{V} = \frac{\pi}{2}$, while i^- labels the point with $\tilde{U} = \frac{\pi}{2}, \tilde{V} = 0$. They correspond to the future and past end points of all timelike curves, respectively. As they label points at infinity, one can see that they are singular points as they coincide with the $r = 0$

singularity. Furthermore, i^0 labels the point $\tilde{U} = -\frac{\pi}{2}, \tilde{V} = \frac{\pi}{2}$, corresponding to the end point of all spacelike curves. This includes the constant time curve shown in figure 3.2. Finally, $\mathscr{J}^+$ labels the points at $-\frac{\pi}{2} < \tilde{U} < 0, \tilde{V} = \frac{\pi}{2}$, while $\mathscr{J}^-$ labels the points at $\tilde{U} = -\frac{\pi}{2}, 0 < \tilde{V} < \frac{\pi}{2}$. One can also define $i^{\pm}$, i^0 and $\mathscr{J}^{\pm}$ for the left region of the diagram. Similarly to the diagram in figure 3.1, the light cones are bounded by 45° lines at each point on the diagram and each point represents a 2-sphere.

In both diagrams, we have shown lines of constant time. From Eq. 3.6 we see that a line of constant time is given by the relation $U = cV$, where c is a constant. Therefore, in the Kruskal diagram, lines of constant time are straight lines through the point $U = V = 0$. On the conformally compactified Kruskal diagram, we note that lines of constant time are spacelike curves that end on i^0, as spacelike curves are mapped to spacelike curves by a conformal compactification. In other words, the tangent vector at every point along the curve of constant time is spacelike. Let's investigate the geometry of a line of constant time, now including the coordinates θ and ϕ. One can consider using isotropic coordinates, a valuable method as it does not require one to embed the geometry into a higher dimensional space [29]. However, here we use an embedding technique and consider Schwarzschild coordinates to build a more intuitive picture of the constant time geometry. Consider Eq. 3.1 at a constant time and $\theta = \frac{\pi}{2}$. From this, we obtain

$$ds^2 = \left(1 - \frac{2M}{r}\right)^{-1} dr^2 + r^2 d\phi^2 \tag{3.11}$$

Our approach is to embed this metric into $\mathbb{R}^3$ in cylindrical coordinates (r, ϕ, z). This metric is given by

$$ds^2_{\mathbb{R}^3} = dr^2 + r^2 d\phi^2 + dz^2 = \left(\left(\frac{dz}{dr}\right)^2 + 1\right) dr^2 + r^2 d\phi^2 \tag{3.12}$$

where we have taken $z = z(r)$ [29]. Comparing Eq. 3.11 and Eq. 3.12, we can identify

$$\frac{dz}{dr} = \pm\sqrt{\frac{2M}{r - 2M}} \tag{3.13}$$

where by performing the substitution $y = r - 2M$,we can integrate this expression to obtain

$$z(r) = \pm\sqrt{8M}\sqrt{r - 2M}. \tag{3.14}$$

Rearranging to obtain r, we arrive at the formula

$$r(z) = 2M + \frac{z^2}{8M}. \tag{3.15}$$

We immediately see that there is a symmetry about $z = 0$, at which the value of r is at its minimum value of $r = 2M$, i.e. at the bifurcation 2-sphere. We call this section of the geometry the 'throat'. We also see that as $z \to \pm\infty$, $r \to \infty$. Using Eq. 3.13, $\frac{dz}{dr} \to 0$ and therefore, Eq. 3.12 approaches $\mathbb{R}^2$. Including the ϕ coordinate, we see that the geometry of a line at constant time is that of a double trumpet as shown in figure 3.3 [29]. This is the Einstein-Rosen bridge. We have omitted θ from this discussion by choosing a fix value of θ to examine this geometry. Therefore, the Einstein-Rosen bridge is actually a 3 dimensional subsurface of Kruskal spacetime and every point on the diagram in figure 3.3 is equivalent to S^1. Of course, the Schwarzschild coordinates are only defined for $r > 2M$ and are singular at $r = 2M$. However, we can see that in the limit that $z \to 0$, $r \to 2M$, so we use the knowledge that $r = 2M$ is a coordinate singularity to include this point in our discussion. Furthermore, while the Schwarzschild coordinates are only defined for the top and right regions of the conformally compactified Kruskal diagram, we find that they describe a three dimensional surface in the right and left regions. This can been seen from the following perspective: due to the symmetry about $z = 0$ and the isometry between the right and left regions, we can map the geometry from the right region to the left region and join the two surfaces at the bifurcation 2-sphere. Following our previous discussion of the Kruskal

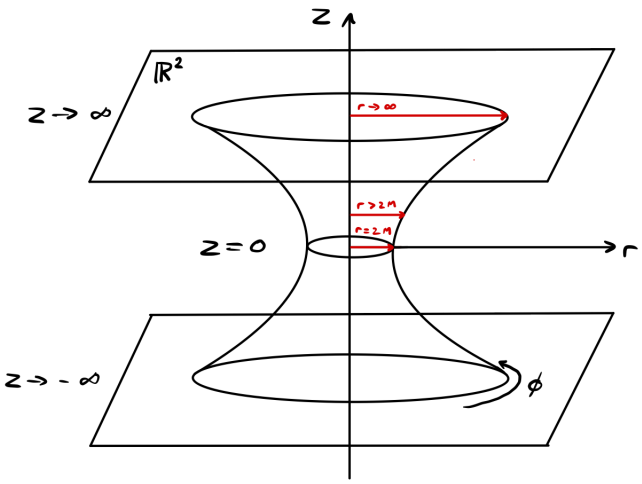

Figure 3.3: The Einstein-Rosen Bridge [29]. The throat of the double trumpet geometry has a minimum value of $r = 2M$ and approaches asymptotically flat space as $z \to \infty$.

diagram, we can note an important point about the Einstein-Rosen bridge. As the Einstein-Rosen bridge is a spacelike surface as time does not pass while remaining on the bridge. Therefore, a causal observer cannot traverse the Einstein-Rosen bridge and cross from the right region to the left region. More specifically, the end point of a causal curve crossing the bifurcate horizon would lie at the singularity, not at a point in the left region.

3.2 The Concept of a Wormhole

The idea of a wormhole floated around the scientific community soon after the announcement of Einstein's general theory of relativity. The first contribution was by Flamm, who was the first to discover the parabolic nature of a wormhole-like structure as shown in equation 3.15 [30]. Following this was the work of Einstein and Rosen, which we discussed in section 3.1. We have seen that the Einstein-Rosen bridge is a geometry that connects the left and right regions of Kruskal spacetime, across which a causal observer cannot travel. We say that this geometrical structure is an example of a non traversable wormhole. While the term wormhole was not used at the time, the Einstein-Rosen bridge is widely regarded as the first example of a wormhole. Although this discovery did not spark any immediate research, there has been a lot of interest in wormholes in the last few decades [28]. In the years following the work of Einstein and Rosen, Wheeler revived the idea of these geometrical structures. He introduced the concept that the physical entity of electric charge is simply a manifestation of the geometry of spacetime coupled with electromagnetism. By considering the Einstein-Maxwell equations, Wheeler determined that electric charge arises from the existence of electric field lines that form closed loops by navigation through a wormhole-like geometry [31]. This idea is depicted in figure 3.4. This concept led Wheeler, alongside Misner, to

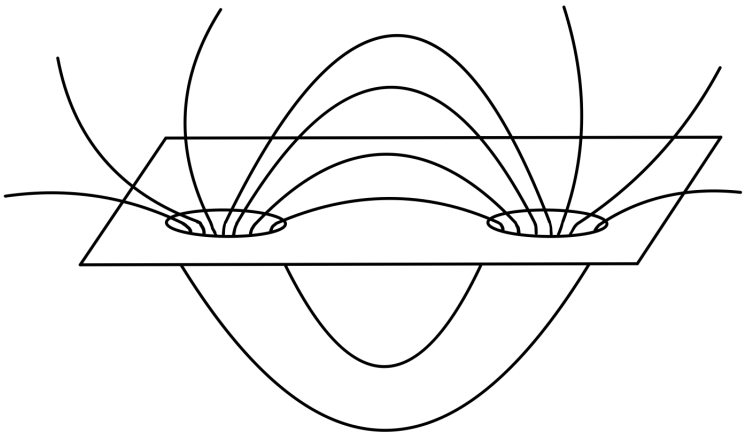

Figure 3.4: A wormhole as depicted by Wheeler. The geometry allows a flux of electric field lines to form closed loops. [31]

propose that all entities of classical physics, i.e. gravitation, electromagnetism, charge and mass, are simply a manifestation of empty curved spacetime [32]. Proceeding these ideas put forth by Wheeler, a paper published by Morris and Thorne explored the possibility of using wormholes for interstellar travel, similar to these seen in works of science fiction. As shown in figure 3.5, these

wormholes create a 'shortcut' through spacetime allowing one to effectively travel long distances in a short amount of time. Morris and Thorne present solutions to the Einstein field equations that could be traversed by causal observers [33]. These solutions omit the traversability issues that are present for the Einstein-Rosen bridge and other non-traversable wormholes. For example, a causal

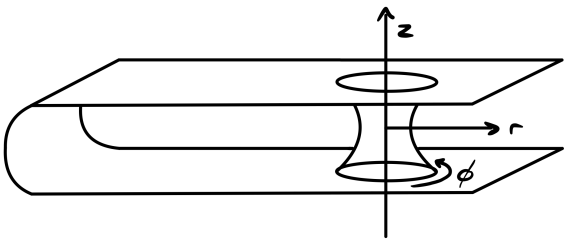

Figure 3.5: An interstellar wormhole as depicted by Morris and Thorne [33]. Spacetime is curved in such a way that two different regions of the same spacetime are connected via a short path.

observer attempting to cross the Einstein-Rosen bridge will cross the event horizon of a black hole and reach the curvature singularity. Therefore, a traversable wormhole should not possess a horizon of any kind, which would prevent travel across the wormhole in at least one direction. Furthermore, the tidal forces acting on a causal observer woul have to be small enough, such that the the journey through the wormhole leaves the observer unharmed [33]. Another obvious point is that an observer must be able to cross the wormhole in finite proper time, otherwise the wormhole does not serve its purpose. Of course, only the Einstein-Rosen bridge is understood to arise naturally. Conversely, traversable wormholes have to be created and sustained. Morris and Thorne discovered that to sustain the wormhole structure, the tension of the throat must be equivalent to the pressure at the centre of neutron stars. Subsequently, the matter necessary to form the wormhole appears to have negative energy density for a sufficiently fast-moving observer. This matter is labelled as 'exotic', as it violates the weak energy condition [33]. Once such a traversable wormhole has been constructed, an observer must be able to pass through without affecting the geometry in such a way that the structure collapses or deformes. Therefore, it is also required that the wormhole geometry must remain stable in the presence of perturbations, either from external objects or from the observer [33]. Perhaps the most important of these conditions to achieve is the violation of the weak energy condition.. Classically this is not possible, however, the discovery of Hawking radiation revealed that quantum fields can violate the weak energy condition [33]. In fact, one can consider the use of the Casimir effect. As the Casimir vacuum violates the weak energy condition, it may be possible to form a wormhole by manipulating such an effect [34]

All of the wormholes that we have considered so far are known as Lorentzian wormholes. These are wormholes which have been created from the deformation of Minkowski space, meaning that the

metric of such a geometrical structure has Lorentzian signature. Having discussed these wormholes, we can see that there are two types: inter-universe wormholes and intra-universe wormholes [28]. The former are wormholes that connect two universes together, which if traversable allow travel or exchange of information between two different universes. The Einstein-Rosen bridge is an example of an inter-universe wormholes and is depicted in figure 3.3. The latter are wormholes that connect two spatially separated points in the same universe. We have seen two different examples of an intra-universe wormholes. The Wheeler wormhole simply allows the flow of electric field lines between two points in spacetime, meaning that these points can interact with eachother as seen in figure 3.4. From a different perspective, we have also seen the Morris and Thorne wormhole which simply allows a causal observer to travel from one point in spacetime to another in a very short amount of time, as shown in figure 3.5. As we will see later, we present recent examples of both inter-unverse and intra-universe wormholes in the context of AdS/CFT. While we have not discussed such wormholes so far, we will also turn our attention to the Euclidean wormholes, a highly active and modern area of research in the realm of AdS/CFT. These wormholes are obtain by performing a wick rotation of the time component of the spacetime from which the wormhole is formed.

4. Quantum Entanglement

Quantum mechanics gives rise to various phenomena of which the properties are very mysterious. One of these phenomena is quantum entanglement, often shortened to entanglement. In this section, we review the basic properties of entanglement and discuss how the famous EPR paradox arises from these properties. We will see that at first glance, entanglement appears to violate the fundamental relativistic property of locality, the inability to send information faster than the speed of light [12]. While we will not provide any formal proof of this in a general case, we will examine the specific situation of quantum teleportation and see that entanglement does not lead to faster than light communication. Of vital importance to our later discussions is the concept of entanglement entropy. Hence, we finish this section by discussing the properties of this quantity and how it measures the entanglement of a system.

4.1 A Review of Entanglement

4.1.1 Entangled States

Let us consider a multipartite system with n subsystems. Classically, the total state of a system is described by the Cartesian product of the individual subsystems [35]. However in quantum mechanics, the total state of the system is a vector in the Hilbert space $\mathcal{H} = \bigotimes_{j=1}^{n} \mathcal{H}_j$, which is a tensor product of the Hilbert spaces of the n individual subsystems. In general, we can use the principle of superposition to write the total state as

$$|\Psi\rangle = \sum_{i_1,\ldots,i_n} \alpha_{i_1 \ldots i_n} |\phi_{i_1}\rangle \otimes |\phi_{i_2}\rangle \otimes \ldots \otimes |\phi_{i_n}\rangle \,, \tag{4.1}$$

where $|\phi_{i_j}\rangle$ is a basis vector which belongs to the Hilbert space of subsystem j, $\mathcal{H}_j$ [35]. In contrast to the classical case, this means that we cannot write $|\Psi\rangle$ as a tensor product of states of

the individual subsystems, i.e it is not possible to write $|\Psi\rangle$ as

$$|\Psi\rangle = |\psi_1\rangle \otimes |\psi_2\rangle \otimes ... \otimes |\psi_n\rangle \,, \tag{4.2}$$

where the j^{th} subsystem is in the state $|\psi_j\rangle$. Therefore, we cannot describe any of the individual subsystems with a single state vector [35]. We say that states of the form in Eq. 4.1 are entangled, while states of the form in Eq. 4.2 are not entangled. In each case, as the total state of the system is known, we call these pure states [36]. In other words, we have complete knowledge of the state and can represent it as a state vector. It is very difficult to understand the dynamics of a multipartite system with large n, so we now restrict our discussion to the simplest situation where $n = 2$, i.e. a bipartite system with particles A and B. Let us further restrict our system such that each subsystem only contains two degress of freedom, i.e. each particle can only exist in one of two states, $|0\rangle$ or $|1\rangle$. Therefore, our Hilbert space is now $\mathcal{H} = \mathcal{H}_A \otimes \mathcal{H}_B$, where $\dim\mathcal{H}_A = \dim\mathcal{H}_B = 2$ [35]. Therefore, the Hilbert space $\mathcal{H}_{A/B}$ is spanned by the two basis vectors, $|0\rangle_{A/B}$ or $|1\rangle_{A/B}$. From these states, one can construct the 4 orthonormal basis vectors of the bipartite Hilbert space $\mathcal{H}$, which are given by

$$\begin{aligned} |\Psi^{\pm}_{AB}\rangle &= \frac{1}{\sqrt{2}} \left(|0\rangle_A \otimes |1\rangle_B \pm |1\rangle_A \otimes |0\rangle_B\right), \\ |\Phi^{\pm}_{AB}\rangle &= \frac{1}{\sqrt{2}} \left(|0\rangle_A \otimes |0\rangle_B \pm |1\rangle_A \otimes |1\rangle_B\right). \end{aligned} \tag{4.3}$$

We call these the Bell states and they form a complete basis of the bipartite Hilbert space $\mathcal{H}$ [35]. A key point of these states is that we cannot describe either of the subsystems individually. In other words, one cannot determine information about subsystem A without disturbing subsystem B and vice versa. It is in this sense that the subsystems are entangled. We will now consider the properties of entanglement of this bipartite system in the context of the EPR paradox.

4.1.2 The EPR Paradox

To understand the EPR paradox, we shall now consider the measurement of spin $\frac{1}{2}$ particles in a bipartite system. Such a system is equivalent to the bipartite system described in section 4.1.1, where we interpret the two degrees of freedom as the two possible spin states, spin $\frac{1}{2}$ (spin up) and spin $-\frac{1}{2}$ (spin down). We denote these states $|\uparrow\rangle$ and $|\downarrow\rangle$, respectively. Let's create a state with a total spin of zero. By the principle of superposition, the state of the bipartite system is given by [37]

$$|\Psi^{-}_{AB}\rangle = \frac{1}{\sqrt{2}} \left(|\uparrow\rangle_A \otimes |\downarrow\rangle_B - |\downarrow\rangle_A \otimes |\uparrow\rangle_B\right). \tag{4.4}$$

We now proceed to move these particles a large distance apart in such a way that does not affect the spin of each particle. Now, if we perform a measurement of the spin of particle A such that the measurement has no effect on particle B, knowing that the total spin of the two particle state is zero, we immediately know the spin of particle B. Classically, there is no issue with the previous statement as the spin of each particle is well defined at all times, regardless of any measurements [37]. However, in a quantum system, Einstein, Rosen and Podolsky (EPR) noted that this statement gives rise to a paradox. Initially, we had no exact knowledge of which spin state particle B was in, only that it could be either $|\uparrow\rangle_A$ or $|\downarrow\rangle_A$ with equal probability. However, by performing a spin measurement on A, we have seemingly gained knowledge of the spin state of particle B without disturbing it. Therefore, EPR stated that the spin of particle B must be a well defined property that is not affected by any measurement. In contrast, the laws of quantum mechanics state that the spin state of particles A and B are ill-defined before measurement [38]. As such, so we arrive at a paradox, namely the EPR paradox. At the time of publishing, EPR's solution was that there exists local hidden variables, or elements of reality, that carry the information that had seemingly travelled faster than the speed of light. However, if one believes the principle of locality is a fundamental property of nature, then this solution is proven incorrect by the violation of the Bell inequalities [38]. Here we note that EPR did not consider the discrete case of spin $\frac{1}{2}$ particles, but considered the continuous variables of position and momentum [39]. However, the outcome of both arguments is the same. In fact, it is not possible to use entanglement to send information faster than the speed of light [12]. We will not provide any formal proof of the principle of locality. However, we will proceed by discussing why locality is not violated in quantum teleportation, a phenomenon which relies entirely on quantum entanglement.

4.1.3 Locality in Quantum Teleportation

Let's consider the scenario whereby observer A wants to send a particle to observer B. The trivial way to accomplish this would be to directly send the particle. However, we shall describe an alternative way of transfering the particle, using the properties of quantum entanglement. Consider a 3 particles system containing particles a, b and c, which is given by [40]

$$|\psi\rangle = |\phi_c\rangle \otimes |\Psi^-_{ab}\rangle \,. \tag{4.5}$$

Here, we see that we have created an entangled state $|\Psi^-_{ab}\rangle$, where particle a belongs to observer A and particle b belongs to observer B. Proceeding this, we introduced a new particle c that is not entangled with $|\Psi^-_{ab}\rangle$, which observer A wishes to send to observer B. To teleport particle

c to observer B, we must entangle the state $|\phi_c\rangle$ with $|\Psi^-_{ab}\rangle$. To do this, observer A performs a measurement on their particles, i.e. on the subsystem containing particles a and c [40]. Let us consider the outcomes of this measurement. If we consider that particle c is also a spin $\frac{1}{2}$ particle, like particles a and b, then we can write

$$|\phi_c\rangle = \alpha\,|\uparrow_c\rangle + \beta\,|\downarrow_c\rangle\,. \tag{4.6}$$

Therefore, the full state of the 3 particle system as a quantum superposition of the 4 possible outcomes of the measurement is [40]

$$\begin{aligned}|\psi\rangle =&\frac{1}{\sqrt{2}}\left(\alpha\,|\uparrow_c\rangle\otimes|\uparrow_a\rangle\otimes|\downarrow_b\rangle - \alpha\,|\uparrow_c\rangle\otimes|\downarrow_a\rangle\otimes|\uparrow_b\rangle\right.\\ &\left.+\beta\,|\downarrow_c\rangle\otimes|\uparrow_a\rangle\otimes|\downarrow_b\rangle - \beta\,|\downarrow_c\rangle\otimes|\downarrow_a\rangle\otimes|\uparrow_b\rangle\right).\end{aligned} \tag{4.7}$$

Now, we can re-write Eq. 4.7 in terms of the newly entangled subsystem containing particles a and c, $|\Psi_{ca}\rangle$. Of course, we see that there are 4 possible states in which observer A may find this subsystem. These are given by the Bell states [40]

$$\begin{aligned}|\Psi^{\pm}_{ca}\rangle &= \frac{1}{\sqrt{2}}\left(|\uparrow_c\rangle\otimes|\downarrow_a\rangle \pm |\downarrow_c\rangle\otimes|\uparrow_a\rangle\right),\\ |\Phi^{\pm}_{ca}\rangle &= \frac{1}{\sqrt{2}}\left(|\uparrow_c\rangle\otimes|\uparrow_a\rangle \pm |\downarrow_c\rangle\otimes|\downarrow_a\rangle\right).\end{aligned} \tag{4.8}$$

Re-writing Eq. 4.7 in terms of these bell states, we find

$$\begin{aligned}|\psi\rangle =&\frac{1}{2}\Big(|\Phi^-_{ca}\rangle\otimes(\alpha\,|\downarrow_b\rangle+\beta\,|\uparrow_b\rangle) + |\Phi^+_{ca}\rangle\otimes(\alpha\,|\downarrow_b\rangle-\beta\,|\uparrow_b\rangle)+\\ &|\Psi^+_{ca}\rangle\otimes(-\alpha\,|\uparrow_b\rangle+\beta\,|\downarrow_b\rangle) - |\Psi^-_{ca}\rangle\otimes(\alpha\,|\uparrow_b\rangle+\beta\,|\downarrow_b\rangle)\Big).\end{aligned} \tag{4.9}$$

Therefore, if observer A performs a measurement, they will find the subsystem of particles a and c to be in one of the bell states with equal probability. Let's say that the after this measurement, $|\psi\rangle$ collapses into the state

$$|\psi\rangle = |\Phi^+_{ca}\rangle\otimes(\alpha\,|\downarrow_b\rangle - \beta\,|\uparrow_b\rangle). \tag{4.10}$$

Observer A will therefore obtain knowledge of the state of particle b. Here we see that the state of particle b differs from that of particle c by the sign of the coefficient β. Therefore, observer A must send a classical message to observer B, informing them to perform a unitary operation on particle b such that the sign of β becomes positive [40]. In doing so, the state of particle b becomes that of Eq. 4.6, meaning that observer A has successfully teleported particle c. If the wavefunction had collapsed into any of the other 3 states, observer A would simply send a different classical message,

directing observer B to perform the relevant unitary operation on particle b such that the state in Eq. 4.6 is obtained. The important point in this example is the use of a classical message to enable this teleportation. While the properties of entanglement are of central importance to this process, the particle was not transferred from one location to another at a speed faster than the speed of light. In a more general sense, we can say that the information of particle c was not transferred faster than the speed of light.

4.2 Measuring Entanglement

4.2.1 The Density Matrix Formalism

In section 4.1.1, we considered pure states. Such states can be expressed by a single state vector. However, we can also use the density matrix formalism to express pure states. The density matrix of a pure state is defined as

$$\rho = |\Psi\rangle \langle\Psi| . \tag{4.11}$$

Taking the trace of this expression we find [36]

$$\mathrm{Tr}(\rho) = \sum_i \langle\Psi_i|\Psi\rangle \langle\Psi|\Psi_i\rangle = \sum_i \langle\Psi|\Psi_i\rangle \langle\Psi_i|\Psi\rangle = \langle\Psi|\Psi\rangle = 1, \tag{4.12}$$

where $|\Psi_i\rangle$ fully span the Hilbert space of the multipartite system, $\mathcal{H}$. Furthermore, we can see that

$$\rho^2 = |\Psi\rangle \langle\Psi|\Psi\rangle \langle\Psi| = \rho, \tag{4.13}$$

so we find the relation [36]

$$\mathrm{Tr}(\rho^2) = \mathrm{Tr}(\rho) = 1. \tag{4.14}$$

However, if we do not have full knowledge of a state, we call this a mixed state. Mixed states cannot be represented by a single state vector, so we must use the density matrix formalism. Let's consider an ensemble of pure states $\{p_i, |\Psi_i\rangle\}$, where p_i is the probability that the quantum state is in the state $|\Psi_i\rangle$ [36]. Using this ensemble, we define the density matrix of a mixed state as

$$\rho = \sum_i p_i |\Psi_i\rangle \langle\Psi_i| = \sum_i p_i \rho_i, \tag{4.15}$$

where we have identified $\rho_i = |\Psi_i\rangle \langle\Psi_i|$ as the density matrix for the i^{th} pure state in the ensemble. We can therefore say that a mixed state is a statistical ensemble, or mixture, of pure states [36].

We can now calculate the trace of the mixed density matrix as

$$\mathrm{Tr}(\rho) = \sum_{i,j} p_i \langle \Psi_j | \Psi_i \rangle \langle \Psi_i | \Psi_j \rangle = \sum_{i,j} p_i \delta_{ji} \delta_{ij} = \sum_i p_i = 1, \tag{4.16}$$

as the probability that the state exists in one of the states in the ensemble is equal to 1. Furthermore, we see that

$$\rho^2 = \sum_{i,j} p_i p_j \left| \Psi_i \right\rangle \langle \Psi_i | \Psi_j \rangle \left\langle \Psi_j \right| = \sum_{i,j} p_i p_j \left| \Psi_i \right\rangle \delta_{ij} \left\langle \Psi_j \right| = \sum_i {p_i}^2 \left| \Psi_i \right\rangle \left\langle \Psi_i \right| \neq \rho. \tag{4.17}$$

Therefore, we can calculate

$$\mathrm{Tr}(\rho^2) = \sum_{i,j} {p_i}^2 \langle \Psi_j | \Psi_i \rangle \langle \Psi_i | \Psi_j \rangle = \sum_{i,j} {p_i}^2 \delta_{ji} \delta_{ij} = \sum_{i,j} {p_i}^2 < 1. \tag{4.18}$$

Here, we note that if $p_k = 1$ and $p_i = 0 \; \forall i \neq k$ then our ensemble reduces to a single state such that our mixed state becomes a pure state. In this case, we find that Eq. 4.18 becomes $\mathrm{Tr}(\rho^2) = p_k^2 = 1$. Therefore, we can see that for all states, the density matrix must obey the conditions $\mathrm{Tr}(\rho) = 1$ and $\mathrm{Tr}(\rho^2) \leq 1$, where pure states satisfy $\mathrm{Tr}(\rho^2) = 1$ and mixed states satisfy $\mathrm{Tr}(\rho^2) < 1$ [36].

4.2.2 Reduced Density Matrices and the Entanglement Entropy

Finally, we discuss how to quantify the degree of entanglement between two systems. For our discussion, the most natural way to measure entanglement is via a quantity called the von Neumann entropy [41]. Let us consider a quantum mechanical system with multiple degrees of freedom, for example a bipartite system. We can describe this system with the wavefunction of Eq. 4.1, where $n = 2$, given by

$$\left| \Psi \right\rangle = \sum_{i,j} \alpha_{ij} \left| \phi_{i,A} \right\rangle \otimes \left| \phi_{j,B} \right\rangle, \tag{4.19}$$

which belongs to the Hilbert space $\mathcal{H}_{AB}$, meaning that our system is in a pure state. Let us also assume that we can split our system into two subsystems, A and B, such that $\mathcal{H}_{AB}$ is decomposed into the tensor product of the Hilbert spaces of the two subsystems. Therefore, we write $\mathcal{H}_{AB} = \mathcal{H}_A \otimes \mathcal{H}_B$, where $\mathcal{H}_A$ and $\mathcal{H}_B$ are the Hilbert spaces of subsytems A and B, respectively. The dynamics of such a system are encoded in the denstiy matrix [42]

$$_{\cdot}\rho_{AB} = \left| \Psi \right\rangle \left\langle \Psi \right| = \sum_{i,j,k,l} \alpha_{ij} \alpha_{kl}^* \left| \phi_{i,A} \right\rangle \left\langle \phi_{k,A} \right| \otimes \left| \phi_{j,B} \right\rangle \left\langle \phi_{l,B} \right|. \tag{4.20}$$

From this, we can compute what is known as the reduced density matrix, which allows us to understand the dynamics of one of the subsystems, A and B. We compute the reduced density marix of subsystem A in the following way [36]

$$\rho_A = \mathrm{Tr}_B(|\psi\rangle\langle\psi|) = \sum_{i,j,k,l} \alpha_{ij}\alpha^*_{kl} |\phi_{i,A}\rangle\langle\phi_{k,A}| \,\mathrm{Tr}(|\phi_{j,B}\rangle\langle\phi_{l,B}|), \tag{4.21}$$

which performing the trace operation gives us [42]

$$\begin{aligned}
\rho_A &= \sum_{i,j,k,l,m} \alpha_{ij}\alpha^*_{kl} |\phi_i\rangle_A \langle\phi_{k,A}| \langle\phi_{m,B}|\phi_{j,B}\rangle \langle\phi_{l,B}|\phi_{m,B}\rangle \\
&= \sum_{i,j,k,l,m} \alpha_{ij}\alpha^*_{kl} |\phi_{i,A}\rangle\langle\phi_{k,A}| \,\delta_{mj}\delta_{lm} \\
&= \sum_{i,j,k} \alpha_{ij}\alpha^*_{kj} |\phi_{i,A}\rangle\langle\phi_{k,A}| \,.
\end{aligned} \tag{4.22}$$

Similarly, we can compute the reduced density matrix of subsytem B as follows

$$\rho_B = \mathrm{Tr}_A(|\psi\rangle\langle\psi|) = \sum_{i,j,k,l} \alpha_{ij}\alpha^*_{kl}\mathrm{Tr}(|\phi_{i,A}\rangle\langle\phi_{k,A}|) |\phi_{j,B}\rangle\langle\phi_{l,B}| \,, \tag{4.23}$$

where taking the traces gives us [42]

$$\begin{aligned}
\rho_B &= \sum_{i,j,k,l,m} \alpha_{ij}\alpha^*_{kl} \langle\phi_{m,A}|\phi_{i,A}\rangle \langle\phi_k|\phi_{m,A}\rangle |\phi_{j,B}\rangle\langle\phi_{l,B}| \\
&= \sum_{i,j,k,l,m} \alpha_{ij}\alpha^*_{kl}\delta_{mi}\delta_{km} |\phi_{j,B}\rangle\langle\phi_{l,B}| \\
&= \sum_{i,j,l} \alpha_{ij}\alpha^*_{il} |\phi_{j,B}\rangle\langle\phi_{l,B}| \,.
\end{aligned} \tag{4.24}$$

Therefore, we have obtained a way to solely describe each of the subsystems individually. Using the reduced density matrices, we can now define the von Neumann entropy for subsystem A as [43]

$$S_A = -\mathrm{Tr}(\rho_A \ln(\rho_A)). \tag{4.25}$$

Similarly, for susbystem B we define

$$S_B = -\mathrm{Tr}(\rho_B \ln(\rho_B)). \tag{4.26}$$

We call the von Neuman entropy of a reduced matrix the entanglement entropy [43]. To understand why we use this quantity to measure the entanglement entropy, we now note some of key properties.

The von Neumann entropy of a state ρ is [44]

$$S_{tot} = -\mathrm{Tr}(\rho \ln \rho) = 0, \tag{4.27}$$

if and only if ρ is a pure state. If ρ is a mixed state, one finds that [44]

$$S_{tot} = -\mathrm{Tr}(\rho \ln \rho) > 0. \tag{4.28}$$

Furthermore, we see for a pure state that the entanglement entropies of each subsystem are equal, i.e. [43]

$$S_A = -\mathrm{Tr}(\rho_A \ln(\rho_A)) = -\mathrm{Tr}(\rho_B \ln(\rho_B)) = S_B. \tag{4.29}$$

From Eq. 4.27, we see that if ρ_A and ρ_B are pure states, then Eq. 4.29 is equal to zero. This means that there is no entangled degrees of freedom between the two subsystems. However, if ρ_A and ρ_B are mixed states, then S_A and S_B are non-zero, meaning that the number of entangled degrees of freedom between subsystems A and B is also non-zero. This allows us to say that a total state is entangled if both subsystems A and B are in mixed states. However, if both subsystems A and B are in pure states, then the total state is not entangled [45]. For example, we see that $|\Psi\rangle$ from Eq. 4.19 is an entangled state, as ρ_A and ρ_B are mixed states of the form in Eq. 4.15. We can also consider the maximum entanglement entropy that a subsystem can have. For a Hilbert space, $\mathcal{H}$ of dimension d, it is possible to determine that the von Neumann entropy is bounded by

$$S \leq \ln(d). \tag{4.30}$$

Here, we have $S = \ln(d)$ if and only if ρ is a maximally mixed state, i.e. a state that is propertional to the identity matrix. Using this, we say that the state ρ_{AB} is maximally entangled if it is pure and the two subsystems ρ_A and ρ_B are maximally mixed [44].

An interesting quantity to consider is the mutual information of ρ_{AB}. Let's consider the von Neumann entropy of the system ρ_{AB}, obtained by the equation [36]

$$S_{AB} = \mathrm{Tr}(\rho_{AB} \ln(\rho_{AB})). \tag{4.31}$$

Using this, we define the mutual information as [44]

$$I_{AB} = S_A + S_B - S_{AB}, \tag{4.32}$$

which is bounded from below by

$$I_{AB} \geq 0. \tag{4.33}$$

Here, we see $I_{AB} = 0$ if and only if $\rho_{AB} = \rho_A \otimes \rho_B$. Mutual information is simply a measure of how much information system A has about system B and vice versa [44]. Let's consider what this means for an entangled system . Let's say that ρ_{AB} is a pure state while the subsystems ρ_A and ρ_B are mixed states. We can immediately see, using Eqs. 4.27, that the von Neumann entropy $S_{AB} = 0$. Furthermore, we can see that $S_A = S_B$ where both entropies are non-zero as ρ_A and ρ_B are mixed states. Therefore, we find

$$I_{AB} = 2S_A, \tag{4.34}$$

so the mutual information of such a system arise purely from entanglement [44].

5. Black Hole Thermodynamics

Among the most successful and funamental laws of physics are the 4 laws of classical thermodynamics. These laws state the following principles [46]: 0th Law - If a body exists in thermal equilibrium, then the temperature T throughout the body must be constant, 1st Law - The change of energy of a system obeys $\Delta E = p\Delta V + T\Delta S$, 2nd Law - The entropy S of a system never decreases moving forward in time, i.e. $\Delta S \geq 0$, 3rd Law - It is not possible to reach the temperature of absolute zero $T = 0K$ in a finite number of processes.

As stated in the introduction, the area theorem states that the area of a black hole never decreases with time, i.e. $\Delta A \geq 0$. We can compare this to the 2nd law of thermodynamics as stated above, showing that the area theorem is the black hole analogue of the 2nd law of classical thermodynamics. From this analogy, we should expect that the three other thermodynamic laws should have black hole counterparts. Indeed, this is the case as we will now discuss [46]. The 0th law states that the surface gravity κ of a stationary black hole is constant over the event horizon. We clearly see here that κ is analogous to T. The 1st law states that the change in mass of a black hole is given by the expression $\kappa\Delta A = 8\pi(\Delta M - \Omega\Delta J)$. Here, we note that the term $-\Omega\Delta J)$ corresponds to $p\Delta V$, the work term of the 1st law of thermodynamics, while we see that ΔA corresponds to ΔS. The 2nd law states that the area of a black hole's event horizon never decreases, i.e. $\Delta A \geq 0$. Here, see that A and S are analogous, c.f. Eq. 1.1. Finally, the 3rd law states that the surface gravity κ cannot be reduced to zero in a finite number of processes. Once again, we see the analogous relation between κ and T.

The analogy between the laws of thermodynamics and the laws of black hole mechanics forms the basis of what is known as black hole thermodynamics. Of course, our discussion until now has been restricted to classical mechanics. We know from Hawking that black holes radiate due to quantum effects, causing the black hole to eventually evaporate. Thus, we see that the black hole counterpart of the 2nd law is violated once quantum mechanics is considered. From this example alone, one might assume that by considering quantum mechanics, that there should be many interesting deviations from the predictions of classical black hole thermodynamics. In this

section, we will consider quantum mechanical effects and discuss the thermodynamic properties Schwarzschild black holes.

5.1 The Rindler Decomposition of Minkowski Spacetime

To understand the dynamics of quantum field theories in AdS-Schwarzschild, we first restrict our discussion to the dynamics in Minkowski spacetime and Schwarzschild spacetime. To proceed, we consider the Rindler decomposition of Minkowski space as shown in figure 5.1. The Rindler coordinates (η, ξ) are given via

$$\begin{aligned} t &= \xi \sinh \eta, \\ x &= \xi \cosh \eta \end{aligned} \tag{5.1}$$

where t and x are the usual coordinates for two dimensional Minkowski spacetime. Then by substitution, the two dimensional Minkowski metric $ds^2 = -dt^2 + dx^2$ becomes

$$ds^2 = -\xi^2 d\eta^2 + d\xi^2. \tag{5.2}$$

where $0 < \xi < \infty$ and $-\infty < \eta < \infty$. As none of the metric components depend on η, we can identify the killing vector ∂_η. Transforming back to Minkowski coordinates, we find that the Killing vector is

$$\partial_\eta = \frac{\partial}{\partial \eta} = \frac{\partial t}{\partial \eta}\frac{\partial}{\partial t} + \frac{\partial x}{\partial \eta}\frac{\partial}{\partial x} = x\partial_t + t\partial_x. \tag{5.3}$$

Therefore, we can see that ∂_η is equivalent to the Killing vector associated with Lorentz boosts in the x direction [47]. Noting that $x^\mu \partial_\mu = \partial_\eta$ and therefore $x^t = x$ and $x^x = t$, we can determine

$$||\partial_\eta||^2 = x^\mu x^\nu g_{\mu\nu} = t^2 - x^2. \tag{5.4}$$

where $g_{\mu\nu}$ is the Minkowski metric. Therefore, we see that ∂_η is timelike in regions where $|x| > |t|$ and spacelike in regions where $|x| < |t|$. Furthermore, we can determine the direction of the orbits of ∂_η directly from Eq. 5.3. The Lorentz boost operator, ζ generates symmetries such that the Killing vector orbits are the same as the orbits of ∂_η, as stated before. This allows us to decompose Minkowski spacetime into four regions, separated by Rindler horizons, where ζ is well-defined: left, right, top and bottom (c.f. Kruskal spacetime) [44]. As before, we note that the Killing vector corresponding to ζ is timelike in the left and right regions where $|x| > |t|$, but spacelike in the top and bottom regions where $|x| < |t|$. Furthermore, from Eq. 5.3, we can determine the direction of

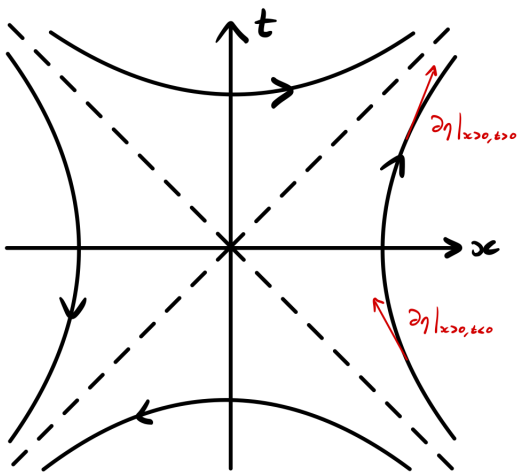

Figure 5.1: The Rindler decomposition of Minkowski spacetime [44]. The dotted lines represent the Rindler horizons, while the curved solid lines represent orbits of the Killing vector, ∂_η. In red, we show specific values of ∂_η.

each orbit using Eq. 5.3. For example, in the right region we have $0 < x < \infty$ and $-\infty < t < \infty$ along an orbit of ∂_η. Therefore, we have

$$\begin{aligned} \partial_\eta|_{x>0,\, t<0} &= |x|\partial_t - |t|\partial_x, \\ \partial_\eta|_{x>0,\, t>0} &= |x|\partial_t + |t|\partial_x, \end{aligned} \tag{5.5}$$

which requires the orbit of ∂_η to be directed forward in time, as depicted in figure 5.1. This prodedure works similarly for the left, top and bottom regions.

We now seek to express the vacuum state in terms of the states $|\phi_L\rangle$ and $|\phi_R\rangle$, the general eigenstates of the Lorentz boost operator in the left and right regions, respectively. Using the Euclidean path integral, we can write the overlap of a state $|\phi\rangle$ with the vacuum as [44]

$$\langle\phi|\Omega\rangle \propto \int_{\Phi(\tau=-\infty)=0}^{\Phi(\tau=0)=\phi} \mathcal{D}\Phi e^{-S_E[\Phi]} \tag{5.6}$$

where the Euclidean action S_E is obtained by taking $t \to -i\tau$ in the original Lorentzian action S [44]. It is also important to note that $\Phi = \Phi(\tau, \vec{x})$ and $\phi = \phi(\vec{x})$. The action of ζ in Minkowski spacetime is to perform hyperbolic rotations, in accordance with its definition. Therefore, by taking time to be imaginary, we see that the action of ζ in the Euclidean spacetime is to perform rotations. Using this property of ζ, we can take the convenient approach whereby we evaluate the path integral along the angle generated by ζ, rather than along the time coordinate generated by the Hamiltonian H [44]. As we are integrating from $\tau = -\infty$ to $\tau = 0$, this corresponds to

the lower half of the Euclidean plane. Therefore, the new integration is evaluated from 0 to π. Therefore, we can re-write our path integral from Eq. 5.6 as

$$\int_{\Phi(\tau=-\infty)=0}^{\Phi(\tau=0)=\phi} \mathcal{D}\Phi e^{-S_E[\Phi]} \xrightarrow{H\to\zeta} \int_{\Phi(\theta=0)=\phi_L}^{\Phi(\theta=\pi)=\phi_R} \mathcal{D}\tilde{\Phi} e^{-\tilde{S}_E[\tilde{\Phi}]}, \tag{5.7}$$

where we have transformed to Rindler coordinates, such that $\tilde{S}_E$ and $\tilde{\Phi}_E$ are the action and fields, respectively, in Rindler coordinates [48]. These two methods of integration are shown in figure 5.2. Therefore, we can see that our integration requires us to decompose $|\phi\rangle$ into fields on the left and

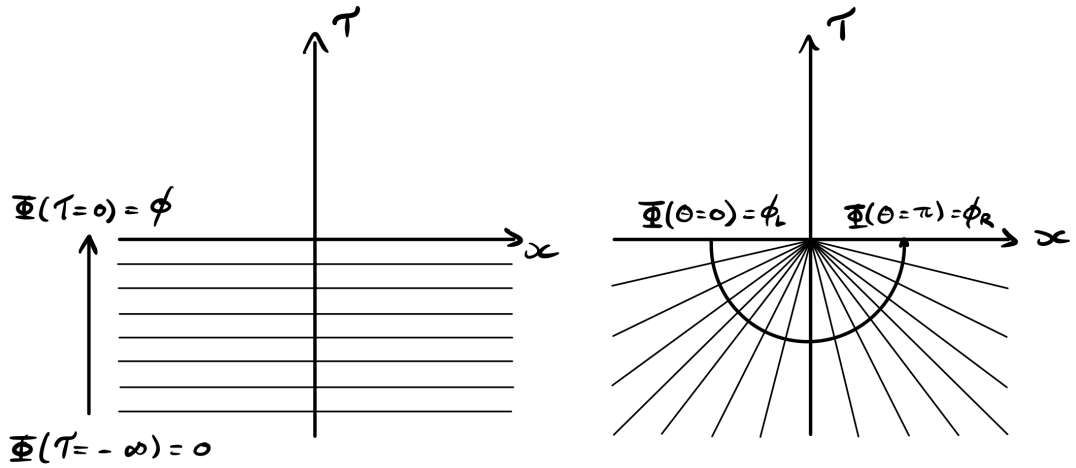

Figure 5.2: Left: Schematic of Eq. 5.6, where we perform the Euclidean path integral along the τ direction. Along each line, we perform a spatial integration so that we cover the whole lower half plane. Right: The new method of integration, whereby we integrate along the angle generated by ζ. Here, we see that to cover the full lower half plane, we must perform our integration along the lines shown [44].

right sections, i.e. $|\phi\rangle = |\phi_L\rangle \otimes |\phi_R\rangle = |\phi_L\phi_R\rangle$. Using this, we can now write our path integral as

$$\langle\phi_L\phi_R|\Omega\rangle \propto \langle\phi_R| e^{-\pi\zeta_R}\hat{A}\,|\phi_L\rangle\,, \tag{5.8}$$

where we have introduced the anti-unitary operator $\hat{A}$, which is called the CPT operator and ζ_R is the restriction of the Lorentz boost operator to the right region [44]. We now have a simple expression which we can calculate by introducing a complete set of states which are eigenstates of the ζ_R operator, i.e. $\mathbb{1} = \sum_i |k_{i,R}\rangle\langle k_{i,R}|$. This gives us

$$\langle\phi_L\phi_R|\Omega\rangle \propto \sum_i e^{-\pi k_i}\langle\phi_R|k_{i,R}\rangle\langle k_{i,R}|\hat{A}|\phi_L\rangle\,, \tag{5.9}$$

where k_i are the eigenvalues of the ζ_R operator in the $|k_{i,R}\rangle$ basis, i.e. $\zeta_R|k_{i,R}\rangle = k_i|k_{i,R}\rangle$. We denote k_i the Lorentz boost energies. Proceeding, we can use the action the anti-unitary operator

on an eigenstate of ζ_R, $\hat{A}^\dagger |k_{i,R}\rangle = |k^*_{i,L}\rangle$, to obtain

$$\langle \phi_L \phi_R | \Omega \rangle \propto \sum_i e^{-\pi k_i} \langle \phi_L | k^*_{i,L} \rangle \langle \phi_R | k_{i,R} \rangle , \tag{5.10}$$

where we note that as $k_{i,R/L}$ is a scalar, we have used the complex conjugate instead of the hermitian conjugate. Now we can clearly see that we have an expression for the vacuum state in Minkowski spacetime

$$|\Omega\rangle = \frac{1}{\sqrt{Z}} \sum_i e^{-\pi k_i} |k^*_{i,L}\rangle \otimes |k_{i,R}\rangle , \tag{5.11}$$

which is given in terms of eigenstates of the Lorentz boost operator [44]. We also note that the normalisation constant involves Z, the partition function. We see that in the vacuum state, entanglement between the right and left regions of Minkowski space is completely manifest. Furthermore, we can compute the reduced density matrix of the vacuum state, by performing a partial trace over the states in the left or right region of Minkowski spacetime. For example, the density matrix for states in the right region is given by

$$\rho_R = \mathrm{Tr}_L(\rho) = \mathrm{Tr}_L(|\Omega\rangle \langle \Omega|), \tag{5.12}$$

which using Eq. 4.24 evaluates to [44]

$$\rho_R = \frac{1}{Z} \sum_i e^{-2\pi k_i} |k_{i,R}\rangle \langle k_{i,R}| . \tag{5.13}$$

Therefore, we can identify $\beta = T^{-1} = 2\pi$, in units where $k_B = 1$. This identification allows us to write Eq. 5.11 for a general temperature, given by

$$|\Omega\rangle = \frac{1}{\sqrt{Z}} \sum_i e^{-\frac{\beta k_i}{2}} |k_{i,L}\rangle \otimes |k_{i,R}\rangle . \tag{5.14}$$

This state is called the thermo-field double state [45]. This state reveals that in a Rindler frame in Minkowski spacetime, the vacuum appears to have a finite temperature, T.

5.2 The Unruh Effect

Up to this point, our argument has avoided any realistic scenarios. Therefore, we will now arrive at this result by considering the more realistic picture of a quantum field theory in Minkowski space. Generalising the metric in Eq. 5.2 to 4 dimensional Minkowski space in both Rindler coordinates

(η, ξ, y, z) and Minkowski coordinates (t, x, y, z), we have

$$ds^2 = -\xi^2 d\eta^2 + d\xi^2 + dy^2 + dz^2 = -dt^2 + d\vec{x}^2 \tag{5.15}$$

where η and ξ are defined as in Eq. 5.1 and $\vec{x} = (x, y, z)$, so they only cover the right region of Minkowski. In Minkowski coordinates, one can execute the canonical quantisation procedure and arrive at the expression for a scalar field Φ in terms of normal modes $\phi_{E,p} \propto e^{-i(Et+\vec{p}\cdot\vec{x})}$, which is given by [49]

$$\Phi = \sum_{E,\vec{p}} a_{E,\vec{p}}\phi_{E,\vec{p}} + a^\dagger_{E,\vec{p}}\phi^*_{E,\vec{p}}, \tag{5.16}$$

which is a solution to the Klein-Gordon equation in Minkowski spacetime. Here, the creation and annihilation operators, $a^\dagger_{E,\vec{p}}$ and $a_{E,\vec{p}}$, respectively, create and destroy states with energy E and momentum $\vec{p}$ in the spatial directions. The Minkowski vacuum, $|\Omega_M\rangle$, is defined by the fact that it must annihilated by a, i.e. $a\,|\Omega_M\rangle = 0$. We now change to Rindler coordinates, where the write Φ in terms of normal modes with the form $\varphi_{k,p} \propto e^{-i(k\eta+p_1 y+p_2 z)}g(\xi)$, where p is the two dimensional momentum vector in Rindler coordinates (not to be mistaken by $\vec{p}$) [49]. By inserting this ansatz for into the Klein-Gordon equation, one can determine the form of $g(\xi)$. Furthermore, we would also prefer to separate φ into fields in the left and right regions of Minkowski space in figure 5.1, φ_L and φ_R, which requires us to extend the Rindler coordinates to cover the left region of Minkowski spacetime. Performing the canonical quantisation procedure, we obtain [49]

$$\Phi = \sum_{k,p}\left(b^R_{k,p}\varphi^R_{k,p} + {b^R_{k,p}}^\dagger {\varphi^R_{k,p}}^* + b^L_{k,p}\varphi^L_{k,p} + {b^L_{k,p}}^\dagger {\varphi^L_{k,p}}^*\right). \tag{5.17}$$

In Rindler coordinates, we find that the canonical quantisation procedure does not form the same creation and annihilation operators as in Minkowski coordinates. Instead, we have the operators $b^\dagger_{k,p}$ and $b_{k,p}$, which create and annihilate states with Lorentz boost energy k and momentum p. Therefore, we define the Rindler vacuum $|\Omega_\mathcal{R}\rangle$ by the fact that it must be annihilated by b, i.e. $b\,|\Omega_\mathcal{R}\rangle = 0$. As we want to determine the form of the Minkowski vacuum $|\Omega_M\rangle$ in terms of Rindler states, we must relate the the the operators a and $a^\dagger$ with b and $b^\dagger$. Specifically, we seek expressions for $a\,|\Omega_M\rangle = 0$ in terms of b and $b^\dagger$. With some work, we find that [50]

$$\begin{aligned}
&\frac{1}{\sqrt{1-e^{-2\pi k}}}\left(b^R_{k,p} - e^{-\pi k}{b^L_{k,p}}^\dagger\right)|\Omega_M\rangle = 0,\\
&\frac{1}{\sqrt{1-e^{-2\pi k}}}\left(b^L_{k,p} - e^{-\pi k}{b^R_{k,p}}^\dagger\right)|\Omega_M\rangle = 0.
\end{aligned} \tag{5.18}$$

From this, we can arrive at the expression

$$|\Omega_M\rangle = \prod_{k,p} \left(\frac{1}{\sqrt{1-e^{-2\pi k}}} \sum_n e^{-\pi n k} |n^L_{k,p}\rangle \otimes |n^R_{k,p}\rangle \right), \tag{5.19}$$

where $|n^{R/L}_{k,p}\rangle$ is a state of n particles in the right or left regions of Minkowski spacetime with Lorentz boost energy k and momentum p [50]. Once again, to determine the reduced matrix of the left or right regions we can take the partial trace of this expression as in Eq. 4.22. For the right region, we obtain the expression

$$\rho_R = \mathrm{Tr}_L(|\Omega_M\rangle \langle\Omega_M|) = \prod_{k,p} \left(\frac{1}{1-e^{-2\pi k}} \sum_n e^{-2\pi n k} |n^R_{k,p}\rangle \langle n^R_{k,p}| \right). \tag{5.20}$$

From this expression, we can identify $\beta = T^{-1} = 2\pi$ as before [50]. This is the Unruh effect. An accelerating observer will observe the vacuum of Minkowski spacetime as a thermal state with temperature T, whereas an inertial observer would not. In our argument, we have not explictily included the acceleration, ξ^{-1}, to maintain consistency with our previous discussion. Including this parameter and returning to SI units, we find that

$$T_U = \frac{\hbar \xi^{-1}}{2\pi c k_B}, \tag{5.21}$$

which is called the Unruh temperature [44].

5.3 A Heuristic View of Hawking Radiation

Of course, we would like to understand the thermodynamic properties of black holes, so one might wonder why we have focused our discussion on Minkowski and Rindler space so far. In fact, the thermodynamics in Schwarzschild spacetime and Rindler spacetime show a remarkable similarity. As we have understood, observers in the Rindler frame move with constant acceleration, ξ. In this frame, one views the Minkowski vacuum as a thermal state with temperature, T. We now invoke the equivalence principle, which states that the Rindler frame is identical to a non-inertial frame in Schwarzschild spacetime, which maintains its position at $r = \text{constant} > 2M$. This explains the large resemblance between figures 5.1 and 3.1. Therefore, we must be able to perform a similar computation for black holes. The main difference between the calculations is the choice of coordinate system. In the Rindler frame, we choose to used Rindler coordinates which naturally lead to the use of the Lorentz boost operator to generate translations in η. In the Schwarzschild case, we will use Kruskal-Szekeres coordinates U and V, as this gives rise to the Kruskal diagram

whose right region resembles our Rindler spacetime. Furthermore, it is no longer natural to consider the Lorentz boost operator ζ , but to consider the generator of time translations in Kruskal-Szekeres coordinates. In Schwarzschild coordinates, the Hamiltonian generates translations in time t, so we define the orbits of the Killing vector ∂_t as the lines of constant r, as shown in figure 5.3. In

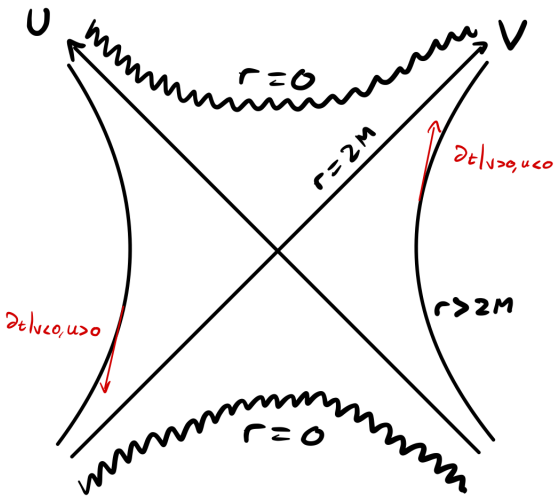

Figure 5.3: Kruskal spacetime with orbits of the Killing vector ∂_t represented by solid black lines in the left and regions [51]. Again, we show specific values of ∂_t.

Kruskal coordinates, we find that ∂_t is given by

$$\partial_t = \frac{\partial U}{\partial t}\frac{\partial}{\partial U} + \frac{\partial V}{\partial t}\frac{\partial}{\partial V} = \frac{1}{4M}\left(V\frac{\partial}{\partial V} - U\frac{\partial}{\partial U}\right). \tag{5.22}$$

Noting that $x^\mu \partial_\mu = \partial_t$, we see that $x^U = -\frac{U}{4M}$ and $x^V = \frac{V}{4M}$. Therefore, we have

$$||\partial_t||^2 = x^\mu x^\nu g_{\mu\nu} = -\left(1 - \frac{2M}{r}\right) \tag{5.23}$$

where $g_{\mu\nu}$ is the metric of Kruskal spacetime. Hence, we see that ∂_t is timelike for $r > 2M$, i.e. the left and right regions, but spacelike for $r < 2M$, i.e. the top and bottom regions. Furthermore, we see that in the right region we have $U < 0$ and $V > 0$. Therefore, we can write Eq. 5.22 as

$$\partial_t = \frac{1}{4M}\left(|V|\frac{\partial}{\partial V} + |U|\frac{\partial}{\partial U}\right). \tag{5.24}$$

so we see that ∂_t is directed forward in time in the right region as shown in figure 5.3. Similar arguments exist for the other three regions. By comparing Eqs. 5.22 and 5.3, we can see that the Lorentz boost operator in Minkowski spacetime is analagous to the Hamiltonian in Schwarzschild spacetime. Therefore, we can see that one can formulate a similar argument as for the Rindler

and Minkowski spacetime comparison, but this time we are comparing an inertial frame in Kruskal coordinates with a non-inertial frame in Schwarzschild coordinates which does not cross the event horizon [51]. As before, one can consider a scalar field Φ in both Kruskal coordinates and non-inertial Schwarzschild coordinates. Quantising the scalar field in Kruskal coordinates we find that in analogy with Eq. 5.16, we decompose Φ into outgoing and ingoing normal modes, which are weighted by creation and annihilation operators $c^\dagger$ and c, respectively. Similarly, one can quantise Φ in the non-inertial coordinates and obtain an expression analogous to Eq. 5.17. In this case, Φ is decomposed into ingoing and outgoing normal modes in the left and right regions of Kruskal spacetime, weighted by creation and annihilation operators, $d^\dagger$ and d, respectively [49]. Here, it is important to understand the meaning of these ingoing and outgoing modes. Consider the right region of Kruskal spacetime as in figure 5.4. We define the outgoing modes as waves that propagate

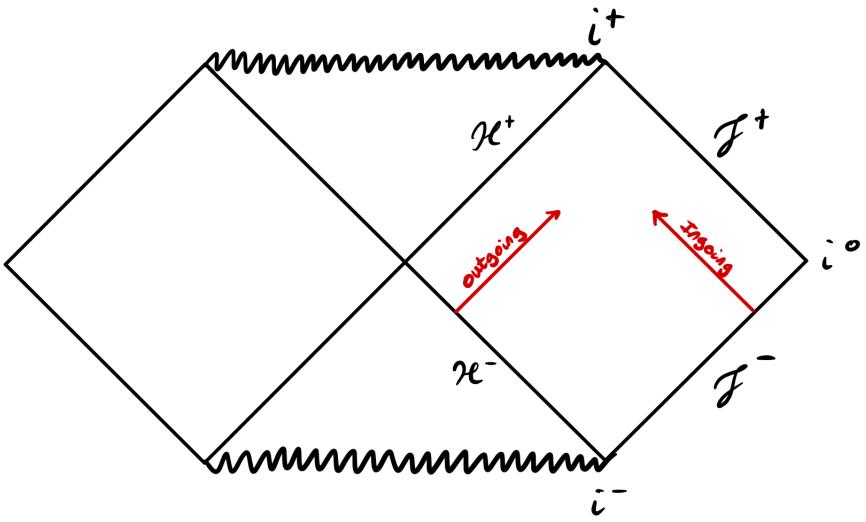

Figure 5.4: Kruskal diagram showing the ingoing and outgoing modes in red. We see that the ingoing modes are directed towards the future event horizon, $\mathcal{H}^+$, whereas the outgoing modes are directed towards $\mathscr{J}^+$ [44].

from the past event horizon $\mathcal{H}^-$ towards $\mathscr{J}^+$, i.e. they have no data on $\mathcal{H}^+$. Similarly, we define the ingoing modes as waves that propagate from $\mathscr{J}^-$ towards the future event horizon $\mathcal{H}^+$, i.e. they have no data on $\mathscr{J}^+$ [49, 3]. Proceeding, we must relate the two different sets of ladder operators via a Bololiubov transformation. This allows us to write the annihilation of the Killing vacuum in terms of the Kruskal ladder operators, which in turn leads to the expression for the Kruskal vacuum [51, 49]

$$|\Omega_K\rangle = \frac{1}{Z}\prod_{\omega,i}\sum_n e^{-4\pi n}\,|n^L_{\omega,i}\rangle \otimes |n^R_{\omega,i}\rangle\,. \tag{5.25}$$

in terms of states in the left and right regions of Kruskal spacetime. Here, we can see that the temperature of the state is $T_H = \frac{1}{4\pi}$, half of the Unruh temperature. Including all the relevant

parameters, we can write this as

$$T_H = \frac{\hbar c^3}{8\pi k_B G M}. \tag{5.26}$$

which is known as the Hawking temperature [44]. The Hawking temperature is often given in terms of the surface gravity, κ, in the form $T_H = \frac{\kappa}{2\pi}$. Therefore, the link between temperature and surface gravity is completely manifest and so Hawking's result supports the analogy between these two quanities [3]. A simple description was put forth by Hawking that the particles of Eq. 5.25 are formed in virtual pairs just outside the event horizon $\mathcal{H}^+$. One of these particles has negative energy and cannot exist in the right region. However, it can tunnel with some probability across $\mathcal{H}^+$ into the top region, i.e. the black hole, where the particle can be real due to the spacelike nature of ∂_t. The other particle has positive energy and so it is real in the right region, i.e. outside the black hole. Therefore, it can escape to $\mathscr{J}^+$ and it is in fact this particle that contributes to the non-zero temperature observed in the right region [49, 3]. This explaination give us an intuitive picture for the relation $T_H = \frac{T_U}{2}$ and how black holes emit radiation.

From classical thermodynamics, we understand that temperature and entropy are linked by the expression [44]

$$\frac{dS}{dE} = \frac{1}{T}. \tag{5.27}$$

Therefore, expect that a black hole with temperature T_H should also have an entropy governed by Eq. 5.27. For this discussion, we will deviate from our use of natural units and use SI units where $\hbar$, G, k_B and c are all restored. Given the famous relation $E = Mc^2$ and the temperature of the black hole, T_H, we can write Eq. 5.27 as

$$S = \int_0^M \frac{8\pi k_B G M'}{\hbar c} dM' = \frac{4\pi k_B G M^2}{\hbar c}. \tag{5.28}$$

Noting that the area of the event horizon $A = 4\pi r_s$, where $r_s = \frac{2GM}{c^2}$, we can write [4, 44]

$$S = \frac{k_B c^3 A}{4\hbar G} = \frac{k_B A}{4 l_p^2} \tag{5.29}$$

where $l_p = \sqrt{\frac{\hbar G}{c^3}}$ is the Planck length. We find that this is the same expression as Eq. 1.1 that we discussed in the introduction. This is the entropy of a black hole. As a final remark of the thermodynamics of Schwarzschild black holes, we return to Bekestein's idea of a generalised second law of thermodynamics, where the combined entropy of black holes and objects in the black hole exterior never decreases. Consider the scenario whereby the exterior of a non-emitting black hole has a lower temperature than that of the black hole. Here, the generalised second law of

thermodynamics is violated. However, if we take Hawking's idea that black holes emit radiation to be true, then the generalised second law holds [3].

5.4 Black Hole Information

Following our discussion of black hole entropy, it is natural to discuss the exchange of information throughout the lifetime of a black hole. To proceed, now turn our attention to black holes that are formed from collapsing matter. Before the start of the collapse, the matter system exists in a specific state, i.e. it will have a unique distribution of mass, charge, energy etc. Then, as the matter collapses beyond its event horizon, all the information about this system is seemingly lost from the universe, as the causal structure of black hole spacetimes do not permit any communication between points on either side of the event horizon [16]. However, we find that some information remains. To determine this, one must extremise the action

$$S = \int d^4x\sqrt{-g}(\mathcal{R} + \mathcal{L}) \tag{5.30}$$

where $\mathcal{R}$ is the Ricci scalar of the curved spacetime and $\mathcal{L}$ is the Lagrangian describing the dynamics of the collapsing matter with constraints determined by mass M, charge Q, angular momentum, J and the presence of an event horizon. This complicated calculation shows that the solution to this equation is the Kerr-Newman metric, the metric outside a rotating, charged black hole. Therefore, we see that despite the specific dynamics encoded in $\mathcal{L}$, the only information accessbile to an observer outside a black hole in its final state are the parameters M, Q and J; this is the no hair theorem [16]. In other words, all black holes with the same parameters M, Q and J appear exactly the same to observers outside the event horizon. However, we have discussed that black holes have an entropy given in Eq. 5.29. The interpretation of this is that information is stored across the event horizon in regions of the size $\sim l_p^2$ [5]. Therefore, it is reasonable to postulate that information about the collapsed matter is stored on the event horizon. Let us assume that this is in fact true. We can consider the black hole to be in some pure quantum state that contains all the information about the matter that formed it. As Hawking concluded, this black hole should emit radiation and begin to evaporate. However, as we can see from Eq. 5.25 that the radiation is in a completely thermal, i.e. statistically determined, state. Furthermore, due to the causal structure of black holes spacetimes, the radiation cannot be causally connected to any information inside the black hole. Therefore, there is no direct correlation between Hawking radiation and the dynamics of the collapsed matter that formed the black hole. Eventually, the black hole should

completely evaporate and disappear, meaning that the radiation is now all that is left. Knowing the statistical nature of the radiation, the final state of this process is a mixed state. In summary, we have evolved a pure state of a black hole, encoding the information of the collapsed matter, into a mixed state describing the radiation from the fully evaporated black hole. Therefore, it is not possible to recover the information of the pure state from the radiation. This is the black hole information paradox [52]. In other words, the map from the inital state of the collapsing matter and the radiation from the fully evaporated black hole it not unitary [44]. Let's see the consequences of this statement on the entropy during black hole evaporation. At the start of the evaporation process, we expect to find the black hole in a pure state and so we have a vanishing entanglement entropy. As the black hole evaporates, the state loses its 'purity' and becomes slightly mixed, meaning that we now have a small, but non-vanishing entanglement entropy. Eventually, the black hole completely evaporates and the final state is mixed with a maximum entanglement entropy. So we see that black hole information loss is equivalent to a black hole evaporation system gaining entanglement entropy. Therefore, we can state that for information to be conserved, at some point during black hole evaporation the entanglement entropy must start to decrease and vanish once the final state has been reached [44]. This is known as the Page curve and is shown in figure 5.5.

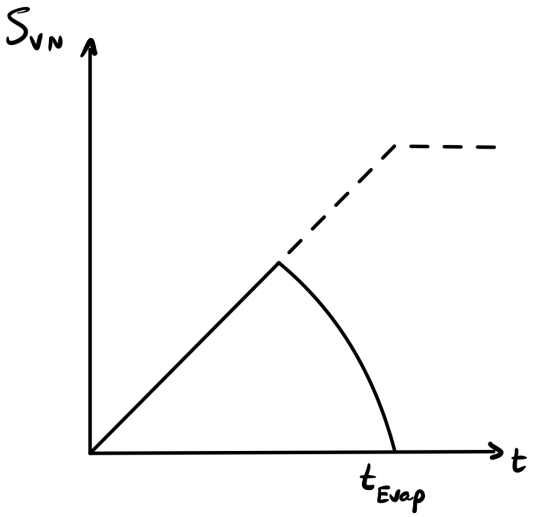

Figure 5.5: A comparison of the Page curve, represented by the solid line, with the predicted curve of Hawking, represented by the dashed line [44].

6. Holography in AdS-Schwarzschild

Having finished our discussion of Schwarzschild black holes, we now turn our attention to Schwarzschild black holes in an anti-de Sitter spacetime, also known as AdS-Schwarzschild black holes. Specifically, we seek to determine the Kruskal and Penrose diagrams of AdS-Schwarzschild, which will be widely used throughout the rest of this section. Furthermore, we will use our results from section 5 to investigate the thermodynamics properties of AdS-Schwarzschild spacetime. Proceeding this, we will review the conjectured relation between wormholes and entanglement, denoted ER = EPR. Naturally, this leads to our discussion on the holographic dual theories of AdS-Schwarzschild spacetime, where we will analyse the role of wormholes in the dual theories.

6.1 AdS-Schwarzschild Black Holes

6.1.1 AdS-Schwarzschild Spacetime

Having discussed AdS in section 2.1, we now turn our attention to Schwarzschild black holes in an AdS background, denoted AdS-Schwarzschild black holes. One way to write the metric for AdS-Schwarzschild spacetime is given by [17]

$$ds^2 = -\left(1 - \frac{2M}{r} - \frac{\Lambda r^2}{3}\right) dt^2 + \left(1 - \frac{2M}{r}\frac{\Lambda r^2}{3}\right)^{-1} dr^2 + r^2 d\Omega^2. \tag{6.1}$$

However, we will focus on a more suitable metric for our discussion. As with the modification of the Minkowski metric to obtain the Schwarzschild metric, we modify the AdS metric given in Eq. 2.8 by

$$ds^2 = -\left(1 - \frac{2M}{r} + \frac{r^2}{R^2}\right) dt^2 + \left(1 - \frac{2M}{r} + \frac{r^2}{R^2}\right)^{-1} dr^2 + r^2 d\Omega^2 \tag{6.2}$$

where M is the mass of the black hole [53]. Note, we will now use R to refer the curvature of AdS (previously we used R_{AdS}) to avoid making our expressions difficult to read. We can clearly see that like Schwarzschild black holes, there is a singularity at $r = 0$. Furthermore, we can determine the remaining singularities by considering the roots of g^{rr}, given by $r^3 + R^2 r - 2MR^2 = 0$. We

find that there exists a single root of this equation, given by

$$r_{AdS} = \frac{2}{3}\sqrt{3}R\sinh\left(\frac{1}{3}\sinh^{-1}\left(3\sqrt{3}\frac{M}{R}\right)\right) \tag{6.3}$$

Expanding Eq. 6.3 by taking $R \gg M$, we obtain

$$r_s \approx r_{AdS} + \frac{8M^3}{R^2} + ... \tag{6.4}$$

where we can see that r_{AdS} is smaller than r_s, so the event horizon of an AdS-Schwarzschild black hole is closer to the singularity compared to Schwarzschild black holes [53]. We can also see that by taking $R \to \infty$, i.e. approaching asympotically flat space, Eq. 6.4 becomes $r_s = r_{AdS}$, while Eq. 6.2 becomes the Schwarzschild metric. In an analogous manner to the Schwarzschild case, it is preferable to analyse the AdS-Schwarzschild spacetime in Kruskal-Szekeres coordinates. Defining the tortoise coordinate as

$$dr_*^2 = \frac{dr^2}{\left(1 - \frac{2M}{r} + \frac{r^2}{R^2}\right)^2}, \tag{6.5}$$

we can integrate this expression to find the tortoise coordinate, given by [19]

$$\begin{aligned} r_*(r) =& \frac{R^2}{3r_{AdS}^2 + R^2}\left(r_{AdS}\ln\left|1 - \frac{r}{r_{AdS}}\right| - \frac{r_{AdS}}{2}ln\left(1 + \frac{r(r + r_{AdS})}{r_{AdS}^2 + R^2}\right)\right. \\ &\left. + \frac{3r_{AdS}^2 + 2R^2}{\sqrt{3r_{AdS}^2 + 4R^2}}\tan^{-1}\left(\frac{r\sqrt{3r_{AdS}^2 + 4R^2}}{2(r_{AdS}^2 + R^2) + rr_{AdS}}\right)\right). \end{aligned} \tag{6.6}$$

Using the tortoise coordinate, we can define the new coordinates

$$\begin{aligned} U &= -\exp\left(-\left(\frac{M}{r_{AdS}^2} + \frac{r_{AdS}}{R^2}\right)(t - r_*(r))\right), \\ V &= \exp\left(\left(\frac{M}{r_{AdS}^2} + \frac{r_{AdS}}{R^2}\right)(t + r_*(r))\right), \end{aligned} \tag{6.7}$$

where, as before, $U < 0$ and $V > 0$. With some calculcations, one finds the AdS-Schwarzschild metric in Kruskal-Szekeres coordinates

$$ds^2 = -4\frac{\left(1 - \frac{2M}{r} + \frac{r^2}{R^2}\right)}{\left(\frac{2M}{r_{AdS}^2} + \frac{2r_{AdS}}{R^2}\right)^2} exp\left(\left(\frac{2M}{r_{AdS}^2} + \frac{2r_{AdS}}{R^2}\right)r_*(r)\right)dUdV + r^2d\Omega_2^2, \tag{6.8}$$

where the radial coordinate is defined implicitly, i.e. $r = r(U, V)$ [19]. The Kruskal diagram for AdS-Schwarzschild is given in figure 6.1. We note there exists a symmetry $U \to -U$, $V \to -V$, allowing us to extend the range of coordinates to $-\infty < U < \infty$, $-\infty < V < \infty$. This allows us to introduce the bottom and left regions of the Kruskal diagram, forming the maximal extension for

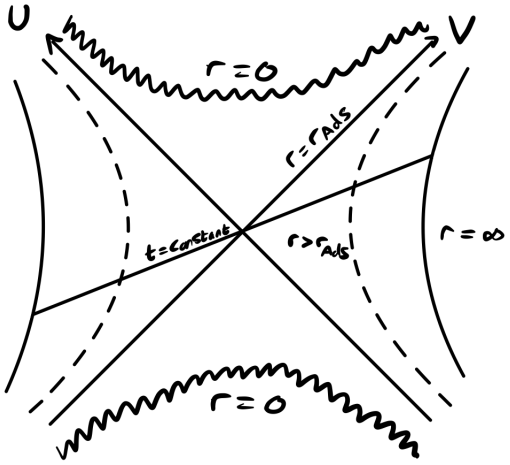

Figure 6.1: AdS-Schwarzschild spacetime in Kruskal coordinates [19]. Here, we show constant t and r lines as the straight solid lines and curved dashed lines, respectively. We also present curved solid lines which represents the boundary of the spacetime.

AdS-Schwarzschild spacetime. We also have the relation

$$UV = -exp\left(\left(\frac{2M}{r_{AdS}^2} + \frac{2r_{AdS}}{R^2}\right) r_*(r)\right), \tag{6.9}$$

in addition to

$$\frac{V}{U} = -exp\left(\left(\frac{2M}{r_{AdS}^2} + \frac{2r_{AdS}}{R^2}\right) t\right), \tag{6.10}$$

which are both defined for $V > 0$ [19]. Therefore, in a similar way to the Schwarzschild black hole case, lines of constant t are straight lines through the origin, while lines of constant r are hyperbolae. Furthermore, we can also see that the light cones at each point are bounded by 45° using the same argument as for the Schwarzschild case. We can clearly see the numerous similarities between the Kruskal diagrams of Schwarzschild spacetime and AdS-Schawrschild spacetime. One noteable difference is the location of the boundary at spatial infinity on the diagrams. The line of constant r at $r = \infty$ is given by a hyperbola with a finite semi-major axis, using Eq. 6.9 where we note that $r_*(\infty) < \infty$. This relates to the discussion in section 2.1 where we noted that massless particles on outwards radial trajectories can reach the boundary of AdS and return in finite time. Before performing a conformal compactification, we note that for Eqs. 6.5 - 6.10, by taking $R \to \infty$, we recover the corresponding expressions for the Schwarzschild black hole in Kruskal-Szekeres coordinates, as in section 3.1. Specifically, for Eq. 6.6, one must taylor expand the second and third terms using $\ln(1 + x) \approx x + ...$ and $\tan^{-1}(x) \approx x + ...$.

To construct the Penrose diagram, we compactify the space in a similar manner to section 3.1, introducing new coordinates that bring infinity to a finite coordinate. We define the coordinates θ and τ via

$$\begin{aligned} U &= -exp\left(\left(\frac{M}{r_{AdS}^2}+\frac{r_{AdS}}{R^2}\right)r_*(\infty)\right)\tan\left(\frac{\theta-\tau}{2}\right), \\ V &= exp\left(\left(\frac{M}{r_{AdS}^2}+\frac{r_{AdS}}{R^2}\right)r_*(\infty)\right)\tan\left(\frac{\theta+\tau}{2}\right) \end{aligned} \tag{6.11}$$

where $-\infty < \theta < \infty$ and $-\infty < \tau < \infty$ [19]. Taking $r = \infty$ in Eq. 6.9, we find

$$\tan\left(\frac{\theta+\tau}{2}\right) = \cot\left(\frac{\theta-\tau}{2}\right), \tag{6.12}$$

which implies $\theta = \pm\frac{\pi}{2}$ and subsequently $-\frac{\pi}{2} < \tau < \frac{\pi}{2}$. Taking $r \to 0$, we have $UV = 1$ so therefore

$$exp\left(\left(\frac{2M}{r_{AdS}^2}+\frac{2r_{AdS}}{R^2}\right)r_*(\infty)\right)\tan\left(\frac{\theta+\tau}{2}\right) = -\cot\left(\frac{\theta-\tau}{2}\right). \tag{6.13}$$

By considering $\theta = 0$ and $\theta = \frac{\pi}{2}$, we find that $0 < \tau < \frac{\pi}{2}$ and $\tau = \pm\frac{\pi}{2}$, respectively [19]. The Penrose diagram for AdS-Schwarzschild spacetime is given in figure 6.2. Here, we see a large

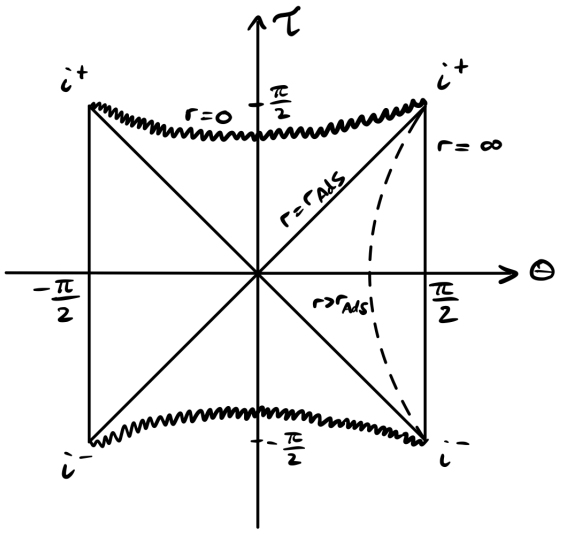

Figure 6.2: The Penrose diagram of AdS-Schwarzschild spacetime [19, 17]. As with the Schwarzschild case, the jagged line represents a curvature singularity and the dashed line represents a line of constant r.

resemblance with the Penrose diagram of AdS, as shown in figure 2.2. We define i^+ (i^-) as in the Schwarzschild case, as the future (past) endpoint of all timelike curves. Shown in figure 6.2 is a constant $r > r_{AdS}$ line, which is determined in the same way as for the Schwarzschild Penrose diagram. Also note that the similarity with the lines of constant r in the Poincaré patch coordinates

as shown in figure 2.2. It is important to note here that null radial geodesics don't necessarily end at $r = \infty$. This is due to the discussion in section 2.1 where we showed that null radial geodesics take a finite amount of proper time to reach the conformal boundary at $r = \infty$ and return the origin. Qualitatively speaking, we can see that we have somewhat 'reshaped' the Kruskal diagram for Schwarzschild spacetime to fit inside conformally compactified $\widetilde{\text{AdS}}$.

6.1.2 Thermodynamics of AdS-Schwarzschild Black Holes

Here, we will briefly comment on a few aspects of the thermodynamics of AdS-Schwarzschild black holes, as this will become very important later on in our discussion. We have shown how Schwarzschild black holes emit radiation, meaning black holes are objects that have a temperature given by the Hawking temperature in Eq. 5.26. From classical thermodynamics, this means that they have an entropy given by Eq. 5.29. Therefore, we expect that AdS-Schwarzschild black holes must also possess similar thermodynamic properties to Schwarzschild black holes; this is indeed the case. Unsuprisingly, we find different properties compared to Schwarzschild black holes due to the unusual nature of AdS. One can identify the temperature of an AdS-Schwarzschild black hole as [54]

$$T = \beta^{-1} = \frac{R^2 + 3r_{AdS}^2}{4\pi R^2 r_{AdS}}, \tag{6.14}$$

which by taking the limits $R \to \infty$ and $r_{AdS} \to r_s$, is equal to the Hawking temperature, T_H. Using this, we consider the canonical ensemble and construct the Euclidean path integral

$$Z(\beta) = \int \mathcal{D}[g_{\mu\nu}] e^{-S_E[g_{\mu\nu}]}. \tag{6.15}$$

where we sum over all metrics, $g_{\mu\nu}$, that are asymptotically AdS whose time coordinate is periodic in β. Here, Z is the partition function and S_E is the Euclidean action given by

$$S_E = \frac{1}{16\pi} \int_0^\beta dt_E \int d^3\vec{x} \sqrt{g} (\mathcal{R} - 2\Lambda), \tag{6.16}$$

where $\mathcal{R} = \mathcal{R}_{\mu\nu} g^{\mu\nu}$ and $t = it_E$ is the analytic continuation of Lorentzian time to Euclidean time [19]. While we have not previously mentioned the semi-classical nature of Hawking's calculation, it becomes important here. By semi-classical, we mean that we have considered a quantum field theory on a non-dynamical, i.e. classical, spacetime background. Therefore, we can approximate the path integral to

$$Z \approx e^{-S_E}. \tag{6.17}$$

From section 2.1, we determined that for AdS, $R = 4\Lambda$. Therfore, we can write Eq. 6.16 as [19]

$$S_E = -\frac{\Lambda}{8\pi}\int_0^\beta dt_E \int d^3\vec{x}\sqrt{g}. \tag{6.18}$$

To compute the entropy of an AdS-Schwarzschild black hole, we consider the difference between the Euclidean action of the AdS-Schwarzschild black hole $S_E^{\text{AdS}-S}$ and the Euclidean action of AdS S_E^{AdS}, both with imaginary time periodic in β [54] . We denote this difference $I = S_E^{\text{AdS-S}} - S_E^{\text{AdS}}$. To compute the former, we take the metric of Eq. 2.8 with $t = it_E$. From this we can conclude $\sqrt{g} = r^2\sin(\theta)$. Therefore, we can evaluate Eq. 6.18

$$S_E^{AdS} = -\frac{\Lambda}{8\pi}\int_0^{\beta_{AdS}} dt_E \int_0^C dr r^2 \int_0^\pi d\theta \sin(\theta) \int_0^{2\pi} d\phi = -\frac{\Lambda\beta_{AdS}C^3}{6}, \tag{6.19}$$

where the radius of S^2 is C. Here, C is a cutoff to regulate the infinite volume one would obtain if we took the upper limit of the r integral to $r \to \infty$ [19]. To compute the latter $S_E^{\text{AdS-S}}$, we use the metric of Eq. 6.2. However, it is important to only integrate from $r = r_{\text{AdS}}$ as the r coordinate is only defined for $r > r_{\text{AdS}}$. Therefore, we obtain the expression for $S_E^{\text{AdS-S}}$ [19]

$$\begin{aligned} S_E^{\text{AdS-S}} &= -\frac{\Lambda}{8\pi}\int_0^\beta dt_E \left(\int \text{Vol}_{S^2}(r=c) - \int \text{Vol}_{S^2}(r=r_{AdS})\right) \\ &= -\frac{\Lambda\beta(C^3 - r_{AdS}^3)}{6}. \end{aligned} \tag{6.20}$$

Here we note that by comparing Eqs. 6.1 and 6.2, $\Lambda = -\frac{3}{R^2}$. Of course, we want an expression only involving β, so we must find a way to relate this parameter to β_{AdS}. This is accomplished by considering the fact that upon removing the cutoff C, i.e. $C \to 0$, the metrics of Eqs. 2.8 and 6.2 should be equal as the AdS-Schwarzschild metric is asymptotically AdS. Therefore, at spatial infinity, we should find that the intervals of proper time are equal, such that [19]

$$\Delta t_E^{\text{AdS}}\sqrt{1 + \frac{C^2}{R^2}} = \Delta t_E^{\text{AdS}-S}\sqrt{1 - \frac{2M}{C} + \frac{C^2}{R^2}}. \tag{6.21}$$

Given our integration ranges, we can identify $\Delta t_E^{AdS} = \beta_{AdS}$ and $\Delta t_E^{AdS-S} = \beta$. Therefore, we can write

$$\beta_{AdS} = \beta\sqrt{\frac{1 + \frac{C^2}{R^2}}{1 - \frac{2M}{C} + \frac{C^2}{R^2}}}, \tag{6.22}$$

which leads to

$$I = \frac{\beta(MR^2 - r_{AdS}^3)}{2R^2}, \tag{6.23}$$

where we can see that removing the cuttoff leaves I to be finite [19]. Now, to calculate the entropy, we recall the result from statistical mechanics [54]

$$S = -\beta \frac{\partial}{\partial \beta} (\ln Z) + \ln Z, \tag{6.24}$$

or equivalently

$$S = \beta \frac{\partial}{\partial \beta} (I) - I. \tag{6.25}$$

To evaluate this expression, we must re-write I in terms of r_{AdS} only. To do this, we must determine β and M in terms of r_{AdS}. Of course, this expression for β is given in Eq. 6.14. To determine M, we note that at the event horizon, the g_{rr} component of the AdS-Schwarzschild metric in Eq. 6.2 must tend to infinity, i.e. $1 - \frac{2M}{r_{AdS}} + \frac{r_{AdS}}{R^2} = 0$. Rearranging, we find that [19]

$$M = \frac{r_{AdS}}{2} \left(1 + \frac{r_{AdS}^2}{R^2} \right). \tag{6.26}$$

Using Eqs. 6.14 & 6.26, we can rewrite Eq. 6.25 as

$$S = \beta \frac{\partial r_{AdS}}{\partial \beta} \frac{\partial}{\partial r_{AdS}} (I) + I. \tag{6.27}$$

It turns out that this expression evaluates to [19]

$$S = \pi r_{AdS}^2 = \frac{A}{4}, \tag{6.28}$$

which, when expressed in SI units, is the same expression for entropy as we found for the Schwarzschild black hole. One of the main differences we find with AdS-Schwarzschild black holes is the ability to maintain thermal equilibrium. As we have seen in section 2.1, massless particles can reach the conformal boundary at spatial infinity and return to its original position in finite proper time. Therefore, we can expect that Hawking radiation will be emitted from a black hole, reach the conformal boundary and return to be reabsorbed by the black hole. However, if a black hole is small enough, it will evaporate before the radiation is reflected back. Subsequently, for a black hole to remain at thermal equilibrium, a black hole must be of a certain size such that the flux of radiation emitted from the black hole and reflected back from the conformal boundary are equal. We refer to these black holes as 'big' and 'small' [44]. It was also determined by Hawking and Page that there exists a phase transition at a temperature T_1 between two systems, an AdS-Schwarzschild black hole with a thermal exterior and a thermal AdS spacetime. To find this temperature, we

consider the Helmholtz free energy

$$F = -T\ln(Z), \tag{6.29}$$

where T is the temperature of the system [54]. Specifically, we consider the free energy difference between an AdS-Schwarzschild black hole and AdS spacetime, given by

$$\Delta F = F_{AdS-S} - F_{AdS} = T(I_{AdS-S} - I_{AdS}) = (R^2 - r_{AdS}^2)\frac{T\pi r_{AdS}^2}{R^2 + 3r_{AdS}^2}, \tag{6.30}$$

where we see that $\Delta F = 0$ for $R = r_{AdS}$ [19]. Therefore, Eq. 6.14 becomes

$$T_c = \frac{1}{\pi R}. \tag{6.31}$$

In fact, this is a very simple analysis of the phase transitions and the calculations by Hawking and Page shows there are 3 characteristic temperatures to consider as we will now discuss [54]. One can show that black hole configurations cannot exist below a temperature $T_0 = \frac{\sqrt{3}}{2\pi R}$, so the thermal AdS spacetime is the only stable state below T_0. Conversely, one can show that thermal AdS configurations cannot exist above a temperature $T_2 = \frac{3^{\frac{1}{4}}}{\sqrt{R}}$, meaning that black hole configurations are the only stable states above T_2. The subtlety of our simple calculation arises between the temperature range $T_0 < T_1 < T_2$. In the range $T_0 < T < T_1$, one finds that while black holes of low mass can form, the thermal AdS spacetime configuration is still more likely to form. Meanwhile, between $T_1 < T < T_2$, one finds that both black hole and thermal AdS states are stable, but black holes are more likely to form. It is in thise sense that we denote T_1 as the Hawking-Page transition temperature, whereby black holes are no longer the energetically favourable state of the spacetime.

6.2 Holographic Description of Wormholes

6.2.1 The ER = EPR Conjecture

In section 5.1, we discussed the construction of the vacuum state of Minkowski spacetime from the perspective of a uniformly acceleration observer. This can be accomplished by performing a path integral evaluated along the Euclidean time, generated by the Hamiltonian, H. However, we discussed a different, but natural approach whereby the path integral was performed along the angle generated by Lorentz boost operator, ζ, in Euclidean signature. Such a calculation leads to the entangled nature of the Minkowski vacuum state, which we call the thermo-field double state due to the identification $\beta^{-1} = T$. We would now like to use this result to understand the ground state of AdS-Schwarzschild spacetime. Let us consider the descrpition of AdS-Schwarzschild spacetime

as we laid out in section 6.1.1. We have determined that the hyperbolae describing $r = \infty$ in the left and right regions of Kruskal spacetime both have a finite semi-major axis, meaning that we can include such hyperbolae on a Kruskal diagram as shown in figure 6.1. Transforming from Lorentzian time to Euclidean time, i.e. $t \to i\tau$, we find Eq. 6.10 becomes of the form

$$\frac{V}{U} = -exp\left(i\frac{2\pi}{\beta}\tau\right), \tag{6.32}$$

where we have written the exponential in this form such that the range of Euclidean time is $0 \leq \tau < \beta$ [11]. Therefore ,we see that the hyperbolae at $r = \infty$ are now replaced by a circle of finite radius as shown in figure 6.3, where we identify τ as an angular coordinate. Now, we see that

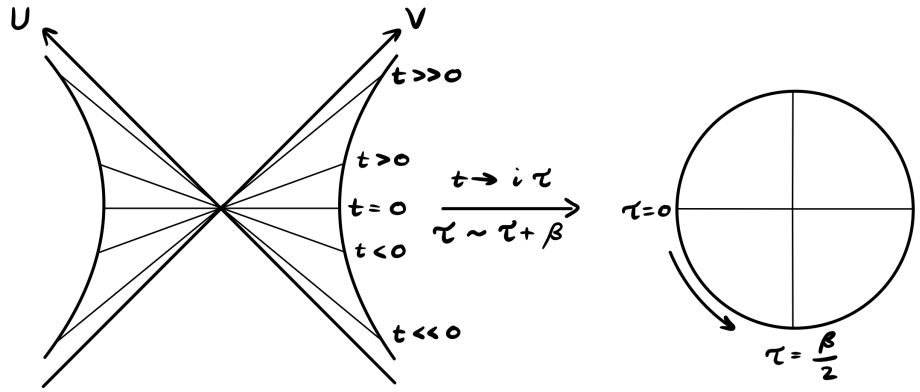

Figure 6.3: Schematic demostrating how Kruskal spacetime transforms from Lorentzian time to Euclidean time [11]. Here we make the identification $\tau \sim \tau + \beta$.

to define the ground state wavefunction of AdS-Schwarzshild, we perform a path integral along the angle generated by H, on the $r = \infty$ boundary in the lower half of the circle. We notice that at $t = \tau = 0$, Eq. 6.32 becomes $\frac{V}{U} = -1$, which is satisfied for the points $V = 1$, $U = -1$ and $V = -1$, $U = 1$, i.e. at the vertices of both hyperbolae in the left and right regions of Kruskal spacetime. Therefore, we see that we can analytically continue the spacetime from the Euclidean signature to Lorentzian signature at the constant $t = 0$ hypersurface. In other words, we can attach the lower semi circle of the Euclidean spacetime to the $t > 0$ region of Kruskal spacetime at $t = 0$ as shown in figure 6.4 [11]. Performing the path integral along the boundary of the Euclidean section of figure 6.4, with angular length $\frac{\beta}{2}$, we find that the wavefunction at $t = 0$ is given by

$$|\Psi\rangle = \frac{1}{\sqrt{Z}} \sum_i e^{-\frac{\beta E_i}{2}} |E_{i,L}\rangle \otimes |E_{i,R}\rangle\,, \tag{6.33}$$

where $|E_i\rangle_{L/R}$ are the energy eigenstates of the CFT defined on the conformal boundary at $r = \infty$ in the left and right regions, respectively [11]. We can make the comparison with Eq. 5.14, where

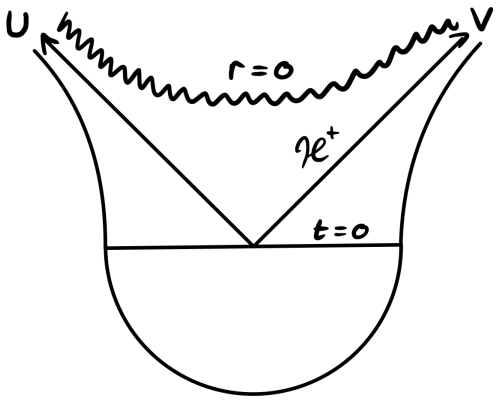

Figure 6.4: Kruskal diagram of AdS-Schwarzschild showing the analytic continuation at $t = 0$ from Euclidean time to Lorentzian time [11].

by taking the partial trace over the left region gives us the reduced density matrix in the right region

$$\rho_R = \frac{1}{Z} \sum_i e^{-\beta E_i} \left| E_{i,R} \right\rangle \left\langle E_{i,R} \right| . \tag{6.34}$$

Similarly, by taking the partial trace over the right region we obtain the reduced density matrix in the left region

$$\rho_L = \frac{1}{Z} \sum_i e^{-\beta E_i} \left| E_{i,L} \right\rangle \left\langle E_{i,L} \right| . \tag{6.35}$$

We see that $|\Psi\rangle$ is constructed from two identical copies of the CFT with finite temperature from Euclidean signature [11]. However, from Eqs. 6.34 and 6.35, we can see that the dynamics of each CFT evolve independently of one another, which reflects the fact that both conformal boundaries are hidden from eachother by the event horizon. From the viewpoint of AdS/CFT, we can evidently state that the gravitational dual theory of $|\Psi\rangle$ is AdS-Schwarzschild spacetime [11]. Now, let us consider a more detailed viewpoint of this duality. Consider a state divided into two subsystems A and B

$$|\Psi'\rangle = |\psi_A\rangle \otimes |\psi_B\rangle , \tag{6.36}$$

where there is no entanglement between subsystems. Due to this lack of entanglement, the states are non-interacting and evolve independently of one another. Now, let's say that $|\psi_A\rangle$ is dual to an asymptotically AdS spacetime A and $|\psi_B\rangle$ is dual to an asymptotically AdS spacetime B. Then, as $|\Psi'\rangle$ describes two independent quantum systems, the dual theory of the wavefunction $|\Psi'\rangle$ is the disconnected spacetimes A and B. Using this, we can build a picture for the dual theory of $|\Psi\rangle$. We can immediately see that $|\Psi\rangle$ is a normalised, weighted sum of states with the form of $|\Psi'\rangle$. From this we can argue that $|\Psi\rangle$ is dual to a quantum superposition of disconnected

asymptotically AdS spacetimes A_i and B_i, where the state $|E_{i,L}\rangle$ is dual to A_i and $|E_{i,R}\rangle$ is dual to B_i. We now have a situation where two gravitational theories are dual to the same CFT. If we believe both of these dualities to be true, then we can state that the quantum superposition of disconnected asymptotically AdS spacetimes is equivalent to the connected AdS-Schwarzschild spacetime as shown in figure 6.5. From this, we arrive at the remarkable conclusion: connectivity

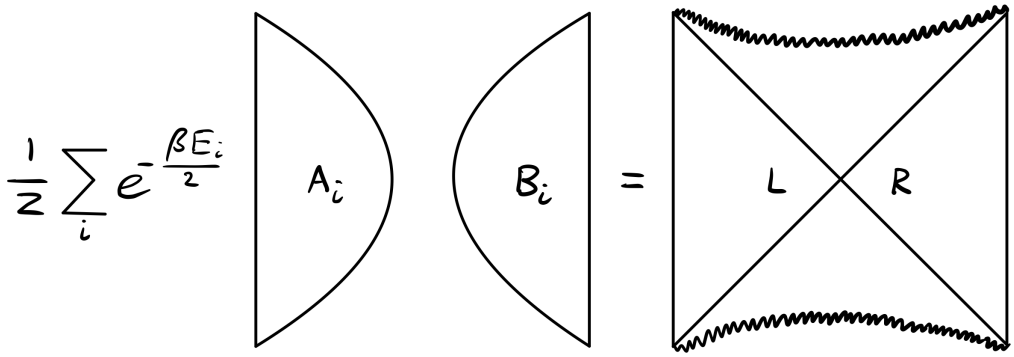

Figure 6.5: Demonstration of the equivalence between the quantum superposition of disconnected asymptotically AdS spacetimes with AdS-Schwarzschild [55].

of the AdS-Schwarschild spacetime arises from the entanglement of the degrees of freedom in Eq. 6.33 [55].

Interestingly, we can also consider another interpretation of our AdS-Schwarzschild spacetime. Up to this point, the Killing vectors corresponding to the time translation symmetry, generated by ∂_t, have been oriented upwards in the right region and downwards in the left region. However, in our second interpretation, we re-orient the Killing vector in the left region such that it points upwards as shown in figure 6.6. In this new interpretation, each CFT has a common time, t, for

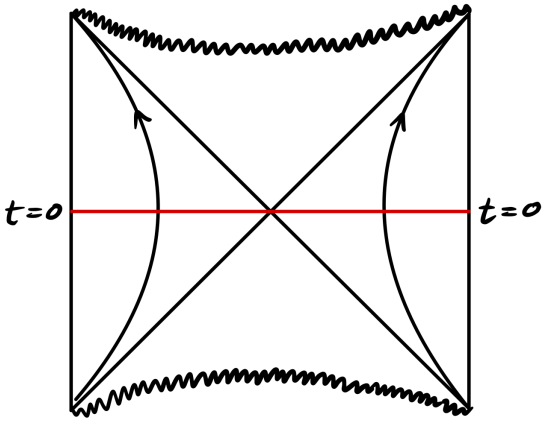

Figure 6.6: AdS-Schwarzschild with a re-orientation of time in the left region and an Einstein-Rosen bridge, given by the red line. This gives rise to the second interpretation of AdS-Schwarzschild [12].

$t \geq 0$. Therefore, we can write the evolution of the state in Eq. 6.33 as

$$|\Psi(t)\rangle = \frac{1}{\sqrt{Z}} \sum_j e^{-\frac{\beta E_j}{2}} e^{-2iE_j t} |E_{j,L}\rangle \otimes |E_{j,R}\rangle \tag{6.37}$$

where the reduced matrices are the same as in Eqs. 6.34 and 6.35 as the complex factors cancel out [12]. Note here that we have changed our summation label to avoid confusion with the imaginary number. The intepretation is that this state represents two black holes in disconnected spacetimes [12]. We say that the degrees of freedom present within the disconnected spacetimes are non-interacting. However, using our previous argument, the geometry is actually connected (c.f figure 6.5). We say that the two black holes are entangled with eachother, where the entanglement entropy is equal to the entropy of either black hole [12]. We can see from figure 6.6 that the conformal boundaries are only connected via spacelike hypersurfaces, i.e. wormholes with the geometry of an Einstein-Rosen bridge. Therefore, we can state that the entanglement between the two black holes arises due to the presence of an Einstein-Rosen bridge. As we can also describe Schwarzschild spacetime using the thermo-field double state, we note that our this discussion also applies for Schwarzschild black holes [12]. In this case, we see that the Einstein-Rosen bridge that gives rise to entanglement has the geometry as discussed in section 3.1.

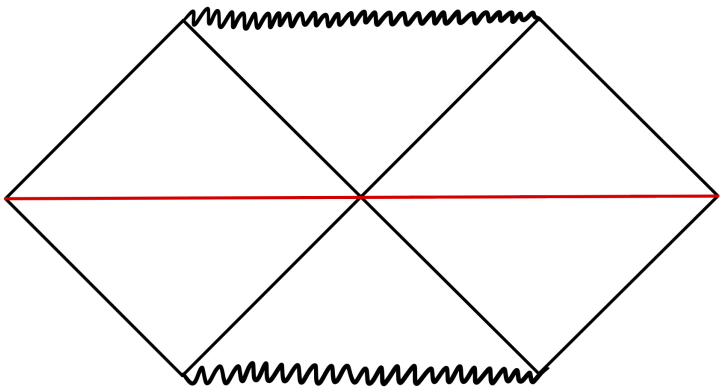

Figure 6.7: Kruskal diagram of Schwarzschild spacetime with an Einstein-Rosen bridge shown in red [12].

In fact, there is a third interpretation of the black hole spacetimes, whereby we consider two black holes in the same spacetime as long as they are sufficiently far apart [12]. It is important to note that our entire discussion has centered around eternal black holes, i.e. black holes that have existed since the start of time. However, one can also consider non-eternal black holes, under the condition that they are created in an entangled state at $t = 0$. [12]. For example, let us create a large number of entangled pairs of particles and separate them into two subsystems, such that the

two subsytems are completely entangled with each other. Then, by collapsing both subsystems into black holes, we will form two entangled black holes connected by an Einstein-Rosen bridge. This concept can be further extended to a single pair of entangled particles. However, the Einstein-Rosen bridge for such an entangled system would be extremely small in size, meaning that the wormhole would have a quantum geometrical structure that could not be described classically [12]. Both types of wormhole are shown in figure 6.8. Having described numerous situations where the entanglement of a system arises due to the presence of an Einstein-Rosen bridge, we are in a position to make a general statement and conjecture the following: wormholes generate entanglement. This conjecture has been given the name 'ER = EPR' , where for completeness we note that ER stands for Einstein and Rosen, while EPR stands for Einstein, Podolsky and Rosen [12]. Of course, we see that the property of locailty is consistent as both entanglement and the Einstein-Rosen bridge geometry do not violate locality (see section 4.1.3 and section 3.1, respecitvely) [12]. Despite these strong comparisons, there is no formal proof for the statement of ER = EPR. However, we will discuss an example supporting the idea of ER = EPR in section 6.2.2.

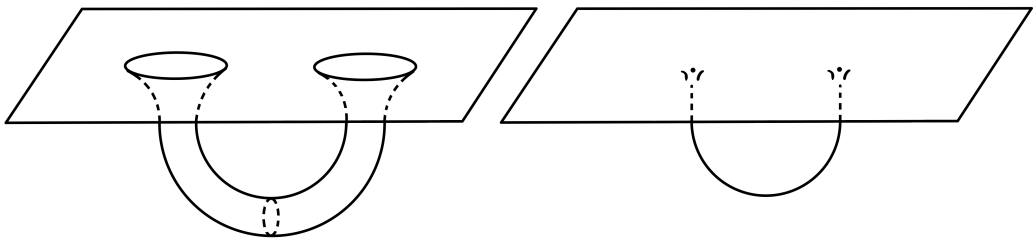

Figure 6.8: Left: Two black holes sufficiently far apart in the same spacetime, connected by a wormhole [56]. Right: Two particles in the same situation, connected by a highly quantum wormhole.

The scientific community is well acquainted with the idea that general relativity and quantum mechanics do not fit together easily. As such, this conjecture raises some important questions. One such question is the following: Does the presence of an Einstein-Rosen bridge allow observation of entanglement? It is well understood from quantum mechanics that one cannot observe a system and determine whether it is entangled or not. However, we understand from ER = EPR that entanglement is generated by wormholes. Therefore, if one could detect this difference in geometry, then the entanglement of the system could be observed, which would violate quantum mechanics [57]. To investigate this, let's consider what an observer in the right and top regions of AdS-Schwarzschild spacetime, as shown in figure 6.9, can measure. As an Einstein-Rosen bridge is a spacelike hypersurface, no observer can traverse this geometry and detect it directly. Therefore, the only means of detecting an Einstein-Rosen bridge is by detecting any affect that the bridge

may have on the geometry that is accessible to the observer [57]. The easiest way to determine this is to compare the geometry of a one-sided AdS-Schwarzschild black hole as shown in figure 6.9, i.e. a black hole formed by the collapse of matter, with the AdS-Schwarzschild spacetime in section 6.1.1, also known as the spacetime of a two-sided AdS-Schwarzschild black hole or an eternal AdS black hole. Consider the metric in Eq. 6.8. For convenience, let us introduce the coordinates

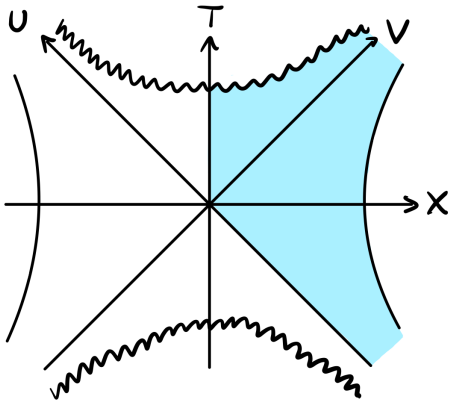

Figure 6.9: Kruskal spacetime in both Kruskal coordinates and light-cone coordinates. The blue region is equivalent to the spacetime of a one-sided black hole [57].

$$\begin{aligned} T &= \frac{V+U}{2}, \\ X &= \frac{V-U}{2}. \end{aligned} \tag{6.38}$$

Substituting these coordinates into Eq. 6.8 gives us [57]

$$ds^2 = 4\frac{\left(1-\frac{2M}{r}+\frac{r^2}{R^2}\right)}{\left(\frac{2M}{r_{AdS}^2}+\frac{2r_{AdS}}{R^2}\right)^2} exp\left(\left(\frac{2M}{r_{AdS}^2}+\frac{2r_{AdS}}{R^2}\right)r_*(r)\right)(-dT^2+dX^2)+r^2d\Omega_2^2. \tag{6.39}$$

Therefore, in addition to the $(U,V)\to(-U,-V)$ isometries of AdS-Schwarzschild, we also have $(T,X)\to(T,-X)$ and $(T,X)\to(-T,X)$ from the new form of the metric in Eq. 6.39. We now note that the geometry of a one-sided AdS black hole covers the region $V>0, X>0$ [57]. We see that no Einstein-Rosen bridge is present in this geometry, as there is no left region of the spacetime. Therefore if one could perform a measurement that would distinguish between two-sided and one-sided AdS black holes, they would be informed of the presence or absence of an Einstein-Rosen bridge, respectively. In this sense, the Einstein-Rosen bridge and hence entanglement could be observed. Due to the $(U,V)\to(-U,-V)$ symmetry of the metric, we see that the top and right regions are completely isomorphic to the bottom and left regions, respectively. Furthermore, due to the $(T,X)\to(T,-X)$ symmetry, we see that the $X<0$ portion of the top region, which is not

accessible to an observer in the one-sided AdS black hole, is isomorphic to the $X > 0$ portion of the top region. Therefore, we can state that an observer in either a one-sided or two-sided AdS black hole cannot perform any local measurement of the geometry that would inform them of which spacetime they are measuring. We can therefore claim that it is not possible for an observer to detect the presence of an Einstein-Rosen bridge [57].

Let's now consider wormholes that connect the conformal boundaries at different times. From figure 6.10, we see that one can construct an infinite number of different wormhole configurations that connect the same two boundary points. In fact, we can summarise this by the region in which all spacelike curves can exist as shown in the blue regions. Of course, this means that each region is bounded by lines parallel to the horizons and is different for states at different times. Therefore, we conclude that a wormhole between two entangled states at specific times is unique [12]. As shown in figure 6.10, we can evolve states on each conformal boundary indepedently of the other to obtain various wormhole configurations. For example, on the left we have three possible wormholes that connect the conformal boundaries at $t = 0$. By performing the same time evolution operation on each state, we obtain the configuration as shown in the center. Alternatively, we can evolve one state while leaving the other state at time $t = 0$ a shown on the right. The states considered in figure

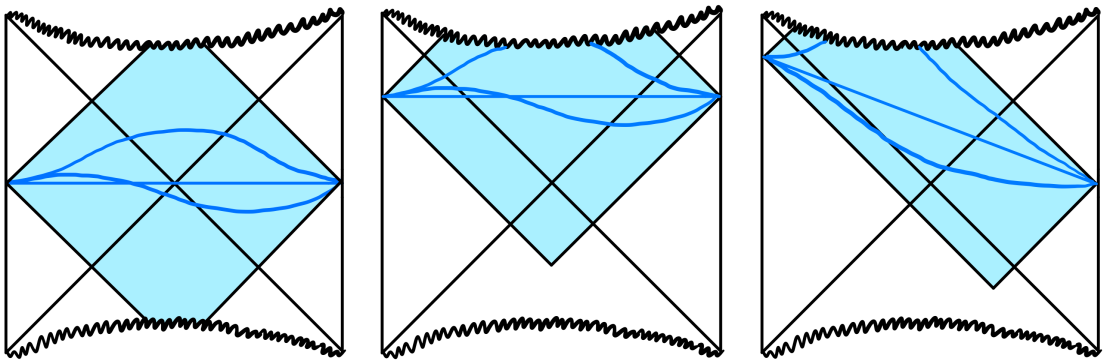

Figure 6.10: Kruskal diagrams showing the possible wormhole configurations [12]. The blue region covers the spacetime in which we can consider such wormholes. Left: Wormholes configurations connecting the asypmtotic boundaries at $t = 0$. Centre: The same configurations considered at $t > 0$. Right: Configurations connecting the asymptotic boundaries at different times, i.e. $t > 0$ and $t = 0$.

6.10 are called maximally entangled states, meaning that each CFT is in a maximally mixed state [12]. Furthermore, we know that the reduced matrices in Eqs. 6.34 & 6.35 are time independent, so each state remains maximally mixed irrespective of any time evolution. Therefore, all wormholes in the eternal AdS black hole spacetime connect states that are maximally entangled. We can also consider wormholes that connect states that are not maximally entangled. To accomplish this, we must consider unitary transformations that alter the density matrices of the CFTs, such that they

are no longer maximally mixed. Consider the penrose diagram of figure 6.4, given by figure 6.11. As we have discussed, performing a path integral along the Euclidean section creates our entangled state $|\Phi\rangle$. This state descibes the physics in the bulk, i.e. the vacuum spacetime of an AdS black hole. Therefore, if we modify our Euclidean path integral to achieve different boundary states, we can alter the physics in the bulk. Specifically, by inserting operators on the boundary as shown

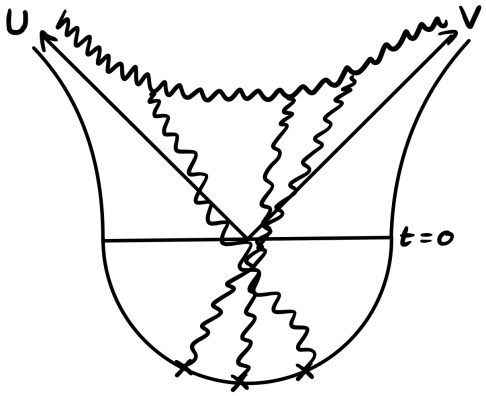

Figure 6.11: Penrose diagram of figure 6.4 [12]. Inserting operators, represented by crosses, on the Euclidean boundary adds particles to the bulk spacetime.

in figure 6.11, we are adding particles to the bulk [11]. In doing so, we subsequently modify the density matrices of each boundary CFT [12]. Therefore, we can add particles to the bulk such that the density matrices are no longer maximally mixed and the CFTs are not maximally entangled. Note, we can add particles such that only one of the density matrices is affected by only acting with the operator one side [12]. It is natural to assume that adding particles to the bulk affects the wormhole geometries of the spacetime, but one may question how wormhole configurations differ when considering different degrees of entanglement, i.e. different entanglement entropies. We will examine this is section 6.2.4.

Let's now discuss what this means for our other interpretations of AdS-Schwarzschild spacetime. As we have discussed, the eternal AdS black hole gives rise to maximal entanglement between states on the conformal boundary at all times. Therefore, if we take the double black hole interpretation of AdS-Schwarzschild to behave similarly, then we conclude that the two black holes are in fact maximally entangled [12].

6.2.2 Wormhole Description of an EPR Pair

Having used the AdS/CFT correspondence to formulate the ER=EPR conjecture, we now proceed to briefly discuss a physical example. Let's consider a colour-neutral quark-antiquark pair. Being colour-neutral, the quark-antiquark pair is naturally entangled. A single quark in Super Yang Mills

theory is dual to a string extending from the Poincaré horizon to the conformal boundary of AdS, where the quark is represented by the endpoint of the string on the conformal boundary [58]. For our quark-antiquark pair, the holographic dual is an open string where the endpoints representing the quarks are on the conformal boundary as shown in figure 6.13. Recall the metric of AdS_5 metric in Poincaré coordinates from Eq. 2.16. By defining $u = z^{-1}$, we rewrite Eq. 2.16 as

$$ds^2 = R^2 \left(u^2 \eta_{\mu\nu} dX^\mu dX^\nu + \frac{du^2}{u^2} \right), \tag{6.40}$$

where $\mu, \nu \in \{0, 1, 2, 3\}$ [59]. To determine the string dynamics, we also recall the Polyakov action from Eq. 2.69. For the case of a string, the Polyakov action reduceds to

$$S = -T_1 \int d^2\xi \sqrt{-\det(h_{ab})} = -T_1 \int d^2\xi \sqrt{-\det\left(\frac{\partial \tilde{X}^\rho}{\partial \xi^a} \frac{\partial \tilde{X}^\sigma}{\partial \xi^b} g_{\rho\sigma} \right)}, \tag{6.41}$$

where ξ^a are the worldsheet coordinates with $a, b \in \{0, 1\}$, T_1 is the tension of the string, $g_{\rho\sigma}$ is the metric of AdS_5 in Poincaré coordinates and $\tilde{X}^\rho = (X^\mu, u)$ where $\rho, \sigma \in \{0, 1, 2, 3, 4\}$ and so $X^4 = u$. To assist our calculation, we can choose the static gauge where we set $(\xi^0, \xi^1) = (t, u)$ and ignore the transverse spatial directions, i.e. set $X^2 = X^3 = 0$. In doing so we have $\tilde{X}^\rho = (t, x(t, u), 0, 0, u)$ [59]. From this, a simple calculation shows that

$$h_{ab} = \begin{pmatrix} h_{00} & h_{01} \\ h_{10} & h_{11} \end{pmatrix} = \begin{pmatrix} R^2 u^2 (\dot{x}^2 - 1) & \dot{x} x' R^2 u^2 \\ \dot{x} x' R^2 u^2 & R^2 (\frac{1}{u^2} + x'^2 u^2), \end{pmatrix} \tag{6.42}$$

which leads to

$$\det(h_{ab}) = -R^4 (1 - \dot{x}^2 + u^4 x'^2). \tag{6.43}$$

Variation of the action gives the equation of motion [59]

$$\frac{\partial}{\partial u} \left(\frac{u^4 x'}{\sqrt{-h}} \right) - \frac{\partial}{\partial t} \left(\frac{\dot{x}}{\sqrt{-h}} \right). \tag{6.44}$$

One can find that the exact solution to this equation which is given by

$$x = \pm \sqrt{t^2 + c^2 - \frac{1}{u^2}} = \pm \sqrt{t^2 + c^2 - z^2}, \tag{6.45}$$

where c is an integration constant [59]. As the quarks are positioned on the conformal boundary of AdS_5, we find that the motion of the quarks obeys $x = \pm\sqrt{t^2 + c^2}$, which is equivalent to the hyperbolic motion that we find for Rindler spacetime as shown in figure 6.12. In terms of the causal

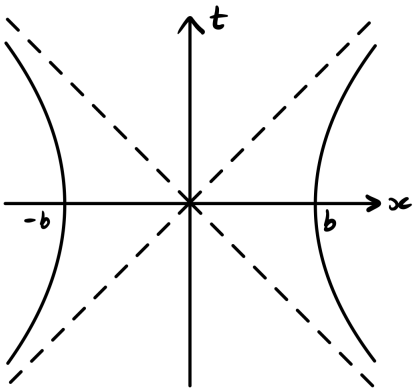

Figure 6.12: Spacetime diagram showing the hyperbolic trajectories of the quark-antiquark pair [58].

structure of the string worldsheet, one can show from the induced metric h_{ab} that all null geodesics trace out straight lines with a gradient equal to or greater than 1 [58]. From this we determine that there exists a horizon at $z = c$ from Eq. 6.45. Due to the causal structure, we notice that the only geometries that connect the regions beyond the horizons are spacelike. In this sense, we see that the causal structure of the string worldsheet is identical to that of the eternal AdS black hole. Hence, we conclude that the holographic dual of the accelerating entangled quarks is a spacetime which is connected by spacelike geometries, i.e. an Einstein-Rosen bridge [58]. In the setup we

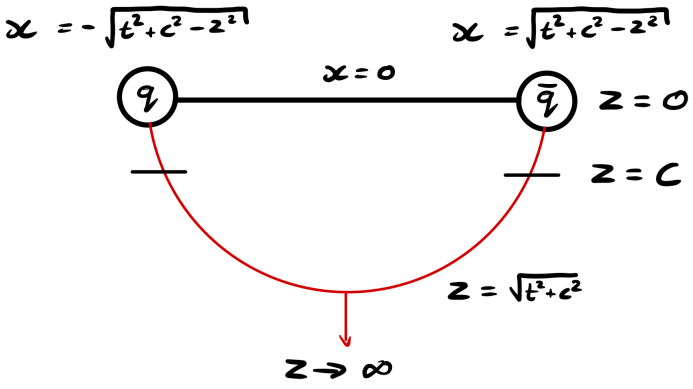

Figure 6.13: Schematic showing the string connecting the quark-antiquark pair at different values of z [58].

have been discussing, the quark-antiquark pair are forever out of causal contant, meaning that for all t no signal can be sent from one quark to the other. However, this restriction is not a defining property of entanglement. As such, we should expect that the holographic wormholes should exist between entangled quarks for more general trajectories, where they are now allowed to come into causal contact. In fact, holographic wormholes do exist for more general trajectories in AdS_5 [60], which provides further evidence of ER=EPR in a general setting.

6.2.3 The Ryu-Takayanagi Formula

Having previously discussed the entanglement entropy of CFTs on the conformal boundary of AdS, we now proceed to discuss how to calculate this in the context pf holography. In other words, we seek a way of calculating the entanglement entropy of the boundary theory from the dual bulk theory. To do this, we use the Ryu-Takyanagi formula. We will now proceed to derive the Ryu-Takyanagi formula as in [18] [43] [13]. To construct such a method, let's consider a 1+1 dimensional quantum field theory which we can separate into two subsytems A and B. We calculate the entanglement entropy of subsystem A the quantum field theory using the replica trick where we have [43]

$$S_A = -\mathrm{Tr}_A(\rho_A \ln(\rho_A)) = -\frac{\partial}{\partial n}\left(\mathrm{Tr}_A \rho_A^n\right)|_{n=1}. \tag{6.46}$$

Therefore, we see that we need to calculate $\mathrm{Tr}_A \rho_A^n$ for our quantum field theory to determine the entanglement entropy. To do this, we return to the Euclidean path integral formalism. As we have only 1 spatial dimension, x, we define the region of subsytem A as the interval $x \in [u, v]$ at $t_E = 0$. We can construct the ground state wavefunction as before by performing the Euclidean path integral from $t_E = -\infty$ to $t_E = 0$ as

$$\Psi(\phi_0(x)) = \int_{\phi(t_E=-\infty,x)}^{\phi(t_E=0,x)=\phi_0(x)} \mathcal{D}\phi e^{-S[\phi]}, \tag{6.47}$$

where $\phi(t_E, x)$ is the field that we are considering for our quantum field theory [43]. The density matrix of the full quantum field theory is given by

$$\rho_{\phi_0 \phi_0'} = \Psi(\phi_0(x))\Psi^*(\phi_0'(x)), \tag{6.48}$$

where $\Psi^*(\phi_0'(x))$ denotes the complex conjugate of $\Psi(\phi_0'(x))$ (c.f $\rho = |\Psi\rangle \langle\Psi|$). To calculate the $\Psi^*(\phi_0'(x))$, we perform the integral in Eq. 6.47 from $t_E = 0$ to $t_E = \infty$ [43]. However, we would like to calculate the reduced density matrix of subsystem A. To accomplish this, we set $\phi_0(x) = \phi_0'(x)$ in the region that defines subsystem B and integrate over this interval, which leaves us with the expression

$$(\rho_A)_{\phi_{1+}\phi_{1-}} = \frac{1}{Z_1}\int_{\phi(t_E=-\infty)}^{\phi(t_E=\infty)} \mathcal{D}\phi e^{-S[\phi]} \prod_{x\in A} \delta(\phi(\epsilon, x) - \phi_{1+}(x))\delta(\phi(-\epsilon, x) - \phi_{1-}(x)), \tag{6.49}$$

where $\epsilon \ll 1$ and Z_1 is the partition function that is required in this expression so that $\mathrm{Tr}_A \rho_A = 1$ [18]. Now that we have a copy of the reduced density matrix $(\rho_A)_{\phi_{1+}\phi_{1-}}$, we can make n copies

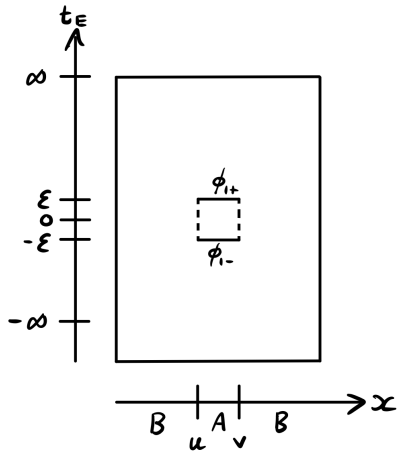

Figure 6.14: Schematic showing the integration ranges of Eq. 6.49 [13].

and determine

$$\mathrm{Tr}_A(\rho_A^n) = \mathrm{Tr}_A((\rho_A)_{\phi_{1+}\phi_{1-}}(\rho_A)_{\phi_{2+}\phi_{2-}}...(\rho_A)_{\phi_{n+}\phi_{n-}}), \tag{6.50}$$

where we have taken the product of the n copies of our quantum field theory [43]. In terms of the path integral, we join the n copies via the identification $\phi_{i-}(x) = \phi_{(i+1)}(x)$ where $i \in \{1, 2, ..., n\}$ to form a Riemann surface, R_n, as shown in figure 6.15. This gives us [43]

$$\mathrm{Tr}_A(\rho_A^n) = \frac{1}{Z_1^n}\int_{R_n} \mathcal{D}\phi e^{-S[\phi]} = \frac{Z_n}{Z_1^n}. \tag{6.51}$$

An important point about R_n is that there are conical singularities at $x = u$ and $x = v$. In other

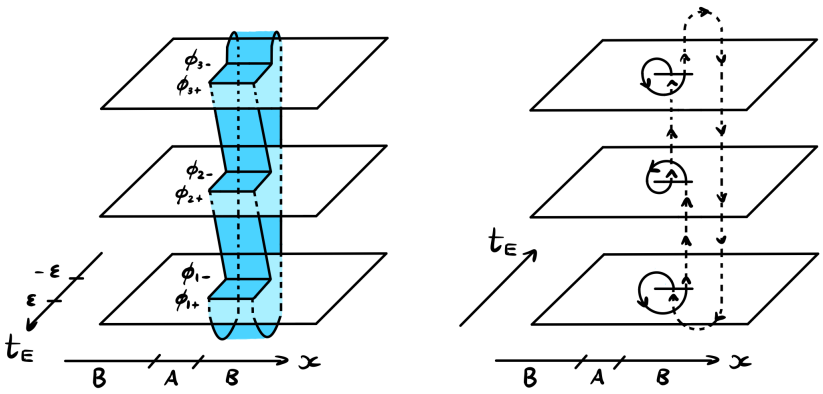

Figure 6.15: Left: Visualisation of the full integration over R_3, which is represented by the blue region [61]. Right: A demonstration of how the phase difference arises from the integration over 3 sheets [13].

words, the boundary of A, ∂A is singular. Therefore, going round a singularity leads to a phase difference of 2π. Of course, as we have n sheets which form R_n, a phase difference of $2\pi(1-n)$ is picked up [13]. This is shown in figure 6.15.

Now, by pluggin Eq. 6.51 into Eq. 6.46, we obtain

$$S_A = -\left(\frac{\partial}{\partial n}(\frac{Z_n}{Z_1^n})\right)|_{n=1}. \tag{6.52}$$

Note that while we derived this expression in 2 dimensions, it is easily generalised to higher dimensions [43]. From Eq. 6.52, we see that to obtain an expression for the entanglement entropy, we must compute the partition function Z_n. To do this, we use the AdS/CFT dictionary as discussed in section 2.3. Let's now construct the AdS/CFT setup in Poincaré coordinates. Consider a CFT in d dimensions, which we now choose to exist on the conformal boundary of an asymptotically AdS spacetime in $d+1$ dimensions. We now take timeslice of this spacetime and divide the CFT into two subsystems, A and B as shown in figure 6.16, separated by the boundary ∂A. As discussed in section 2.1, a timeslice of AdS_{d+1} is equivalent to the hyperbolic plane H^d; we denote this surface $\mathcal{M}$. To represent ∂A in the bulk spacetime, we form a surface, γ_A, which extends into $\mathcal{M}$ with the condition that $\gamma_A|_{z=0} = \partial\gamma_A = \partial A$ [43]. Assuming we have a weakly curved spacetime, we can

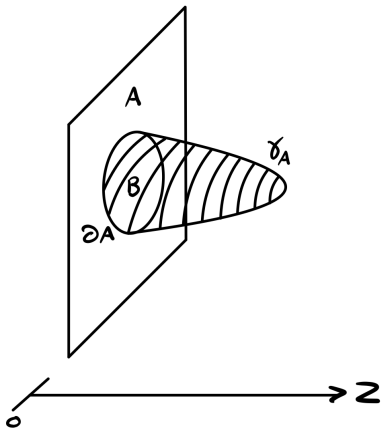

Figure 6.16: An example of a minimal surface in the bulk, separating the regions containing two subsystems A and B [43].

use Eq. 2.89 from the AdS/CFT dictionary to compute the partition function of the CFT. Using this, we write

$$Z_n = \exp(-S_{SG}) = \exp(\frac{1}{16\pi G^{(d+1)}}\int_{\mathcal{M}} dX^{d+1}\sqrt{g}(\mathcal{R}+\Lambda+...)), \tag{6.53}$$

where $G^{(d+1)}$ is the gravitational constant in $d+1$ dimensions and we have omitted all other terms from the supergravity action as they cancel out in the fraction in Eq. 6.51 [43]. To determine $\mathcal{R}$, we seek a bulk AdS spacetime that, as $z \to 0$, asymptotically approaches R_n with the phase

difference of $2\pi(1-n)$ on ∂A. It turns out that this restricts the form of $\mathcal{R}$ to [43]

$$\mathcal{R} = 4\pi(1-n)\delta(\gamma_A) + ..., \tag{6.54}$$

where we have omitted a further term as it is independent of n and therefore does not contribute to the entanglement entropy [18]. Plugging Eq. 6.54 into Eq. 6.53, we obtain

$$\begin{aligned} Z_n &= \exp(-S_{SG}) = \exp(\frac{1}{16\pi G^{(d+1)}}\int_{\mathcal{M}} dX^{d+1}\sqrt{g}(4\pi(1-n)\delta(\gamma_A) + \Lambda + ...) \\ &= \exp(\frac{(1-n)\text{Area}(\gamma_A)}{4G^{d+1}} + ...), \end{aligned} \tag{6.55}$$

where we have once again omitted terms that are independent of n [18]. Interestingly, if we set $n = 1$, we find that $Z_1 = 1 + ...$. Therefore, we can now use this to evaluate the entanglement entropy as

$$\begin{aligned} S_A &= -\left(\frac{\partial}{\partial n}\exp(\frac{(1-n)\text{Area}(\gamma_A)}{4G^{d+1}}\right)|_{n=1} \\ &= -\left(\frac{-\text{Area}(\gamma_A)}{4G^{d+1}}\exp(-\frac{(1-n)\text{Area}(\gamma_A)}{4G^{d+1}}\right)|_{n=1}, \end{aligned} \tag{6.56}$$

which when evaluated for $n = 1$ becomes

$$S_A = \frac{\text{Area}(\gamma_A)}{4G^{d+1}}. \tag{6.57}$$

Furthermore, by taking the supergravity action S_{SG} on shell, we require that γ_A is a surface of minimal area. Taking this into account, we slightly adjust our formula to read [18]

$$S_A = \frac{\text{Area}(\gamma_A, \text{min})}{4G^{d+1}}. \tag{6.58}$$

This is the Ryu-Takyanagi formula. In summary, this formula allows us to compute the entanglement entropy of a CFT using a surface, γ_A, in the bulk AdS spacetime with the conditions that $\partial\gamma_A = \partial A$ and the surface area of γ_A is minimised [13]. Intuitively, we can think of this formula in the following way. The entanglement entropy of subsystem A is obtained by tracing out the degrees of freedom in subsystem B. In other words, the entanglement entropy of subsystem A is equal to the entropy that is only accesible to an observer in region A. We can relate this to our discussion by noticing that the surface γ_A hides region B from an observer in region A [43]. In this sense, the degrees of freedom of subsystem B are not accesible to an observer in region A.

A well established demonstration of the Ryu-Takyanagi formula is the application to the $\text{AdS}_3/\text{CFT}_2$ correspondence [62]. To begin, consider the Poincaré metric in 3 dimensions from

Eq. 2.15

$$ds^2 = \frac{R^2}{z^2}(dz^2 - dT^2 + dX_1^2). \tag{6.59}$$

The CFT exists on the conformal boundary at $z = 0$, parametrised by the coordinates T and X_1. Now, we must define a region on the boundary that contains subsystem A. We choose this region to be $X_1 \in [-\frac{l}{2}, \frac{l}{2}]$. We now seek to determine the entanglement entropy between subsystems A and B at a certain time, so we must take a timeslice of the AdS_3 spacetime. In this timeslice, the surface with a minimised area, γ_A, is given by the geodesic $X_1 = \sqrt{\frac{l^2}{4} - z^2}$ joining the two points at $X_1 = -\frac{l}{2}$ and $X_1 = \frac{l}{2}$ on the boundary [62]. Therefore, the metric on γ_A is obtained by plugging this into Eq. 6.59 and taking $dT = 0$, which gives

$$ds^2_{\gamma_A} = \frac{R^2 l^2}{4z^2(\frac{l^2}{4} - z^2)} dz^2. \tag{6.60}$$

We equate $\text{Area}(\gamma_A, \text{min})$ to the length of γ_A for the case of AdS_3, such that Eq. 6.58 becomes [62]

$$S_A = \frac{1}{4G^{(3)}} \int ds_{\gamma_A} = \frac{R}{4G^{(3)}} \int_a^{\frac{l}{2}} dz \frac{l}{z\sqrt{\frac{l^2}{4} - z^2}}. \tag{6.61}$$

This integral evaluates to

$$S_A = \frac{R}{2G^{(3)}} \ln\left(\frac{l}{a}\right), \tag{6.62}$$

which is the same expression obtained in the CFT framework [62]. Note, we introduced a UV cutoff, a, near $z = 0$ to avoid the divergence of the metric at $z = 0$. We can identify this UV cutoff as the lattice spacing in the CFT [63].

As we discussed in section 6.2.1, the presence of entanglement between two disconnected boundary CFTs at finite temperature in AdS-Schwarzschild spacetime generates a wormhole connecting the two boundaries. Therefore, we can clearly see that the Ryu-Takyanagi formula provides a method of relating the entanglement entropy to the geometry of the wormhole in AdS-Schwarzschild. Before we apply this reasoning, let's discuss this formula in the context of black holes in $3 + 1$ dimensions. Let's define region A to be outside the event horizon, while region B defines the region inside the event horizon. As discussed before, we now seek a surface that hides region B from an observer in region A. Clearly, this surface coincides with the event horizon, $\mathcal{H}^+$, of the black hole [13, 43]. Therefore, our formula becomes

$$S_A = \frac{\text{Area}(\mathcal{H}^+)}{4G^{(4)}} \tag{6.63}$$

which is equal to the usual Bekenstein-Hawking entropy in $3+1$ dimensions.

6.2.4 The Effect of Entanglement Entropy on Lorentzian Wormholes

So far, we have determined the holographic dual of a pair of maximally entangled CFTs with finite temperature at specific times on the conformal boundary of AdS-Schwarzschild spacetime. We discussed that this is equivalent to a non-traversable wormhole in the bulk AdS-Schwarzschild spacetime that connects the boundaries at the specific times as in figure 6.10. Furthermore, we have discussed how to relate the entanglement entropy of the CFTs to the bulk asymptotically AdS spacetime via the Ryu-Takyanagi formula in Eq. 6.58. Combining these two ideas, we now proceed to use the Ryu-Takyanagi formula to understand how the geometry of holographic wormholes in AdS-Schwarzschild spacetime change by varying the entanglement entropy of the CFTs.

Using the Euclidean path integral formalism, we can construct a pair of maximally entangled states at $t = 0$ where each state exists on one of the disconnected boundaries. As these states are entangled, the $t = 0$ region of each boundary is connected by spacelike hypersurfaces, which we call Lorentzian wormholes, as shown in figure 6.10. Let's consider the wormhole configuration that connects the boundaries at $t = 0$ as shown in figure 6.17. For Schwarzschild spacetime we

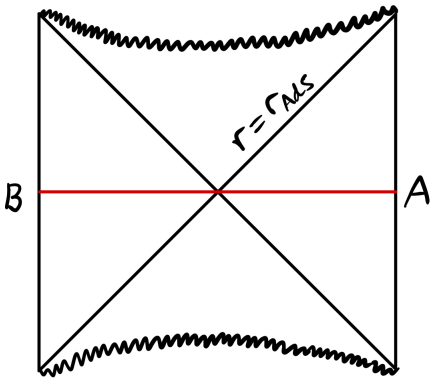

Figure 6.17: Kruskal diagram of AdS-Schwarzschild, where an Einstein-Rosen bridge, shown by the red line, connects the asymptotically AdS boundaries which contain subsystems A and B [64].

have determined the geometry of such wormholes as in figure 3.3. We found that the minimum radius of the wormhole is $r = 2M$, which occurs at the bifurcation 2-sphere. While we haven't explicitly determined the structure of a wormhole in AdS-Schwarzschild, we can make some assumptions regarding its geometry due to the vast similarities between AdS-Schwarzschild spacetime and Schwarzschild spacetime. We expect that the wormhole should resemble the double trumpet geometry, in the sense that the surface of the wormhole asymptotically approaches $\mathbb{R}^2$ as $r \to \infty$ and has a minimal radius at the bifurcation 2-sphere. Furthermore, we see that the bifurcation

2-sphere of AdS-Schwarzschild has a radius of r_{AdS}, as it is the point on the spacetime diagram that joins the two horizons at r_{AdS}. Importantly, we note that by taking the $R \to \infty$ limit, the AdS-Schwarzschild wormhole should approach the geometry of the Schwarzschild wormholes. Therefore, while the geometries of wormholes differ between AdS-Schwarzschild spacetime and Schwarzschild spacetime, we will consider the case of large R where the geometries are approximately identical. As such, we will continue our discussion using the embedding diagram of a wormhole in Schwarzschild spacetime, noting that the geometry approximates to an AdS-Schwarzschild wormhole in weakly curved AdS. Fortunately, we will see that our discussion soley focuses on the section of the wormhole with minimal radius, which is a spatial section of the geometry that we understand well. As such, our discussion should also be applicable to AdS-Schwarzschild wormholes in strongly curved AdS spacetime.

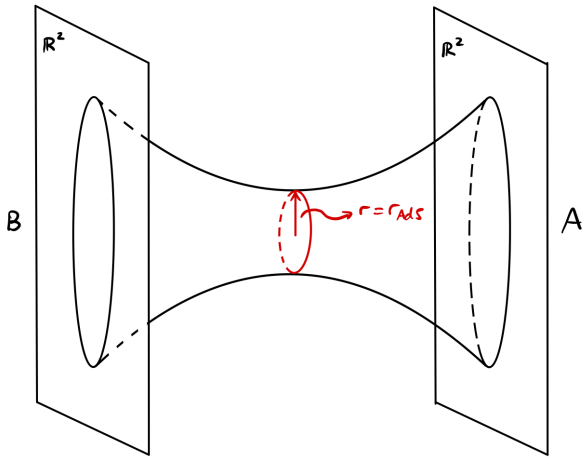

Figure 6.18: The geometry of the Einstein-Rosen bridge in figure 6.17.

We wish to understand how the geometry of the AdS-Schwarzschild wormhole is affected by the entanglement entropy. To use the Ryu-Takyanagi formula, we must identify the surface of minimal area, γ_A, which 'hides' region A from region B. In figure 6.18, we identify γ_A as the circle that wraps around the wormhole at the bifurcation 2-sphere [64]. However, recall that to generate this embedding diagram we supressed the angular coordinate, θ. Therefore, the circle actually represents a 2-sphere of radius r_{AdS}. Trivially, we find the area of this surface is $4\pi r_{\text{AdS}}^2$. Therefore, the entanglement entropy of this system is given by

$$S_A = \frac{4\pi r_{\text{AdS}}^2}{4G}. \tag{6.64}$$

As the state of the total system AB is pure, we see that $S_A = S_B$. Recall the second interpretation of AdS-Schwarzschild spacetime, whereby two black holes are maximally entangled and the

entanglement entropy is equal to the entropy of either black hole. Using the Bekenstein-Hawking formula, one can calculate the entropy of either black hole whose event horizon has an area of $4\pi r^2_{\text{AdS}}$. Indeed, this result matches with the one produced by the Ryu-Takyanagi formula.

Now, let's consider a system at $t = 0$ such that systems A and B now have a smaller entanglement entropy than in Eq. 6.64. This can be achieved in a number of ways. For example, we could add particles to the bulk as in figure 6.11, making the entanglement between the CFTs less than maximal. Alternatively, we can decrease the temperature of the system so that entropy of the system also decreases [55]. Note, however, that in this case the states are still maximally entangled. In either case, we find that

$$S_A < \frac{4\pi r^2_{\text{AdS}}}{4G}. \tag{6.65}$$

Clearly, we see that the area of the minimal surface is has decreased. Eventually, by decreasing the entanglement entropy to zero, the area of the minimal surface also decreases to zero. Hence, decreasing the entanglement entropy of the CFTs causes the wormhole to 'pinch off' [55], disconnecting the two conformal boundaries completely (c.f. figure 6.5).

Another useful quantity to analyse is the mutual information between subsytems A and B, given by Eq. 4.32. We showed that for a pure system AB, where the subsystems A and B are mixed, that the mutual information of AB is $I_{AB} = 2S_A$. Therefore, as the entangledment entropy of a system decreases so does the mutual information. Interestingly, one can relate the mutual information to correlation functions of general operators between the two subsytems A and B as [55]

$$I_{AB} \geq \frac{(\langle \mathcal{O}_A \mathcal{O}_B \rangle - \langle \mathcal{O}_A \rangle \langle \mathcal{O}_B \rangle)^2}{2|\mathcal{O}_A|^2 |\mathcal{O}_B|^2}, \tag{6.66}$$

where $\mathcal{O}_A$ and $\mathcal{O}_B$ are any operators acting on subsystems A and B, respectively. Now, we recall the discussion of correlation functions of scalar fields in section 2.2. We found the form to be that of Eq. 2.52. Clearly, if the correlation function between the scalar field at two different spacetime points goes to zero, the proper distance between the two points becomes infinite if $C_{\Phi_1 \Phi_2}$ remains non-zero. In fact, this holds similarly for operators that are dual to massive particles in the bulk spacetime [55], as in figure 6.11. Therefore, we find that if the mutual information between subsystems A and B becomes zero, then all the correlation functions in Eq. 6.66 also become zero. As such, we find that decreasing the entanglement entropy has the affect of increasing the distance between points in regions A and B.

Combining these two effects, we conclude the following: decreasing the entanglement entropy between our two subsytems A and B causes the wormhole connecting these regions to elongate and 'pinch off'. This process is depicted in figure 6.19, where we see that the effect of decreasing

the temperature of the CFTs causes the distance of the wormhole to increase and the minimal area to decrease [55].

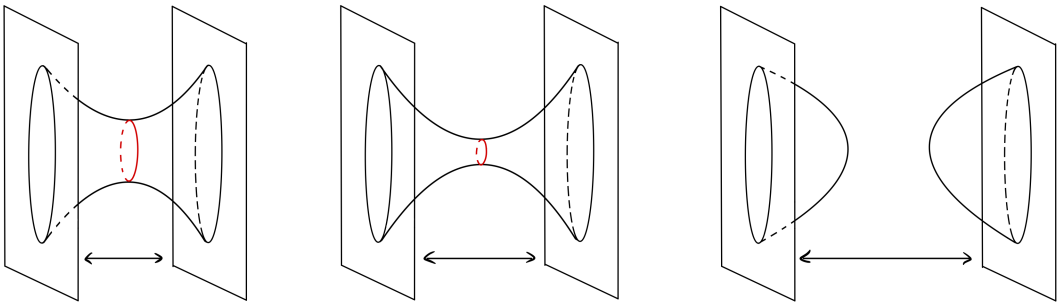

Figure 6.19: Schematic showing the effect of decreasing entanglement entropy, moving from left to right. We see that the wormhole elongates and 'pinches off' [55].

6.2.5 The Future of ER=EPR

To conclude our discussion of the holographic description of Lorentzian wormholes, we will now briefly discuss the future of ER=EPR as well as an apparent failure of the ER=EPR proposal. As such, it appears that the curent state of the ER=EPR proposal needs some modifications, despite the promising ideas we have discussed.

Recall our previous discussion of black hole information in section 5.4. We concluded that the evolution of the collapsed matter to Hawking radiation is non-unitary, as the state evolves from an initial pure state to a final mixed state. This implies that information regarding the initial system of collapsing matter is lost during the evaporation of a black hole. However, let's consider the evaporation of a black hole in the context of AdS/CFT. We can create an infalling shell of matter in the bulk AdS spacetime using CFT operators on the boundary and let it collapse. Proceeding, we can evolve the dual CFT state forward in time using a unitary operator. Therefore assuming that our AdS/CFT bulk to boundary relation is correct, the bulk theory of black hole evaporation must also be unitary, suggesting that information is preserved [44]. If this concept is in fact true, then we should expect the Page curve to correctly determine the entanglement entropy of the system. As ER=EPR suggests a relation between wormholes and entanglement entropy, one might speculate that there exists a relation between the Page curve and the evolution of wormholes. Among other possible open questions, this could certainly be an avenue of future research in ER=EPR. For speculation on the relation between wormholes and black hole evaporation, see [12].

While our discussion surrounding ER=EPR has been positive so far, there exists arguments against such a proposal. It has been suggested that the correspondence between the thermo-field double state and the eternal AdS-Schwarzschild black hole is incorrect, which in turn suggests that

the ER=EPR relation is also incorrect. One of the main reasons this correspondence is believed to be true is the causal structure of AdS-Schwarzschild spacetime. It is impossible for observers in the right and left regions to communicate with each other while remaining in their respective regions. Thsi reflects the fact that the dual CFTs on the conformal boundaries are non-interacting. However, should at least one of the observers in the bulk AdS-Schwarzschild spacetime cross their horizon, communication between the observers becomes possible [12]. It has been suggested that this requires an interaction term in the gravitational theory which allows interactions between degrees of freedom in the right and left regions. However, the dual CFT is non-interacting and so does not contain such an interaction term. Therefore, if we take this point of view to be correct, the proposed duality between the thermo-field double state and the eternal AdS-Schwarzschild black hole must not be true [65].

7. Euclidean Wormholes in AdS

Until now, we have only considered the holographic description of Lorenztian wormholes, those that exists in a spacetime with Lorentzian signature. In particular, we have discussed the specific example whereby the thermo-field double state is holographically dual to AdS-Schwarzschild spacetime. As a final remark, we will now comment the Euclidean wormholes in the context of AdS/CFT. We will review the factorisation problem in AdS/CFT and its possible resolution, leading to the application of the SYK model to holography. Specifically, we will review the work by Garcia-Garcia and Godet, who showed that the statistical averaging of the SYK model leads to Euclidean wormholes in the dual theory [15].

7.1 The Factorisation Problem in AdS/CFT

Let's explore the AdS/CFT dictionary, as discussed in section 2.3, in further detail. Recall Eq. 2.90, which states that the partition function of a string theory on an asymptotically AdS spacetime background evaluated at the boundary is equivalent to the partition function of a CFT that exists on the boundary. For a general string theory, we can write the partition function as

$$Z_{String} = \int \mathcal{D}X\mathcal{D}g_{\mu\nu}e^{-S_E}, \tag{7.1}$$

where S_E is the Euclidean action of the theory [66]. Applying this to the AdS/CFT dictionary, we see that the string theory partition function is a functional integral which sums over all geometries with the boundary conditions that match the boundary CFT. Therefore, if we consider the partition function, Z, of a CFT that exists on a single boundary of an asymptotically AdS spacetime, then the dual theory should be represented by the path integral which sums over such geometries with only one boundary and repects the conditions on that boundary [14]. An issue arises when a product of CFT partition functions are considered. We expect that for the product of CFT partition functions which exist on separate boundaries, say Z^2, the dual theory should be represented by the path integral which sums over geometries with two disconnected boundaries [14]. We give a pictoral

representation of this in figure 7.1. From the bulk point of view, we see that the CFTs cannot communicate in any way through the bulk as the spacetimes are disconnected, so the CFTs are completely decoupled [10]. If we only consider disconnected geometries, then our current view of AdS/CFT is remains consistent, as the square of our single boundary theory is exactly the same as the double boundary theory. However, we are also aware of geometries that connect the two

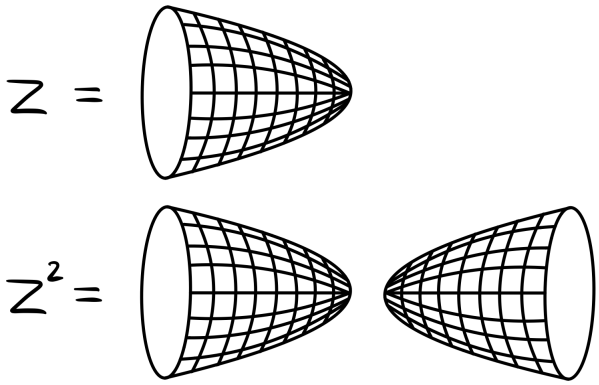

Figure 7.1: The relation between the partition function and the gravitational dual spacetimes. Clearly, we see that if we consider Z^2, we must have two disconnected asymptotically AdS spacetimes (Adapted from a figure in a presentation of [14] given by J. Santos, given online on 26/04/21).

boundaries via the bulk spacetime, i.e. wormholes. Therefore, these geometries also contribute to the construction of Z^2. By including these geometries, we see that Z^2 no longer the square of the single boundary partition function, Z [14]. For this reason, we need to modify our current view of AdS/CFT and assign a new meaning to these partition function dualities. One resolution which

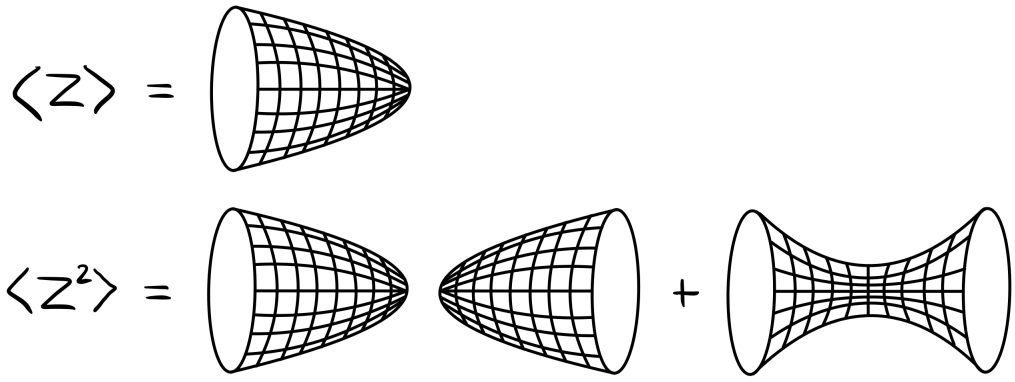

Figure 7.2: The new interpretation of AdS/CFT, where if wormhole configurations are present in the gravitational theory, then the dual theory is equivalent to the statistical average of the partition function [14].

has been recently researched is the possibility that the bulk asymptotically AdS path integrals are actually equivalent to a statistical average of CFTs, i.e. an ensemble of CFTs [14]. In this new picture, which is shown in figure 7.2, we use the notation $\langle Z \rangle$ and $\langle Z^2 \rangle$ to denote the statistical

averaging of the CFTs. Clearly, we see that the wormhole contributions are given by the expression $\delta Z^2 = \langle Z^2 \rangle - \langle Z \rangle^2$, which can be interpreted as the difference between picking out any CFT in the ensemble and the full statistical averaging over all CFTs in the ensemble [14]. If we consider the case where $\delta Z^2 = 0$, then $\langle Z^2 \rangle = \langle Z \rangle^2$, this implies that there are no contributions from bulk spacetimes which connect the two boundaries [14], so we have returned to our previous interpretation of AdS/CFT.

7.2 The Role of The SYK Model in Holography

In our newly modified version of AdS/CFT, we now have a correspondence between asymptotically AdS gravitational theories and an ensemble of CFTs. In recent years, a new avenue of research has opened up surrounding a particular quantum field theory, namely the SYK model, for its applications in the context of our new interpretation of AdS/CFT. We will now briefly discuss this model in further detail before moving on to the proposed holographically dual gravitational theories.

7.2.1 An Brief Introduction to The SYK Model in AdS/CFT

The Sachdev-Ye-Kitaev Model, shortened to the SYK model, is an exactly solvable quantum mechanical model of N Majorana fermions with random interactions between an even number of fermions, q, at a given time [67]. The interaction Hamiltonian of the SYK model is given by [68]

$$H = \frac{i^{\frac{q}{2}}}{q!} \sum_{i_1 i_2 \ldots i_q} J_{i_1 i_2 \ldots i_q} \psi_{i_1} \psi_{i_2} \ldots \psi_{i_q}. \tag{7.2}$$

The distribution of these interactions among the fermions is given by a Gaussian distribution with zero mean and variance

$$\langle J^2_{i_1 i_2 \ldots i_q} \rangle = \frac{J^2 (q-1)!}{N^{q-1}}, \tag{7.3}$$

where J is a parameter that can be identified with the characteristic energy scale of the quantum field theory [68]. In later discussions, we will consider a system of with 4 interacting Majorana fermions at a given time. Setting $q = 4$ we find that the interacting Hamiltonian becomes

$$H = -\frac{1}{4!} \sum_{i,j,k,l=1}^{N} J_{ijkl} \psi_i \psi_j \psi_k \psi_l, \tag{7.4}$$

where the Majorana fermions obey the usual anticommutation relations $\{\psi_a, \psi_b\} = \delta_{ab}$ [68]. Furthermore, we find the variance of J becomes

$$\langle J^2_{ijkl} \rangle = \frac{6J^2}{N^3}. \tag{7.5}$$

In this sense, we see that the SYK model appears to suit the requirements of a CFT in our new interpretation of AdS/CFT due to the statistical averaging of the interaction couplings.

The original purpose of the SYK model was to describe condensed matter systems, specifically the properties of quantum magnets with total spin S and infinitely long range random exchange interactions that obey a Gaussian probability distribution [69]. However, the SYK model has recently sparked interest for its applications in AdS/CFT due to the interesting property that it is nearly invariant under conformal transformations at low energies [67]. For this reason, the SYK model is usually referred to as a nearly conformally invariant theory, denoted $NCFT_1$. To find a dual gravitational theory, it is important that it displays the same symmetries as the CFT. It turns out that there exists a gravitational theory in 2 dimensions with a nearly extremal black hole which displays similar symmetry properties. The near extremal black hole produces a background spacetime that is nearly AdS_2, denoted $NAdS_2$ [67].

To further understand why it is possible to obtain the correspondence $NAdS_2/NCFT_1$, consider the action of Jackiw-Teitelboim (JT) gravity

$$S_{JT} = -\frac{1}{16\pi G}\left(\int d^2x\phi\sqrt{g}(\mathcal{R}+2) + 2\int_{\partial\mathcal{M}} \phi_0\mathcal{K}\right), \tag{7.6}$$

where ϕ is the dilaton, whose value at the boundary is ϕ_0, $\partial\mathcal{M}$ is the boundary of the spacetime and $\mathcal{K}$ is the extrinsic curvature [70]. Clearly, we see that the equation of motion by varying S_{JT} with respect to the dilaton shows that the metric leaves us with the familiar Einstein gravity with a negative cosmological constant, meaning that the metric is that of AdS_2. Furthermore, one can derive the equation of motion for the metric, which restricts the form of the dilaton to [70]

$$\phi = \frac{\alpha + \gamma t + \delta(t^2 + z^2)}{z}. \tag{7.7}$$

It turns out that this solution for the dilaton causes an explicit breaking the conformal symmetry of the theory [70]. While we won't discuss the calculations, it is possible to show that this symmetry breaking leads to the equivalence of the JT gravity theory and the SYK theory at low energies [70] [71].

7.2.2 Euclidean Wormholes in JT Gravity

Now that we have identified the correspondence between the SYK model and JT gravity, we shall construct a specific set up of the SYK model whose gravitational dual theory manifests Euclidean wormholes as in the work by Garcia-Garcia and Godet [15]. Let's consider left and right copies of the SYK model with complex couplings as given by

$$\begin{aligned} H_L &= \frac{1}{4!}\sum_{i,j,k,l=1}^{\frac{N}{2}} (J_{ijkl} + i\kappa M_{ijkl})\psi_{L,i}\psi_{L,j}\psi_{L,k}\psi_{L,l}, \\ H_R &= \frac{1}{4!}\sum_{i,j,k,l=1}^{\frac{N}{2}} (J_{ijkl} - i\kappa M_{ijkl})\psi_{R,i}\psi_{R,j}\psi_{R,k}\psi_{R,l}, \end{aligned} \tag{7.8}$$

where $\kappa \in \mathbb{R}_{>0}$ and the Majorana fermions obey the anticommutation relation $\{\psi_{A,a}, \psi_{B,b}\} = \delta_{AB}\delta_{ab}$. As before, the real and imaginary components of the complex coupling obey a Gaussian probability distribution with zero mean and variance

$$\langle J_{ijkl}^2 \rangle = \langle M_{ijkl}^2 \rangle = \frac{96}{N^3}. \tag{7.9}$$

By looking at H_L and H_R, we see that there are no terms that explicitly couple the two systems, so they are completely non-interacting. Clearly, we see that the two Hamiltonians, H_L and H_R, are complex conjugates of each other. Therefore, denoting the full Hamiltonian of the system as $H = H_L + H_R$, we see that the full system exhibits complex conjugation symmetry, i.e. $H = H_L + H_R = H_R^* + H_L^* = H^*$. Due to this symmetry, we find that the partition function of the total system, $Z(\beta) = \mathrm{Tr} e^{-\beta H}$, is a real parameter of the theory [15].

The work of Garcia-Garcia and Godet was to numerically compute the statistically averaged free energy of the theory, $\langle F(T) \rangle = -T \langle \ln(Z(\beta)) \rangle$, for different values of κ and N to analyse any phase transitions that may occur. They found that for large values of N the averaged free energy is constant at low values of T, followed by a sharp decrease, indicating the presence of a first order phase transition. Furthermore, they found that the temperture at which this phase transition occured increases with increasing κ [15]. In other words, as the total system becomes more 'complex', the phase transition occurs at higher temperatures.

It turns out that the low temperature phase only occurs for large N. As the Hamiltonians are complex, the eigenvalues are also complex and so have the form $E_n = a_n + ib_n$, where $a_n, b_n \in \mathbb{R}$.

Using this, it is possible to write the partition function for a particular state in the ensemble as

$$Z(\beta) = e^{\beta E_0} + 2\sum_n \cos(\beta b_n) e^{-\beta a_n}, \tag{7.10}$$

where we note that E_0 is real [15]. The importance of this expression arises by taking low and high temperature limits. In the high temperature limit, we see that the imaginary component, b_n, is suppressed and has very little effect on the system. Therefore, only the real components of the system contribute, so we see that $H_L = H_R$. Therefore, we see that the system at high temperature behaves like that of two identical, non-interacting SYK systems. Now, taking the low temperature limit, the cosine term becomes rapidly oscillatory as β behaves like a frequency term in the cosine argument [15]. Here, we see the importance of statistically averaging of the system. Computing the averaged free energy

$$\langle F(T) \rangle = -T \left\langle \ln \left(e^{-\beta E_0} + 2\sum_n \cos(\beta b_n) e^{-\beta a_n} \right) \right\rangle, \tag{7.11}$$

for $N = 1$, i.e. no statistical averaging as there is only one Majorana fermion in consideration for each subsystem, the oscillatory behaviour of the free energy is prominent in the low temperature regime. However, by considering larger N, the effect of the statistical averaging is to suppress the eigenvalues with $n > 0$ and thus leveling off the free energy in the low temperature limit. Therefore, we see that at large N, the system has a gap between the ground state, E_0, and the first excited state, E_1, that is not present at low N [15].

It turns out that similar phase transitions occur in JT gravity with matter. In fact, the low temperature gapped phase of the SYK model is actually dual to a Euclidean wormhole in JT gravity with matter. To see this, let's consider the example of a massless scalar field in JT gravity [15]. The wormhole solution we would like to consider is a double trumpet with two asymptotic boundaries connected through the bulk. We can describe this with the metric (c.f Eq. 2.6)

$$ds^2 = \frac{1}{\cos^2(\theta)}(dT^2 + d\theta^2), \tag{7.12}$$

where $T = i\tau$ is the Euclidean time which has the identification $T \sim T + b$. As we discussed before, the SYK model in Eq. 7.4 is holographically dual to JT gravity. In this setup, the Euclidean wormhole is not a solution of the gravitational theory. However, if we consider the SYK model with complex couplings, as in Eq. 7.8, then it turns out that the imaginary components allow the Euclidean wormhole to be a solution [15]. We see that by changing the original SYK Hamiltonians

by

$$\begin{aligned}\delta H_L &= \frac{i\kappa}{4!}\sum_{i,j,k,l=1}^{\frac{N}{2}} M_{ijkl}\psi_{L,i}\psi_{L,j}\psi_{L,k}\psi_{L,l},\\ \delta H_R &= -\frac{i\kappa}{4!}\sum_{i,j,k,l=1}^{\frac{N}{2}} M_{ijkl}\psi_{R,i}\psi_{R,j}\psi_{R,k}\psi_{R,l},\end{aligned} \tag{7.13}$$

we obtain the equations of Eq. 7.8 and it is indeed these terms which contribute to the wormhole. Due to the correspondence, we expect this change to deform the JT gravity theory. This is accomplished by introducing dual operators into the JT gravity action with coefficients ik and $-ik$, where the conformal dimensions of the operators respect the massless scalar field [15]. We will not proceed with the details of the calculation, but it can be shown that the free energy of the gravitational system has two regimes. In the high temperature limit, the free energy of the gravitational system obeys

$$F_{BH} = -2CT - 4\pi^2T^2, \tag{7.14}$$

where C is a constant. This expression is the free energy of two black holes in JT gravity [15]. Furthermore, in the low temperature limit the free energy becomes

$$F_W = -\frac{k^4}{\pi^2}, \tag{7.15}$$

which does not vary with temperature. It turns out that this expression is the free energy of a large Euclidean wormhole, where large simply means that b is large [15]. Clearly, we see a resemblance between the free energy of the JT gravity system and the SYK model with imaginary interaction couplings. In the high temperature regimes, both systems exhibit a decrease in free energy with an increase in temperature, while in the low temperature regime both expressions for the free energy are constant up to the phase transition. Therefore, we can identify the holographic gravity dual of the low energy non-interacting SYK model with a Euclidean wormhole and the holographic dual of the high energy non-interacting SYK model with two black holes [15].

The point of our discussion so far has been that the statistical averaging in the SYK model gives rise to Euclidean wormholes in the holographic gravitational dual theory. As such, we have found a promising example of our new interpretation of AdS/CFT. However, it has also been shown that Euclidean wormholes can still arise when removing the statistical averaging of the SYK interaction couplings and fixing them to a particular value [72].

8. Discussion

The holographic principle has certainly created a new era of modern theoretical physics, possibly taking us one step closer to a quantum theory of gravity. Furthermore, the discovery of AdS/CFT and the specific correspondence between $\mathcal{N} = 4$ Super Yang Mills theory in 4 dimensions and type IIB String Theory compactified on $AdS_5 \times S^5$ by Maldacena has allowed physicists to understand the relationship between gravitational and quantum field theories in greater detail than in previous times. In recent times, this realisation of the holographic principle has been applied to the realm of wormholes, a concept in theoretical physics which has been seemingly dormant in recent times. However, the introduction of AdS/CFT has allowed the topic of wormholes to move towards the forefront of scientific research, with some of the great intellects of our time making great strides in this area. Specifically, the work of Maldacena and Susskind to develop the ER=EPR conjecture, uncovering the relation between Lorentzian wormholes and entanglement, could completely change the way we currently view both gravity and quantum mechanics. While there is no current proof of the connection between wormholes and entanglement, there have been attempts to demonstrate ER=EPR in physical systems.

Following our discussion of black hole thermodynamics, we gave evidence to support the claim that two identical, non-interacting copies of a CFT at finite temperature is holographically dual to an eternal AdS-Schwarzschild black hole. Here, the entanglement between the CFTs generate a Lorentzian wormhole connecting the two asymptotically AdS boundaries. Having determined this duality, we focused our discussion around the thermodynamic quantitiy of entropy. The generalisation of the Bekenstein-Hawking entropy formula by Ryu and Takayanagi allows one to relate the entanglement entropy of the CFTs to the bulk asymptotically AdS spacetime. Using this, we were able to understand the effect of entanglement entropy on the Lorentzian wormhole. We demonstrated that by decreasing the entanglment entropy of the CFTs, the wormhole elongated and 'pinched off', having the effect of disconnecting the AdS-Schwarzschild spacetime. This conclusion is consistent with our understanding that entanglement generates wormholes. Furthermore, we have discussed the role of entropy in black hole evaporation. Among the big unanswered questions

in physics is the black hole information paradox, which states that information that falls into a black hole is lost from the universe. There is speculation that wormholes may be related to black hole evaporation, signaling that ER=EPR may assist progress towards a solution to the black hole information paradox. However, despite the promising arguments supporting ER=EPR, there have been suggestions that this relation between entanglement and wormholes is not correct.

Despite the strong evidence in favour of AdS/CFT, there is one particular issue which has been addressed in the last few years. The original understanding of AdS/CFT does not appear to be consistent due to the possibility of wormhole configurations in the gravitational theory, suggesting that AdS/CFT in its current form must be modified. One proposal that has been explored is that on the CFT side of the correspondence, one must consider the statistical average of an ensemble of CFTs. The SYK model, an exactly solveable quantum mechanical model whose interaction couplings obey a Gaussian probability distibution, has recently be used in AdS/CFT as it can effectively be treated as an ensemble of CFTs. It has been shown by Garcia-Garcia and Godet that a two site SYK model with complex interaction couplings is holographically dual to a Euclidean wormhole in JT gravity. They demonstrated that the free energy of the gapped phase at low temperatures in the SYK model correlates to the free energy of a large wormholes in JT gravity. However, it has also been demonstrated that the statistical averaging of the couplings is not necessary to form wormholes. Therefore, it appears that there are some unanswered questions surrounding the SYK model in AdS/CFT that could be explored in the near future.

References

[1] Jacob D. Bekenstein. Black holes and the second law. *Lett. Nuovo Cim.*, 4:737–740, 1972. doi:10.1007/BF02757029.

[2] Jacob D. Bekenstein. Black holes and entropy. *Phys. Rev. D*, 7:2333–2346, Apr 1973. doi:10.1103/PhysRevD.7.2333.

[3] Stephen. W. Hawking. Particle Creation by Black Holes. *Commun. Math. Phys.*, 43:199–220, 1975. doi:10.1007/BF02345020. [Erratum: Commun.Math.Phys. 46, 206 (1976)].

[4] Raphael Bousso. The holographic principle. *Reviews of Modern Physics*, 74(3):825–874, aug 2002. doi:10.1103/revmodphys.74.825.

[5] Gerard 't Hooft. Dimensional reduction in quantum gravity. *Conf. Proc. C*, 930308:284–296, 1993. doi:10.48550/ARXIV.GR-QC/9310026.

[6] Leonard Susskind. The world as a hologram. *Journal of Mathematical Physics*, 36(11):6377–6396, nov 1995. doi:10.1063/1.531249.

[7] Juan M. Maldacena. *Black Holes in Higher Dimensions*, chapter The Gauge/Gravity Duality, pages 325–347. Cambridge University Press, 2012. doi:10.48550/ARXIV.1106.6073. editor G. Horowitz.

[8] Martin Ammon and Johanna Erdmenger. *Gauge/Gravity Duality: Foundations and Applications*. Cambridge University Press, 2015. doi:10.1017/CBO9780511846373.

[9] Juan M. Maldacena. The Large N limit of superconformal field theories and supergravity. *Adv. Theor. Math. Phys.*, 2:231–252, 1998. doi:10.1023/A:1026654312961.

[10] Juan M. Maldacena and Liat Maoz. Wormholes in AdS. *JHEP*, 02:053, 2004. doi:10.1088/1126-6708/2004/02/053.

[11] Juan M. Maldacena. Eternal black holes in anti-de Sitter. *JHEP*, 04:021, 2003. doi:10.1088/1126-6708/2003/04/021.

[12] Juan M. Maldacena and Leonard Susskind. Cool horizons for entangled black holes. *Fortsch. Phys.*, 61:781–811, 2013. doi:10.1002/prop.201300020.

[13] Shinsei Ryu and Tadashi Takayanagi. Aspects of Holographic Entanglement Entropy. *JHEP*, 08:045, 2006. doi:10.1088/1126-6708/2006/08/045.

[14] Donald Marolf and Jorge E. Santos. AdS Euclidean wormholes. *Class. Quant. Grav.*, 38(22): 224002, 2021. doi:10.1088/1361-6382/ac2cb7.

[15] Antonio M. García-García and Victor Godet. Euclidean wormhole in the Sachdev-Ye-Kitaev model. *Phys. Rev. D*, 103(4):046014, 2021. doi:10.1103/PhysRevD.103.046014.

[16] Charles W. Misner, Kip. S. Thorne, and John. A. Wheeler. *Gravitation*. W. H. Freeman, San Francisco, 1973. ISBN 978-0-7167-0344-0, 978-0-691-17779-3.

[17] Jerry B. Griffiths and Jiri Podolsky. *Exact Space-Times in Einstein's General Relativity*. Cambridge Monographs on Mathematical Physics. Cambridge University Press, Cambridge, 2009. ISBN 978-1-139-48116-8. doi:10.1017/CBO9780511635397.

[18] Horatiu Nastase. *Introduction to the ADS/CFT Correspondence*. Cambridge University Press, 9 2015. ISBN 978-1-107-08585-5, 978-1-316-35530-5. doi:10.1017/CBO9781316090954.

[19] Miguel Socolovsky. Schwarzschild Black Hole in Anti-De Sitter Space. *Adv. Appl. Clifford Algebras*, 28(1):18, 2018. doi:10.1007/s00006-018-0822-6.

[20] Philippe Di Francesco, Pierre Mathieu, and David Senechal. *Conformal Field Theory*. Graduate Texts in Contemporary Physics. Springer-Verlag, New York, 1997. ISBN 978-0-387-94785-3, 978-1-4612-7475-9. doi:10.1007/978-1-4612-2256-9.

[21] Joseph Polchinski. Scale and Conformal Invariance in Quantum Field Theory. *Nucl. Phys. B*, 303:226–236, 1988. doi:10.1016/0550-3213(88)90179-4.

[22] Ofer Aharony, Steven S. Gubser, Juan M. Maldacena, Hirosi Ooguri, and Yaron Oz. Large N field theories, string theory and gravity. *Phys. Rept.*, 323:183–386, 2000. doi:10.1016/S0370-1573(99)00083-6.

[23] Eric D'Hoker and Daniel Z. Freedman. Supersymmetric gauge theories and the AdS / CFT correspondence. In *Theoretical Advanced Study Institute in Elementary Particle Physics (TASI 2001): Strings, Branes and EXTRA Dimensions*, pages 3–158, 1 2002. doi:10.48550/arXiv.hep-th/0201253.

[24] Joseph Polchinski. *String theory. Vol. 2: Superstring theory and beyond.* Cambridge Monographs on Mathematical Physics. Cambridge University Press, 12 2007. ISBN 978-0-511-25228-0, 978-0-521-63304-8, 978-0-521-67228-3. doi:10.1017/CBO9780511618123.

[25] Paolo Di Vecchia. An Introduction to AdS / CFT correspondence. *Fortsch. Phys.*, 48:87–92, 2000. doi:10.1002/(SICI)1521-3978(20001)48:1/3<87::AID-PROP87>3.0.CO;2-S.

[26] Daniel Z. Freedman, Samir D. Mathur, Alec Matusis, and Leonardo Rastelli. Correlation functions in the CFT(d) / AdS(d+1) correspondence. *Nucl. Phys. B*, 546:96–118, 1999. doi:10.1016/S0550-3213(99)00053-X.

[27] Albert Einstein and Nathan Rosen. The Particle Problem in the General Theory of Relativity. *Phys. Rev.*, 48:73–77, 1935. doi:10.1103/PhysRev.48.73.

[28] Matt Visser. *Lorentzian wormholes: From Einstein to Hawking.* 1995. ISBN 978-1-56396-653-8.

[29] Oscar Brauer and Miguel Socolovsky. On schwarzschild anti de sitter and reissner-nördstrom wormholes. *Theoretical Physics*, 4(4), dec 2019. doi:10.22606/tp.2019.44001.

[30] Ludwig Flamm. Republication of: Contributions to einstein's theory of gravitation. *Gen Relativ Gravit*, 47(72), 2015. doi:10.1007/s10714-015-1908-2. Translation of original paper: Beiträge zur Einsteinchen Gravitationstheorie, Physikalische Zeitschrift, 17:448-454, 1916.

[31] John A. Wheeler. Geons. *Phys. Rev.*, 97:511–536, Jan 1955. doi:10.1103/PhysRev.97.511.

[32] Charles W. Misner and John A. Wheeler. Classical physics as geometry: Gravitation, electromagnetism, unquantized charge, and mass as properties of curved empty space. *Annals Phys.*, 2:525–603, 1957. doi:10.1016/0003-4916(57)90049-0.

[33] Michael S. Morris and Kip S. Thorne. Wormholes in space-time and their use for interstellar travel: A tool for teaching general relativity. *Am. J. Phys.*, 56:395–412, 1988. doi:10.1119/1.15620.

[34] Michael S. Morris, Kip S. Thorne, and Ulvi Yurtsever. Wormholes, Time Machines, and the Weak Energy Condition. *Phys. Rev. Lett.*, 61:1446–1449, 1988. doi:10.1103/PhysRevLett.61.1446.

[35] Ryszard Horodecki, Pawel Horodecki, Michal Horodecki, and Karol Horodecki. Quantum entanglement. *Rev. Mod. Phys.*, 81:865–942, 2009. doi:10.1103/RevModPhys.81.865.

[36] Michael A. Nielsen and Isaac L. Chuang. *Quantum Computation and Quantum Information: 10th Anniversary Edition*. Cambridge University Press, 2010. doi:10.1017/CBO9780511976667.

[37] David Bohm and Yakir Aharonov. Discussion of Experimental Proof for the Paradox of Einstein, Rosen, and Podolsky. *Phys. Rev.*, 108:1070–1076, 1957. doi:10.1103/PhysRev.108.1070.

[38] Guy Blaylock. The EPR paradox, bell's inequality, and the question of locality. *American Journal of Physics*, 78(1):111–120, jan 2010. doi:10.1119/1.3243279.

[39] Albert Einstein, Boris Podolsky, and Nathan Rosen. Can quantum mechanical description of physical reality be considered complete? *Phys. Rev.*, 47:777–780, 1935. doi:10.1103/PhysRev.47.777.

[40] Charles H. Bennett, Gilles Brassard, Claude Crepeau, Richard Jozsa, Asher Peres, and William K. Wootters. Teleporting an unknown quantum state via dual classical and Einstein-Podolsky-Rosen channels. *Phys. Rev. Lett.*, 70:1895–1899, 1993. doi:10.1103/PhysRevLett.70.1895.

[41] Tadashi Takayanagi. Entanglement Entropy from a Holographic Viewpoint. *Class. Quant. Grav.*, 29:153001, 2012. doi:10.1088/0264-9381/29/15/153001.

[42] Artur Ekert and Peter L. Knight. Entangled quantum systems and the schmidt decomposition. *American Journal of Physics*, 63(5):415–423, 1995. doi:10.1119/1.17904.

[43] Tatsuma Nishioka, Shinsei Ryu, and Tadashi Takayanagi. Holographic Entanglement Entropy: An Overview. *J. Phys. A*, 42:504008, 2009. doi:10.1088/1751-8113/42/50/504008.

[44] Daniel Harlow. Jerusalem Lectures on Black Holes and Quantum Information. *Rev. Mod. Phys.*, 88:015002, 2016. doi:10.1103/RevModPhys.88.015002. See also: Supplemental Material.

[45] Gustavo Cesar Valdivia Mera. A review on the Unruh Effect and the Thermofield-double state. *arXiv: High Energy Physics - Theory*, 1 2020.

[46] Robert M. Wald. *Quantum Field Theory in Curved Space-Time and Black Hole Thermodynamics*. Chicago Lectures in Physics. University of Chicago Press, Chicago, IL, 1995. ISBN 978-0-226-87027-4.

[47] Miguel Socolovsky. Rindler Space and Unruh Effect. *arXiv: General Relativity and Quantum Cosmology*, 4 2013.

[48] William G. Unruh and Nathan Weiss. Acceleration Radiation in Interacting Field Theories. *Phys. Rev. D*, 29:1656, 1984. doi:10.1103/PhysRevD.29.1656.

[49] William G. Unruh. Notes on black hole evaporation. *Phys. Rev. D*, 14:870, 1976. doi:10.1103/PhysRevD.14.870.

[50] William G. Unruh and Robert M. Wald. What happens when an accelerating observer detects a Rindler particle. *Phys. Rev. D*, 29:1047–1056, 1984. doi:10.1103/PhysRevD.29.1047.

[51] Werner Israel. Thermo field dynamics of black holes. *Phys. Lett. A*, 57:107–110, 1976. doi:10.1016/0375-9601(76)90178-X.

[52] John Preskill. Do black holes destroy information? In *International Symposium on Black holes, Membranes, Wormholes and Superstrings*, 1 1992.

[53] Norman Cruz, Marco Olivares, and Jose R. Villanueva. The Geodesic structure of the Schwarzschild anti-de Sitter black hole. *Class. Quant. Grav.*, 22:1167–1190, 2005. doi:10.1088/0264-9381/22/6/016.

[54] Stephen W. Hawking and Don N. Page. Thermodynamics of Black Holes in anti-De Sitter Space. *Commun. Math. Phys.*, 87:577, 1983. doi:10.1007/BF01208266.

[55] Mark Van Raamsdonk. Building up spacetime with quantum entanglement. *Gen. Rel. Grav.*, 42:2323–2329, 2010. doi:10.1142/S0218271810018529.

[56] Herman Verlinde. ER = EPR revisited: On the Entropy of an Einstein-Rosen Bridge. *arXiv: High Energy Physics - Theory*, 3 2020.

[57] Ning Bao, Jason Pollack, and Grant N. Remmen. Wormhole and Entanglement (Non-)Detection in the ER=EPR Correspondence. *JHEP*, 11:126, 2015. doi:10.1007/JHEP11(2015)126.

[58] Kristan Jensen and Andreas Karch. Holographic Dual of an Einstein-Podolsky-Rosen Pair has a Wormhole. *Phys. Rev. Lett.*, 111(21):211602, 2013. doi:10.1103/PhysRevLett.111.211602.

[59] Bo-Wen Xiao. On the exact solution of the accelerating string in AdS(5) space. *Phys. Lett. B*, 665:173–177, 2008. doi:10.1016/j.physletb.2008.06.017.

[60] Mariano Chernicoff, Alberto Güijosa, and Juan F. Pedraza. Holographic EPR Pairs, Wormholes and Radiation. *JHEP*, 10:211, 2013. doi:10.1007/JHEP10(2013)211.

[61] John L. Cardy, Olalla A. Castro-Alvaredo, and Benjamin Doyon. Form factors of branch-point twist fields in quantum integrable models and entanglement entropy. *J. Statist. Phys.*, 130: 129–168, 2008. doi:10.1007/s10955-007-9422-x.

[62] Tadashi Takayanagi. Entanglement entropy from a holographic viewpoint. *Classical and Quantum Gravity*, 29(15):153001, jun 2012. doi:10.1088/0264-9381/29/15/153001.

[63] Shinsei Ryu and Tadashi Takayanagi. Holographic derivation of entanglement entropy from AdS/CFT. *Phys. Rev. Lett.*, 96:181602, 2006. doi:10.1103/PhysRevLett.96.181602.

[64] Mark Van Raamsdonk. Lectures on Gravity and Entanglement. In *Theoretical Advanced Study Institute in Elementary Particle Physics: New Frontiers in Fields and Strings*, pages 297–351, 2017. doi:10.1142/9789813149441_0005.

[65] Steven G. Avery and Borun D. Chowdhury. No Holography for Eternal AdS Black Holes. *arXiv: High Energy Physics - Theory*, 12 2013.

[66] Joseph Polchinski. *String theory. Vol. 1: An introduction to the bosonic string.* Cambridge Monographs on Mathematical Physics. Cambridge University Press, 12 2007. ISBN 978-0-511-25227-3, 978-0-521-67227-6, 978-0-521-63303-1. doi:10.1017/CBO9780511816079.

[67] Juan M. Maldacena and Douglas Stanford. Remarks on the Sachdev-Ye-Kitaev model. *Phys. Rev. D*, 94(10):106002, 2016. doi:10.1103/PhysRevD.94.106002.

[68] Alexei Kitaev and S. Josephine Suh. The soft mode in the Sachdev-Ye-Kitaev model and its gravity dual. *JHEP*, 05:183, 2018. doi:10.1007/JHEP05(2018)183.

[69] Subir Sachdev and Jinwu Ye. Gapless spin-fluid ground state in a random quantum heisenberg magnet. *Phys. Rev. Lett.*, 70:3339–3342, May 1993. doi:10.1103/PhysRevLett.70.3339.

[70] Juan M. Maldacena, Douglas Stanford, and Zhenbin Yang. Conformal symmetry and its breaking in two dimensional Nearly Anti-de-Sitter space. *PTEP*, 2016(12):12C104, 2016. doi:10.1093/ptep/ptw124.

[71] Vladimir Rosenhaus. An introduction to the SYK model. *J. Phys. A*, 52:323001, 2019. doi:10.1088/1751-8121/ab2ce1.

[72] Phil Saad, Stephen H. Shenker, Douglas Stanford, and Shunyu Yao. Wormholes without averaging. 3 2021. doi:10.48550/arXiv.2103.16754.